# Nanoparticles of short cationic peptidopolysaccharide self-assembled by hydrogen bonding with antibacterial effect against multidrug-resistant bacteria

Hou, Zheng; Shankar, Yogesh Vikhe; Liu, Yang; Ding, Feiqing; Subramanion, Jothy Lachumy; Ravikumar, Vikashini; Zamudio-Vázquez, Rubí; Keogh, Damien; Lim, Huiwen; Tay, Moon Yue Feng; Bhattacharjya, Surajit; Rice, Scott A.; Shi, Jian; Duan, Hongwei; Liu, Xue-Wei; Mu, Yuguang; Tan, Nguan Soon; Tam, Kam C.; Pethe, Kevin; ...Chan-Park, Mary B.

2017

Hou, Z., Shankar, Y. V., Liu, Y., Ding, F., Subramanion, J. L., Ravikumar, V., et al. (2017). Nanoparticles of Short Cationic Peptidopolysaccharide Self-Assembled by Hydrogen Bonding with Antibacterial Effect against Multidrug-Resistant Bacteria. ACS Applied Materials & Interfaces, 9(44), 38288-38303.

https://hdl.handle.net/10356/80357

https://doi.org/10.1021/acsami.7b12120

# Nanoparticles of Short Cationic Peptidopolysaccharide Self-Assembled by Hydrogen Bonding with Antibacterial Effect against Multi-Drug Resistant Bacteria

*Zheng Hou[†1,2], Yogesh Vikhe Shankar[†1,2], Yang Liu[†3], Feiqing Ding[1,2], Jothy Lachumy Subramanion[1,2], Vikashini Ravikumar[5], Rubí Zamudio-Vázquez[1,2], Damien Keogh[1,2], Huiwen Lim[8], Moon Yue Feng Tay[1,9], Surajit Bhattacharjya[3], Scott A. Rice[3,5], Jian Shi[6], Hongwei Duan[1,2], Xue-Wei Liu[2,4], Yuguang Mu[3], Nguan Soon Tan[3,8], Kam (Michael) Chiu Tam[7], Kevin Pethe[8], Mary B. Chan-Park*[1,2,3]*

[1]School of Chemical and Biomedical Engineering, Nanyang Technological University (NTU), 62 Nanyang Drive, Singapore 637459

[2]Centre for Antimicrobial Bioengineering, NTU, 62 Nanyang Drive, Singapore 637459

[3]School of Biological Sciences, NTU, 60 Nanyang Drive, Singapore 637551

[4]Division of Chemistry and Biological Chemistry, NTU, 50 Nanyang Ave, 639798

[5]Singapore Center for Environmental and Life Sciences (SCELSE), 60 Nanyang Drive, Singapore 637551

[6]NUS Centre for Bioimaging Sciences, National University of Singapore, 14 Science Drive 4 Singapore 117557

[7]Department of Chemical Engineering, Waterloo Institute for Nanotechnology, University of Waterloo, Canada, 200 University Ave. W. Waterloo, ON. N2L 3G1

[8]Lee Kong Chian School of Medicine, NTU, 11 Mandalay Road. Singapore 308232

[9]Nanyang Technological University Food Technology Centre (NAFTEC), NTU, 62 Nanyang Drive, Singapore 637459

*mbechan@ntu.edu.sg

†These authors contribute equally.

Keywords: antibacterial, short peptidopolysaccharide, self-assembly, hydrogen bonding, nanoparticle, biocompatible

## Abstract

Cationic antimicrobial peptides (AMPs) and polymers are active against many multi-drug resistant (MDR) bacteria but only a limited number of these compounds are in clinical use due to their unselective toxicity. The typical strategy for achieving selective antibacterial efficacy with low mammalian cell toxicity is through balancing the ratio of cationicity to hydrophobicity. Herein, we report a cationic nanoparticle self-assembled from chitosan-*graft*-oligolysine (CSM5-K5) chains with ultra-low molecular weight (1450 Daltons) that selectively kills bacteria. Further, hydrogen bonding rather than the typical hydrophobic interaction causes the polymer chains to be aggregated together in water into small nanoparticles (with about 37nm hydrodynamic radius) to concentrate the cationic charge of the lysine. When complexed with bacterial membrane, these cationic nanoparticles synergistically cluster anionic membrane lipids and produce greater membrane perturbation and antibacterial effect than would be achievable by the same quantity of charge if dispersed in individual copolymer molecules in solution. The small zeta potential (+15 mV) and lack of hydrophobicity of the nanoparticles impedes the insertion of the copolymer into the cell bilayer to improve biocompatibility. *In vivo* study (using a murine excisional wound model) shows that CSM5-K5 suppresses the growth of methicillin-resistant *Staphylococcus aureus* (MRSA) bacteria by 4.0 orders of magnitude, an efficacy comparable to that of the last resort MRSA antibiotic vancomycin; it is also non-inflammatory with little/no activation of neutrophils (CD11b and Ly6G immune cells). This study demonstrates a promising new class of cationic polymers -- short cationic peptidopolysaccharides -- that effectively attack MDR bacteria due to the synergistic clustering of, rather than insertion into, bacterial anionic lipids by the concentrated polymers in the resulting hydrogen bonding-stabilized cationic nanoparticles.

## 1. Introduction

Drug-resistant bacterial infections challenge the efficacy of antibiotic therapies and result in major healthcare-associated problems[1-2]. With the increasing number of multidrug-resistant (MDR) bacterial strains, antimicrobial peptides (AMPs) have become an attractive potential alternative form of therapy[3]. AMPs are usually constituted of cationic and hydrophobic residues and primarily function somewhat like surfactants by physically disrupting cellular membranes. In contrast to antibiotics, the frequency of bacterial AMP-resistance emergence is typically very low[3-4]. However, poor biocompatibility is one of the major obstacles to the clinical exploitation of the large number of characterized AMPs[5]. The interaction of AMPs with cellular membranes typically involves the electrostatic attraction to anionic lipid head groups followed by peptide insertion into the hydrophobic interior of membrane aided by its hydrophobic residues [3, 6]. Both leaflets of the cytoplasm membrane of bacteria are rich in anionic lipids, such as phosphatidylglycerol, cardiolipin and phosphatidylserine. On the other hand, the similar outer leaflet of cytoplasmic mammalian membranes is composed mainly of zwitterionic lipids such as phosphatidylethanolamine, phosphatidylcholine or cholesterol which are net neutral[7-8]. The differences in anionic charge of cytoplasmic membranes of bacterial cells compared with mammalian cells, though small, may possibly be exploited for selective killing. On the other hand, the hydrophobic component of these peptides facilitates the peptide insertion into the bacterial lipid bilayer but results in non-selective toxicity. Tuning the hydrophobic to charge balance has been a common strategy for improving the bactericidal efficacy of AMPs. However, the inability of many AMPs to differentiate the subtle differences between the plasma membranes of mammalian cells from those of bacterial cells is a major limitation to their clinical potential. Increasing biocompatibility of cationic antimicrobial agents through alternative rational design is an attractive research agenda.

Cationic polymers, unlike sequence-dependent AMPs, have also been exploited as antibacterial agents and they are usually more economical to make and are attractive materials for coatings, personal care formulations, rinse, etc. Amongst these, chitosan (CS) has been extensively explored for antibacterial effect

since it is biocompatible and relatively cheap. Various cationic derivatives of chitosan based on quaternary ammonium[9-10], quaternary pyridinium[11], quaternary piperazinium[12], quaternary phosphonium[13], sulfonamide[14] functional groups, *etc* have been made for improving antibacterial efficacy. However, the antibacterial effects of these quaternized chitosan derivatives are also based on their charge and hydrophobicity.

On the other hand, chitosan is known to have strong intra-/inter-molecular hydrogen bonding, so that suitably designed chitosan derivatives based on hydrogen bonding and cationic charge may offer an alternative strategy for biocompatible antibacterial effect. Chitosan-*graft*-polycationic polymers have been demonstrated to have good antimicrobial activities[15-16]. We have previously reported that medium molecular weight cationic chitosan-*graft*-oligolysine (CS-K16) bromide salt has good antibacterial killing effect on some laboratory bacterial strains with excellent non-hemolytic property[17]. To improve the toxicity of this class of compound so that it may be applied for *in vivo* application, we postulate that ultrashort chitosan-*graft*-cationic peptides may offer better biocompatibility since the charge differential between bacterial and mammalian cells is subtle. However, lowering the molecular weight of cationic polymer reduces charge density which may possibly result in sacrifice of the bactericidal effect and so that there is possibly a contradiction in this strategy of toxicity reduction unless the shorter molecular weight molecule may be self-assembled into nanoparticles, as the antimicrobial activity of nanoparticles were well-studied[18]. There has been numerous reports on short AMPs[19-20] and lipopeptides[21-22] that are antibacterial but there has been no reports yet of short peptidopolysaccharides. Additionally, there has been also no demonstration of peptidopolysaccharides efficacy towards multi-drug resistant (MDR) superbugs with *in vitro* nor *in vivo* models.

In this study, a short chitosan-*graft*-oligolysine chloride salt (Scheme 1) was synthesized via an optimized procedure. The molecular weight of the copolymer was controlled to be around 1450 Daltons by pre-sonication of the starting chitosan molecule and employing hydrochloric acid (HCl) for the post-polymerization deprotection. From Matrix Assisted Laser Desorption/Ionization –time of flight (MALDI-TOF) analysis, the chemical structure of the polymer may be represented by CSM5-K5 (CSM denotes one chitosan monomer

repeat). We show that these short CSM5-K5 molecules self-assembled into nanoparticles because of strong hydrogen bonding due to the chitosan chains[23] causing synergistic selective bacterial cell membrane damage[24]. We showed that CSM5-K5 chloride salt is bactericidal against methicillin- and oxacillin-resistant *S. aureus* (MRSA and ORSA), and pathogenic strains of *E. coli* and *P. aeruginosa*, with minimum inhibitory concentrations of 16-64μ/mL and hemolytic concentration (HC10) of greater than 5000μg/mL which is much higher compared with the MIC values. We also showed that CSM5-K5 is effective at treating MRSA infections in a murine excisional wound infection model and measured the neutrophils (CD11b and Ly6G immune cells) activation. To characterize the nanoparticle solution properties (*i.e.* size, pH-responsiveness, proton sponge effect and interaction forces), we applied light scattering, pH-potentiometric titrations, transmission electron microscopy (TEM) and computer simulation. To show that CSM5-K5 is membrane active, we applied membrane assays, confocal microscopy and cryo-TEM. To understand the interaction forces between copolymer particles with bacterial membranes and compare CSM5-K5 with homo-polylysine, we applied isothermal calorimetric titration (ITC) and molecular dynamics (MD) computer simulation.

## 2. Results and Discussion

### 2.1. *In vitro* and *in vivo* antibacterial activities of CSM5-K5 nanoparticle

Low molecular weight chitosan-*graft*-oligolysine (**Scheme 1**) was synthesized via a multi-step reaction involving the protection of chitosan (CS), N-carboxyanhydride (NCA) polymerization from the $-NH_2$ group on the CS backbone followed by HCl deprotection (**Figure S1A).** The molecular weight of the resulting graft polymer measured by MALDI-TOF was 1450 Daltons (**Figure S2**). The actual structure of the copolymer molecule is likely to be CSM5-Kn where there are 5 chitosan monomer (CSM) repeat units with a total of 'n' lysine amino acids and 'n' ranges from 3 to 8 (the polymer shall be abbreviated hereafter just as CSM5-K5, **Scheme 1**). The number/ weight-average molecular weights (Mn/Mw) of the polymer determined by GPC was 3648Da/4084Da respectively **(Table 1 and Figure S3)**.

CSM5-K5 is broad spectrum active against various bacterial strains (**Table 2**) including multi-drug resistant (MDR) Gram-positive MRSA/ORSA and clinical MDR Gram-negative *E. coli* EC8739 and *P. aeruginosa* PAD25 strains. The MICs against MRSA, ORSA, *E. coli* EC958 and *P. aeruginosa* PAD25 are 16, 16, 64 and 64 μg/mL, respectively, which are comparable with most published AMPs[25-27]. The antimicrobial activity towards Gram-positive bacteria is slightly better compared with Gram-negative bacteria, probably due to the barrier imposed by the outer membrane of Gram-negative bacteria which generally restricts cationic hydrophilic molecules from trespassing. However, more hydrophobic cationic molecule generally leads to better bacteria penetration but also more toxicity to mammalian cell.

The *in vivo* antimicrobial efficacy of CSM5-K5 against MRSA (BAA-40) was measured using a murine excisional wound model. The CSM5-K5 treated wounds resulted in significantly lower MRSA bacteria concentration. With a dosage of 2.5 mg/kg of CSM5-K5 applied to the murine wound, the MRSA burden has a statistical significant lowering of 4.0 orders compared to that of the control without treatment, making it comparable in efficacy to that with vancomycin which is a last resort antibiotic against MRSA (**Figure 1A**). The immune response of the infected skin was also quantified by fluorescence activated cell sorting (FACS) of Lymphocyte antigen 6 complex locus G6D (Ly6G) and CD11b immune cells (neutrophils)[28] (**Figure 1B**), where Ly6G is a marker on the surface of neutrophils and may be used for neutrophil detection and quantification, regardless of the cause for neutrophil increase[29]; CD11b expression of wound tissues is a marker for leukocytes such as monocytes, neutrophils, natural killer cells, granulocytes and macrophages. The negative control group (*i.e.* wound without bacterial infection and without polymer addition) gives a 3.2% activation of $CD11b^+$ and $Ly6G^+$ neutrophils, while the MRSA infection group gives 21% activation of $CD11b^+$ and $Ly6G^+$ neutrophils, suggesting that inflammatory response is caused by bacteria infection. The neutrophils activation were 13 % and 10% for vancomycin and CSM5-K5 respectively, showing statistically insignificant difference between these 2 treatment groups. Comparing CSM5-K5 with the negative control, there was significant activation of neutrophils (*$p<0.1$); however, as compared with infection control mice,

CSM5-K5 treated mice shows lower neutrophils activation suggesting CSM5-K5 reduces inflammation compared with the untreated wound. (negative control is wound without bacterial infection and without polymer addition.)

The *in vitro* cytotoxicity against 3T3 fibroblasts and human red blood cell hemolysis were also measured (**Table S1**); the 3T3 cell viability with 100 μg/mL CSM5-K5 is 83.34% indicating good biocompatibility. The CSM5-K5 copolymer has 10% hemolytic concentration (HC10) above 5000 μg/mL (1hr and 8hr treatment) (**Table S1**) indicating that it is highly non-hemolytic compared to most AMPs[30-31]. The *in vitro* immunomodulatory ability of CSM5-K5 to prevent LPS/LTA-mediated activation of TLR4/TLR2 is proved by measurement of pro-inflammatory cytokines secretion (IL-6, IL-8 and TNF-α)[32] from cultured macrophage cells. We see that LPS and CSM5-K5 both individually induce the secretion of IL-6, IL-8 and TNF-α secretion by the macrophages (Figure 1C). With LPS mixed with CSM5-K5 at 1:1 weight ratio, the cytokines secretions are lower compared with only LPS or CSM5-K5, suggesting that CSM5-K5 nanoparticle can suppress the cytokines secretion caused by LPS, which is a common endotoxin found in bacterial infection.

For studying the importance of having chitosan backbone in the graft copolymer of CSM5-K5, a series of linear poly(L-lysine) (denoted by K10, 20, 30, 40 and 100) were also synthesized via NCA polymerization (**Figure S1B**). However, this series of homopolylysine (PK) without the chitosan backbone shows poor bactericidal activity but has good fibroblast and human red blood cell compatibility (**Table 2**, **Table S1**).

## 2.2. Nanoparticle Formation and Hydrogen Bonding Effect

Using a Dynamic Light Scattering (DLS) setup (where intensity changes with time), we can determine the particle hydrodynamic radius ($R_h$) by first calculating the diffusion coefficient ($D_T$) from the measured slope of decay rate ($\Gamma$) versus wave factor ($q^2$) (Figure 2A) and applying the Stokes-Einstein Equation (1):

$$R_h = \frac{k_B T}{6\pi\eta D_T} \qquad where \qquad D_T = \frac{\Delta\Gamma}{\Delta q^2} \tag{1}$$

($\Gamma$ is reciprocal of time; q is a function of angle and wavelength).

In an aqueous environment with neutral pH, CSM5-K5 copolymers aggregate into nanoparticles with $R_h$ of 36.5±3.5 nm, (**Figure 2A**).

From a Static Light Scattering (SLS) setup (where intensity is measured over a short time) to get the plot of intensity reciprocal ($I^{-1}$) versus wave factor ($q^2$) and applying the Rayleigh-Debye-Zimm formulism[33], the radius of gyration ($R_g$) of CSM5-K5 can be obtained; the Rg of CSM5-K5 is measured to be 42.7±5.6nm. The aggregated molecular weight of CSM5-K5 is measured to be $4.03\times10^5$ g/mol using via a Zimm plot with different polymer concentrations. (The calculation procedure of $R_g$ and $R_h$ follows those of references.[34-35] The Dynamic Light Scattering (DLS) analysis is presented in **Figure S5** and the calculated size distribution is summarized in **Figure S6**). The nanoparticles are in equilibrium with individual polymer chains with $R_h$ smaller than 10 nm. The average radius of the polymer nanoparticle determined by TEM is 27.4 nm (**Figure 2B**), qualitatively corroborating the size distribution determined by light scattering. The dynamic light scattering studies of CSM5-K5 nanoparticle were also done at different fluids to confirm the stability of the nanoparticle (**Table S2**).

From the light scattering study, if the $R_g/R_h$ is greater than 1, we can infer that the polymer forms a Gaussian chain aggregation[34] (**Figure S4**). The CSM5-K5 has a $R_g/R_h$ ratio of 1.17, as well as an average aggregation number of 110 (**Figure S4**, Zimm Plot), indicating that our nanoparticle is probably a Gaussian chain aggregation.[36] As the solution pH value was reduced below 3.5, the aggregates disappeared probably due to increased repulsion of the more protonated CSM5-K5 and then only individual CSM5-K5 polymer chains with $R_h$ of 7.75nm were detected by DLS (**Figure 2A**). In contrast, linear K100 does not aggregate in solution but rather exists as individual polymer chains with hydrodynamic radius ($R_h$) less than 10 nm (**Figure 2A, Table 1**).

The circular dichroism (CD) spectra of CSM5-K5 and linear K100 in DI water were also measured (**Figure S7**). CSM5-K5 exhibits a positive band appearing at 218 nm that resembles that of collagen[37-38] suggesting aggregation of rigid rod-like chitosan backbone which corroborates the particle aggregation

detected by DLS.

Computer simulation was performed to understand the interaction forces causing the CSM5-K5 nanoparticle formation. The simulation shows that pairs of the CSM5-K5 copolymer molecules aggregate in solution because of hydrogen bonding between two –NHC(=O) groups (**Figure 3A1 and A2; Figure S8A**), as well as two –OH groups (**Figure 3A3**). It appears that dimerization maximizes the hydrogen bonding interaction between 2 chitosan backbones and minimizes the energy of unfavorable side chain Kn-Kn contacts (**Figure S8B, C**). The computer simulation corroborates the light scattering observation of nanoparticle formation from CSM5-K5.

CSM5-K5 exists as nanoparticles because of hydrogen bonding between two –NHC(=O), as well as between two –OH groups on two chitosan backbones.

### 2.3. Surface charge and proton sponge effect of CSM5-K5 nanoparticle

pH-potentiometric titration of CSM5-K5 and linear K100 (**Figure S9A**) with pH varying from 12 to 2 were performed to track the protonation process. From the pH-potentiometric titration curve, the degree of protonation (α) can be estimated from the plateau region of the conductivity curve (**Figure S9B**). The apparent dissociation constant ($pK_\alpha$) can also be calculated from the pH-potentiometric curves by the Henderson-Hasselbalch equation (**Figure S9**).

The variation of the apparent dissociation constant ($pK_\alpha$) with the degree of protonation (α) for both CSM5-K5 and K100 is shown in **Figure 2C** and they are quite different. Unlike linear K100, CSM5-K5 is only partially protonated: for example, at neutral pH, the latter is only 46 % protonated (**Figure S9A**). For the linear K100, the apparent $pK_\alpha$ varies linearly with α, suggesting that protonation is a simple one-stage process in which addition of $H^+$ leads to incremental protonation of the amine groups. In contrast, the plot of $pK_\alpha$ against α for CSM5-K5 shows two regions, one (from $pK_\alpha$ of 13 to around 3) at the initial protonation stage in which $pK_\alpha$ decreases rapidly with increasing α, and a second (for $\alpha > 0.6$, pKa<3) regime in which the pKa

change is much slower and the slope of $\Delta pK_\alpha/\Delta\alpha$ becomes much more negative and similar to that of K100 (**Figure 2C**). This suggests that there are two mechanisms of protonation for the graft CSM5-K5 copolymer compared to the linear K100 polymer[39-40]: in the first stage, $H^+$ enters the spaces between the polylysine side chains and in the second stage, protonation of the amine groups on polylysine side chain occurs. At physiological pH (around 7), the CSM5-K5 copolymer aggregates into nanoparticles which can absorb more protons into the interior but when pKa<3, the free protons cause the sharp in the degree of protonation (α) (**Figure 2C**); the absorption of protons by CSM5-K5 which is probably due to the branched cationic copolymer structure makes it behave like a "proton sponge" [39]. Additionally, the surface charges of CSM5-K5 at different pH values were measured in water (**Figure S9C)**; protonation of nanoparticle begins at the basic pH of 9 indicated by a zeta potential of +15mV which increases to +26.5mV as pH decreases to 4 and plateaus off, which is consistent with the pH-potentiometric trend (Figure S9B).

The surface charges of CSM5-K5 and linear K100 in PBS buffer solution (pH=7.4, *i.e.* physiological pH) and DI water at 3 concentrations (1000, 100 and 10 μg/mL) were determined by zeta potential measurements (**Figure 2D and Figure S9D**). In both media, CSM5-K5 copolymer possesses higher zeta potential than K100 (**Figure 2D**), indicating greater surface cationic charge. The zeta potential values, as well as particle size, in PBS with the 2 higher concentrations were quite close to each other (Table S2), suggesting their stabilities under these conditions. The difference in cationic surface charge may be attributable to the aggregated structure of CSM-K5 nanoparticles and to its higher amine concentration density per unit mass. Based on the pH-potentiometric titration, CSM5-K5 has about 2.6 times more amine groups on the polymer backbone than linear K100 (0.121 mole/g versus 0.047 mole/g) (**Figure S9A and Table S3**). Since there are more amines on CSM5-K5 and it tends to aggregate, whereas K100 remains in the form of individual polymer chains, the overall surface charge density of CSM5-K5 nanoparticle is higher.

The "proton sponge" character with "free" protons within the nanoparticles, together with higher cationic zeta potential (a surface charge measure), would favor the interaction of the copolymer with negatively

charged bacteria cell membrane compared to the linear K100 that lacks the "proton sponge" effect[41]. Upon binding with the cytoplasm membrane, the excess protons can increase the local osmotic pressure, eventually leading to membrane rupture[42]. This may be the cause for the higher potency of antimicrobial efficacies of CSM5-K5 versus K100 (**Table S1**).

## 2.4 Hydrogen bonding and electrostatic interaction between CSM5-K5 and bacterial membrane models

To study the interaction of CSM5-K5 with different model membranes, we utilized Isothermal Titration Calorimetry (ITC) (**Figure S10A, B, and C, Table 3**) and Dynamic Light Scattering (DLS) **(Figure S11).** Three kinds of liposome models were prepared (Table 3) to mimic the bacterial outer membrane (OM), bacterial inner membrane (IM), and cytoplasmic membrane of human red blood cells respectively; specifically, the liposomes were composed of POPC(4):LPS(1), POPC(4):POPG(1) and pure POPC[43] respectively. To mimic the OM of Gram-negative bacteria *E. coli* or *P. aeruginosa*, their respective LPS molecules were used.

For both the POPC:LPS and POPC:POPG liposomes, the ITC measurements show that their binding with CSM5-K5 is favorable as the Gibbs energy change is negative (**Table 3)**. (DLS shows increase of the hydrodynamic diameter ($R_h$) of POPC:LPS and POPC:POPG liposomes after CSM5-K5 treatment (**Table S4**), corroborating the ITC results indicating favorable interaction with CSM5-K5.) In contrast, pure POPC liposome (mimicking human red blood cell membrane) titrated with CSM5-K5 shows no change in Gibbs energy from ITC (**Figure S10B iv and C iv**) and no increase in hydrodynamic diameter from light scattering (**Table S4 and Figure S11**), hence no interaction with CSM5-K5 copolymer.

The negative $\Delta H$ value for the bacterial OM and IM liposomes (Table 3, a-c) indicates that the interactions are electrostatic-driven. Also, the lower affinity towards LPS from *P. aeruginosa* indicated by a smaller association constant ($K_A$) suggests a possible explanation for the poorer bactericidal activity against *P. aeruginosa* compared with *E. coli* **(Table 1)**. The electrostatic basis of binding of CSM5-K5 with IM is also consistent with positive zeta potential of CSM5-K5 **(Figure 2D)**.

For the interaction of CSM5-K5 with POPC: LPS of *E. coli* or *P. aeruginosa* **(Table 3, a-b)**, the positive ΔS indicates that the interaction between the bacterial OM and CSM5-K5 is also contributed by entropy increase. The increase in entropy is probably caused by conformational change: expulsion of water molecules at the lipid/water interface into the bulk surrounding water due to hydrogen bonding between saccharide-rich LPS molecules and CSM5-K5.[44-45]

The interactions between CSM5-K5 nanoparticle and the bacterial inner membrane (IM) versus mammalian cell membrane (MM) were also analyzed by computer simulation (see Methods). The CSM5-K5 nanoparticle comprised many copolymer molecules aggregated together but for simplicity, we modelled a dimer of the CSM5-K5 copolymer. Compared with the MM-dimer system, binding in IM-dimer system was stronger (**Figure 3B**) because of the large amount of negatively charged POPG in IM. The computer simulation shows that the binding was driven initially by long-range electrostatic attraction between lysine residues of the CSM5-K5 dimer and the $PO_4^-$ head groups of IM, and further stabilized by H-bonds (also between the lysine of CSM5-K5 and head groups of membranes) when contacts between the dimer and IM were established; the predominant H-bonding interaction is with head groups of lipids, but some could reach deeper to H-bond with carbonyl groups of lipids (**Figure 3C**).

We also compared the effect of different oligomerization forms of CSM5-K5 versus individual homopolylysine (PK) chain on anionic lipid domain formation in the model inner bacterial membranes (*i.e.* a POPC: POPG (4:1) mixture). We investigated 4 bacterial inner membrane(IM)-polycation systems: i) a control without any polymers (IM); ii) IM interacting with two individually dispersed CSM5-K5 copolymers (IM-2mon; where mon stands for monomeric form of CSM5-K5), iii) IM interacting with a dimer comprising 2 of CSM5-K5 chains (IM-dimer); and iv) IM interacting with two individual PK chains (IM-2PK) (**Table S5** and **Figure S12A, B, and C).** Based on the calculated lateral radial distribution function **(Figure 3D)**, we see spikes only in the IM-2mon and IM-dimer systems showing the CSM5-K5 individual chain as well as the CSM5-K5 dimer cause the anionic POPG lipids to be concentrated into domains in these 2 systems compared

with the IM control and IM-2PK systems, indicating that the CSM5-K5 copolymer more favorably induces POPG domain formation than the polylysine molecules. Although the IM-2PK system has 2 positive charge centers, each belonging to one PK chain (**Figure S12B**), which are comparable to that in the IM-2mon system, enrichment of POPG was lower than in the IM-2mon system. This is reasonable since positive charges grafted around the chitosan backbone in the CSM5-K5 have a higher charge density than those involving PK which is linear with charges more spread out. Further, the CSM5-K5 dimer exhibited a stronger propensity to gather POPG into domains (with the highest spike in **Figure 3D**) than two individual CSM-K5 monomers, due to its higher charge density and avoidance of competition between the two copolymer monomers (**Figure S12B**). The much higher clustering of anionic POPG by CSM5-K5 corroborates that it kills bacteria by the carpet model which is consistent to it not having the hydrophobic residues.

### 2.5. Mechanistic studies with membrane assays, confocal microscopy and Cryo-TEM with bacteria

To confirm the mechanism of the penetration of CSM5-K5 or K100 of bacteria cell membrane, membrane assays with *1*-N-phenylnaphthylamine (NPN) and Adenosine Triphosphate (ATP) bioluminescence assay were performed. NPN fluoresces inside a phospholipid bilayer but does not in solution and is used to probe bacterial OM permeabilization. The sharp rise of NPN fluorescence intensity with CSM5-K5 (**Figure 4A**) shows that it effectively permeabilizes the outer membrane (OM) of the Gram-negative *E. coli* K12 and to a limited extent that of *P. aeruginosa* PAO1 (**Figure 4B**) but the linear K100 is ineffective for both bacteria (**Figure 4A, B**). The ATP bioluminescence assays were performed (**Figure 4C, D**) to study the extent of permeabilization into the bacterial inner membrane respectively. The intracellular ATP release test shows that there were only increase of intracellular ATP detected, when both *E. coli* K12 and MRSA BAA-40 were treated with polymer concentration greater than the MIC values (**Table 2**); suggesting the antimicrobial activity of CSM5-K5 nanoparticle is strongly related to cytoplasm membrane interruption. Also, MRSA BAA-40 has a more anionic cytoplasm membrane than *E. coli* and hence also a stronger interaction with CSM5-K5 as this

interaction is dominated by charge interaction (**Table 3**), and proved by stronger ATP release. Our computer simulation shows that CSM5-K5 leads to anionic lipid clustering and this corroborates with the ATP bioluminescence assays which indicates cytoplasm membrane interruption is the main antimicrobial mechanism. Taken together, CSM5-K5 is membrane-active and is more effective than K100 in permeabilizing the OM of *E. coli* and P. aeruginosa and the cytoplasm membrane (IM) of *E. coli* and *S. aureus*.

Super resolution STED microscopy experiment was performed on polymer-treated bacteria. Lissamine rhodamine (Rho) B sulfonyl chloride fluorescent dye was used to label CSM5-K5 copolymer (**Figure S1C**) to study the localization of the copolymer within different strains of bacteria. The MIC of Rho-CSM5-K5 was tested to be similar to pristine CSM5-K5 (**Table S1**). Two Gram-positive bacteria (*E. faecalis* V583 and MRSA BAA-40) and one Gram-negative strain (*E. coli* K12) were incubated for 1 hour with 50 μg/mL of rhodamine-labeled CSM5-K5 (in red) and the plasma membrane was stained using FM1-43FX probe (in green). For the three strains tested, we observed colocalization of the rhodamine-labeled CSM5-K5 with the bacteria membrane as well as internalization of the polymer into the cell cytoplasm (**Figure 5**). The relative degrees of internalization of CSM5-K5 among the three strains correlate well with the relative magnitudes of the MICs (**Table 2**). MRSA BAA-40 showed the best copolymer uptake together with the best MIC of the three tested bacteria, and the copolymer probably enters the disrupted membrane bacteria. Altogether, it is observed that CSM5-K5 copolymer binds to the bacteria membrane and gets internalized into the cytoplasm.

Cryo-TEM was utilized to visualize nanoscale effects of CSM5-K5 copolymer on the IM of Gram-positive MRSA BAA-40 at 1×, 2×, 4× and 8× MICs. Our discussion here is based on 8x MICs which are representative of the images with other concentrations (**Figure S13**). Without treatment, the bacterial cell membrane and cell wall are intact (**Figure 6A**); also, the cell wall is thin and of defined and regular thickness. **Figure 6B** (red circle) shows that after treatment with CSM5-K5, large vesicle-like space formed between cell membrane and cell wall, suggesting the separation of cell membrane from cell wall[46-47]. The vesicle may be caused by permeabilization of cytoplasmic membrane by CSM5-K5, resulting in leakage and accumulation

outside the membrane of low density constituents from the cytoplasm[47]. Also, the damaged cytoplasmic membrane can separate from the cell wall during sample preparation[47]. Membrane ripples were also observed (**Figure 6C Blue circle)**, suggesting cell membrane shrinking from the cell wall, due to leakage of cytoplasm of dead bacteria[46] caused by CSM5-K5.

We also observed that in CSM5-K5 treated MRSA, the cell wall became irregular in thickness and generally thicker; furthermore the septum growth and cell division were inhibited[48] (**Figure 6D Yellow circle**). Further, in untreated cells, we found 17 Cryo-TEM images (out of 57 Cryo-TEM images taken) of cell division whilst in treated cells, we found only 2 cases of cell division (out of 83 Cryo-TEM images taken). We hypothesize that CSM5-K5 may be "mistaken" by bacterial cells to be lipid II as the former is similar in its backbone to the latter and also contains lysine and so it may get incorporated into the cell wall which becomes thicker[49]. It also may bind to glycoltransferase[50]. We postulate that cell division is impeded by CSM5-K5 due to the thicker cell wall; this also has been reported for other systems[51]. Also, the disruption of cytoplasm membrane may interrupt the cell division **(Figure 6D)** which requires invagination of the membrane[52]. Our proposed hypothesis of cell membrane disruption leading to inhibition of cell growth has also been observed with daptomycin which disrupts cytoplasmic membrane; in the cell wall synthesis pathway, the Lipid II needs to bind to the MurJ flippase[52] of Penicillin Binding Protein (PBP) anchored on IM but this process is interrupted by the membrane disruption caused by daptomycin or CSM5-K5 preventing cell wall synthesis and septum formation[53].

## 2.6 Discussions

CSM5-K5 is a unique short cationic peptidopolysaccharide that self-assembles into nanoparticles which effectively kill various Gram-positive and Gram-negative MDR bacteria such as MRSA, VRE and pathogenic *E. coli*. The membrane activity of CSM5-K5 was confirmed by Confocal microscopy and cryo-TEM, as well as NPN membrane assay and ATPase assay with model bacterial membranes.

The CSM5-K5 chains self-assemble into nanoparticles (of around 36.5 nm in hydrodynamics radius) in solutions as shown by DLS and TEM studies. The CSM5-K5 nanoparticles act to concentrate charges and exert the "proton sponge" effect for effective bactericidal effect. Compared with individual CSM5-K5 chains, the aggregated CSM5-K5 nanoparticles more easily lead to clustering and domain formation of the anionic POPG lipids in the IM (that also contains zwitterionic lipids); this effect likely leads to bacterial membrane phase boundary defects and increases membrane leakage[54-55], which could be the first step of experimentally-observed membrane disruption. The nanoparticles, rather than the individual molecules, collectively exert their antibacterial effect mainly through electrostatic interaction between the copolymer lysine side chain and head groups ($PO_4^-$) of bacterial lipids as shown by ITC and simulation results.

The two parts of CSM5-K5, *i.e.* the chitosan backbone and lysine side chain, work together synergistically to achieve effective bactericidal activity: hydrogen bonding due to the chitosan backbone results in aggregation into nanoparticles while the multiple lysine side chain of the aggregated nanoparticle causes bacterial damage through electrostatic interaction. Hence, the good bactericidal activity of CSM5-K5 is due to hydrogen bonding between chitosan chains and electrostatic interaction of lysine side chains with bacteria, and not due to hydrophobic interaction as in most other AMP.

CSM5-K5 copolymer causes the bacteria cell wall to become thicker and cell division is retarded (possibly due to thicker cell wall and membrane disruption). CSM5-K5 also causes separation between cell wall and cytoplasmic membrane of bacteria[56], possibly contributing to the erratic growth of thicker bacteria cell wall, and inhibition of cell division. The peptidoglycan mimic copolymer of CSM5-K5 has backbone structure similar to Lipid II, the peptidoglycan precursor; it may be mistaken for Lipid II and participate in the synthesis route of peptidoglycan cell wall of bacteria[57,49] as an intermediate compound to cause thicker cell wall.

The CSM5-K5 MICs are generally similar or higher than those of other cationic chitosan derivatives or antimicrobial peptides (**Table S6, Table S7**)[25, 58-60] . However, though other cationic antimicrobial polymers or chitosan derivatives have better MICs, they are also usually more cytotoxic to mammalian cells and/or more

hemolytic. Biocompatibility of these other cationic polymers are generally lower due to their constituent hydrophobic components together with cationic charges. With CSM5-K5, the low molecular weight of the single polymer chain is compensated by self-assembly of multiple chains leading to aggregated nanoparticles which are the entities meeting the bacteria to kill them effectively.

The low molecular weight of CSM5-K5 makes its toxicity lower than most other reported cationic chitosan derivatives, albeit its single molecule charge density may be lower [59-62]. For example, Yu et al have demonstrated that high molecular weight (Mw of 38.1kDa) poly(L-lysine-graft-chitosan) (PLL-g-Chi) effectively complexes DNA and possibly acts as a Toll-Like Receptor 9 (TLR9) agonist[63]. Compared with their high molecular weight chitosan, our CSM5-K5 may not act so effectively for the gene transfer. However, the toxicity of the naked PLL-gr-Chi towards mammalian cell may be high because of its high molecular weight.

## 3. Conclusion

Short CSM5-K5 peptidopolysaccharide with only a few (about 5) repeats of chitosan monomer in the backbone can effectively reduce the MRSA bacterial burden in a murine excisional wound model by 4.0 orders of magnitude, and can eradicate clinically important MDR MRSA and Gram-negative *E. coli* and *P. aeruginosa* in *in vitro* studies. CSM5-K5 spontaneously self-assembles in water and the consequent concentration of multiple charged polymer chains in a single nanoparticle causes high localized charge density and enhanced bactericidal activity. Hence, the good bactericidal activity of CSM5-K5 is due to hydrogen bonding between chitosan chains and electrostatic interaction with bacteria, and not due to hydrophobic interaction as in most other AMPs. When complexed with bacterial membrane, these highly charged nanoparticles cluster anionic membrane lipids and result in greater membrane perturbation and antibacterial effect than would be achievable by the same quantity of charge if dispersed in individual copolymer molecules in solution. CSM5-K5 does not rely on membrane insertion for its kill mechanism – indeed its lack of

hydrophobic content makes such insertion energetically unfavorable – and so by design it is intrinsically more biocompatible than agents which are able to insert into lipid bilayers. Due to its concentrated charge, it more strongly interacts with anionic than zwitterionic membrane components and so, by design, more strongly interacts with bacterial membrane than with mammalian membrane.

CSM5-K5 represents a novel approach to rational design of selective peptide-based antimicrobial nanoparticles based totally on hydrogen bonding, rather than hydrophobic interaction, for particle assembly and based on electrostatic interaction without bilayer insertion for membrane perturbation effects. This new approach may accelerate the development of a wide range of next-generation membrane-targeting anti-microbial therapies.

## Experimental Section

### Materials

Low molecular weight chitosan (200 KDa), Nε-benzyloxycarbonyl-L-lysine, triphosgene, ethyl acetate (anhydrous), hexane, phthalic anhydride, triphenylchloromethane, hydrazine solution, hydrochloric acid (37 v/v% in water), hydrogen bromide (33% in acetic acid), *N*,*N*- dimethylformamide (DMF dried on $CaH_2$ and freshly distilled before use), pyridine, trifluoracetic acid (TFA), Lisamine rhodamine B sulfonyl chloride, sodium hydroxide, Lipopolysaccharide (LPS) (extracted from *Pseudomonas aeruginosa* 10 and *Escherichia coli* 0111: B4), and vancomycin HCl salt were purchased from Sigma-Aldrich Corp. 1-palmitoyl-2-oleoyl-sn-glycero-3-phosphocholine (POPC) and palmitoyl-oleoyl phosphatidylglycerol (POPG) were purchased from Avanti Polar Lipid.

Bacteria: *S. aureus* strains ATCC 29213, MRSA BAA-40 and ORSA USA-300, *E. coli* strain ATCC 8739, ATCC 25922 and *P. aeruginosa* PAO1, *Salmonella enterica subsp. enterica* ATCC 13076, and *Vibrio*

*parahaemolyticus* ATCC 17802 were obtained from the ATCC. *E. coli* K12 and *E. coli* W3110 were obtained from laboratory stocks. MRSA 1-7 are clinical strains from Tan Tock Seng Hospital (TTSH); Pan-sensitive strain of *Pseudomonas aeruginosa* (PAES) and Pan-resistant strain of *Pseudomonas aeruginosa* (PAER) were clinical strains from Tan Tock Seng Hospital (TTSH) Singapore. *Enterococcus faecalis* OG1RF, V583, *E. coli* UTI89, EC958, PTR3 were obtained from Singapore Center for Environmental and Life Sciences (SCELSE). Balb/C mice were obtained from InVivos, Singapore.

**Synthesis**

**Synthesis of N-Phthaloyl Chitosan (**Figure S1A): A mixture of chitosan (10 g, 55.86 mmol) and DMF (anhydrous, 200 mL) was bath (preheated at 80 $^{o}$C) sonicated for 1 hour. Then phthalic anhydride (27.6 g, 186.4 mmol) was added into the mixture and heated at 130 $^{o}$C for 24 hours under argon atmosphere. Then mixture was precipitated into distilled water and solid was collected by suction filtration. The solid was washed multiple times with DI water, ethanol, acetone, respectively and dried overnight at 80 $^{o}$C under vacuum. The NMR analysis shows that >96% of chitosan amine groups are phthaloyl-protected. $^{1}$H NMR (300 MHz) (spectrum can be found in Supporting Information Synthesis Scheme S1) DMSO-D6, 25C: $\delta_H$ (ppm) 8-7.5 (m, 5H, phthalic) 5-3.5 (m, overlap, 7H chitosan backbone).

**Synthesis of N-Phthaloyl-*6*-O-triphenylmethyl chitosan (3)**: To a solution of N-phthaloyl chitosan (14 g, 45.27 mmol) in anhydrous pyridine (250 mL) was added triphenylmethyl chloride (41.9 g, 150.3 mmol) at room temperature under argon atmosphere. The solution was heated at 100 $^{o}$C for 24 hours. Then mixture was precipitated into distilled water and solid was collected by suction filtration. The solid was washed multiple times with water, ethanol, acetone, respectively and dried overnight at 80 $^{o}$C under vacuum. $^{1}$H NMR (300MHz) (Spectrum can be found in Supporting Information Synthesis Scheme S2) DMSO-D6, 25C: $\delta_H$ (ppm) 8-7.5 (m, 5H, phthalic) 7.5-6.5 (m, 15H, trityl) 5-3.5 (m, overlap, 7H chitosan backbone). The NMR

analysis shows that >89% of 6-OH groups are trityl protected.

**Synthesis of *6*-O-triphenylmethyl chitosan (4)**: A mixture of N-Phthaloyl-6-O-triphenylmethyl chitosan (10 g) and hydrazine hydrate (200 mL, 50%wt solution) was heated at 100 $^{o}$C for 24 h. The mixture was cooled, diluted with distilled water and suction filtered. The solid product was washed multiple times with water, ethanol and acetone. The derived macroinitiator **4** was re-purified by dissolution in DMF followed by precipitation in diethyl ether to remove traces of trapped hydrazine. The dissolution and precipitation process was repeated two more times. Finally, precipitate was washed multiple times with diethyl ether and dried for overnight at 55 $^{o}$C. $^{1}$H NMR (300MHz) (Spectrum can be found on Supporting Information Synthesis Scheme S3) DMSO-D6, 25C: $\delta_H$ (ppm) 7.5-6.5 (m, 15H, trityl) 5-3.5 (m, overlap, 7H chitosan backbone).

**Synthesis of NCA monomers (5);** The NCA monomer was synthesized by a previously described method[64]. Briefly, a mixture of amino acid (5 g, 17.8 mmol) and anhydrous ethyl acetate (150 mL) in a flask fitted with reflux condenser was heated to reflux under $N_2$ atmosphere. Triphosgene (6 g, 20.2 mmol) was added to the mixture and refluxing continued for next 6 hours. The reaction mixture was then filtered and the filtrate was cooled to -5 $^{o}$C. Separately, de-ionized water and $NaHCO_3$ (0.5% W/V) was chilled to 0 $^{o}$C. The cooled filtrate was transferred to a separation funnel and washed with cooled de-ionized water followed by the cooled $NaHCO_3$ solution. The organic layer containing the partially purified monomers was separated and then dried over $MgSO_4$, filtered and 1/3 evaporated with a rotary evaporator. Then an equal volume of anhydrous hexane was poured into the organic solution. The obtained solid was suction filtered under Ar atmosphere and then vacuum dried overnight. The product yield was 60%. $^{1}$H NMR (300MHz) (Spectrum can be found in Supporting Information Synthesis Scheme S4) $CDCl_3$, 25C: $\delta_H$ (ppm) 7.5-7.1 (m, 5H, benzyl) 5 (s, 2H COC$H_2$O) 4.1(s, 1H, α-H) 3.2-3.1 (s, 2H, C$H_2$NH) 2-1(m, 6H, side chain of lysine).

**Representative Procedure for Synthesis of CSM5-K5 copolymers (6):** The 6-O-triphenylmethyl chitosan

macroinitiator (200 mg, 0.474 mmol) was dried overnight at 80 ºC under vacuum and pre-dissolved in anhydrous DMF (6 mL) before use. Separately, lysine NCA monomer (2.32 g, 7.58 mmol) was dissolved in anhydrous DMF (14 mL) under Ar atmosphere and the 6-O-triphenylmethyl chitosan macroinitiator solution was added immediately. The solution was stirred at room temperature for 3 days. The product was precipitated into diethyl ether, washed multiple times with the same and dried under vacuum at 55 ºC overnight. $^{1}$H NMR (300MHz) (Spectrum can be found on Supporting Information Synthesis Scheme S5) DMSO-D6, 25C: $\delta_H$ (ppm) 7.5-6.5 (m, trityl and benzyl) 5 (m, α-H of polylysine and COC$H_2$O) 4.5-3.5 (m, overlap, 7H chitosan backbone) 2-1 (m, side chain of polylysine).

**Deprotection of CS-Kn(CBz) with conc. HCl (7):** 6-O- triphenylmethyl chitosan-*g*-NCA copolymers (CS-Kn(CBz)) were typically deprotected as follows: To 1.0 g of the powdered copolymer in a round bottom flask, 20 mL conc. HCl (37%) was added under closed system. The mixture was stirred in preheated oil bath at 60 ºC for exactly 100 min, then cooled to room temperature and adjusted to pH 7 with NaOH solution (1M). The obtained solution was dialyzed with cellulose membrane (Spectrum Chemical, M.W. 1000 Da.) for 5 days and then freeze-dried (Figure S1A). $^{1}$H NMR (300 MHz) (Spectrum can be found in Supporting Information Synthesis Scheme S6) $D_2O$, 25C: $\delta_H$ (ppm) 4.2 (m, 1H, α-H of polylysine) 4.0-3.0 (m, overlap, chitosan backbone), 2.5 (m, 2H, C$H_2$$NH_2$), 2-1 (m, 6H, side chain of polylysine).

**Synthesis of Lisamine Rhodamine B dye attached CSM5-K5 (12):** To a solution of CSM5-K5 (20 mg) in 0.1 M sodium carbonate/bicarbonate buffer (4 mL, pH 9.0) (5 mg/mL) was added Lisamine Rhodamine B sulfonyl chloride (200 µL, 1 mg/mL in DMF) solution under dark conditions. The solution was stirred at room temperature for 1 h and dialyzed with cellulose membrane (Spectrum Chemical, M.W. 1000 Da.) for 2 days and then freeze-dried (Figure S1C).

**Gel Permeation Chromatography (GPC) study of molecular weight:** The molecular weight of protected

product 4 was measured with an Agilent PolarGel column using HPLC grade dimethylformamide (DMF) with 1mg/mL LiBr as effluent. The molecular weight of deprotected product 5 was determined by water phase GPC using a Waters Ultrahydrogel column with acidic buffer (0.5M Sodium acetate and 0.5M Acetic acid, with pH=4.5) as eluent.

**Preparation of Liposome models:** Combinations of the lipids 1-palmitoyl-2-oleoyl-sn- glycero-3-phosphocholine (POPC), palmitoyloleoyl phosphatidylglycerol (POPG) and Lipopolysaccharide (LPS) were used to model the cell membranes of different types of cells. Mammalian cell membrane from mammalian cell was modeled as pure POPC lipid bilayer. The outer cell membrane of Gram-negative bacteria was modeled by a mixture of POPC and LPS with mass ratio 4:1. The plasma membrane of Gram-positive bacteria was modeled by a mixture of POPC with POPG with mass ratio 4:1.

Typically, the liposomes were prepared at a scale of 10 mg. 10 mg of lipid was dissolved in methanol/chloroform (v/v=3:1). The solution was then evaporated. The residue was re-suspended in 1mL of 10 mM potassium phosphate buffer solution. The suspension was sonicated for 2 hrs for more even dispersion in the buffer. After sonication, the suspension was frozen in liquid nitrogen and thawed in 40 $^{o}$C water. The freeze-thaw process was performed repeatedly for a total of 5 cycles include the first cycle. The suspension was filtered 10 times using 200 nm polycarbonate membrane. The prepared liposome suspension was stored at 4 $^{o}$C prior to use in various tests. For light scattering measurements, the suspension was diluted 100-fold.

**Light Scattering study of polymer aggregation:** The Light Scattering study of polymer aggregation and interaction with liposomes were performed with a BI-200SM light scattering system (Brookhaven Instruments).

For study of polymer aggregation, 1 mg of polymer was dissolved in 1 mL of DI water and filtered against

0.45 μm PES filter. The Radius of Gyration ($R_g$) and Zimm plot were measured using Static Light Scattering with scattering angles from 30 to 90 degrees. The hydrodynamic radius ($R_h$) was calculated based on Dynamic Light Scattering (DLS) measurements at 30, 45, 60, 75, 90, 105, 120, 135, and 150 degree scattering angles. The method of mathematical analysis of autocorrelation function based on light scattering follows the protocol published by Schillen *et al*[65] using the GENDIST package (Figure S4, Figure S5).

**Light Scattering study of polymer binding with model liposomes:** Liposome suspensions were prepared as previously described. 100 μg/mL of polymer solution was mixed with liposome suspension (mass ratio of polymer: lipid=1:1) and after standing for 20 min to allow the mixture to stabilize, Dynamic Light Scattering measurements were performed.

**pH-potentiometric titration:** pH titration was performed according to a published procedure[66] with modification. A polymer solution of 5 mM actual amine repeat unit in the polymer was prepared in 0.01M NaOH solution (with pH=12). 15 mL of the prepared solution was titrated with 10 μL droplets of 0.1M HCl until pH reached 2. The pH potentiometer used was a 809 Titrando, Metrohm. The pH and conductivity of the solution in the beaker changed with addition of HCl and was plotted. The calculations based on pH-potentiometric titration curve are presented in Figure S9.

**Circular Dichroism Measurement:** Far-UV Circular Dichroism measurements were done over the wavelength range 190 nm to 260 nm at 298.13K in DI water solution, with 0.4 mM concentration based on amine unit using Chirascan CD spectrometer from Applied photophysics.

**Surface charge characterization of nanoparticle:** The surface charge of nanoparticle was characterized in DI water as well as PBS buffer, which provides a constant pH environment (pH=7.4, physiological pH) using

a Malvern Nano ZS sizer.

**Isothermal Titration Calorimetry**

Isothermal titrations were performed using PEAQ-ITC from MicroCal Malvern. Polymer and liposomes were dispersed in MES buffer at pH=6.5. The background Gibbs energy change is firstly tested using 2 μL of polymer solution titrated against MES buffer (Figure S10A). 2 μL aliquots of polymer solutions were added via syringe to 270 μL liposome solution in the cell at 150s intervals with 750 rpm stirring speed. Nineteen injections were performed in each experiment. The temperature was held at 37 $^{o}$C with reference power set at 10 μcal/s. The concentrations of polymer and lipid were adjustable parameters. Thermodynamic parameters were determined from the Gibbs free energy equation:

$$\Delta G = \Delta H - T\Delta S = -RT\ln K_D$$

Where ΔG is Gibbs free energy for binding, ΔH is enthalpy change of binding, ΔS is entropy change of binding. $K_D$ is the association constant.

**ATP bioluminescence assay of cytoplasm membrane interruption**

The overnight culture of *E. coli* K12 and MRSA BAA-40 were firstly prepared by picking a few colonies from bacteria streaked plate into 10mL of fresh MHB broth. The MHB broth were incubated overnight at 37oC, 200rpm in an incubator. The subculture was prepared by diluting overnight culture to 0.01 in fresh MHB media and grown until OD600 of 0.2 reached. Bacteria were washed at 3800rpm for 10mins and resuspend the bacteria pellet with fresh MHB and adjust the starting OD of bacteria inoculum, OD600: 0.2 (108cfu/mL). Aliquot 200uL of bacteria suspension into each well of 96-well flat bottom clear plate incubated with corresponding antibiotics. After 1hour of incubation, transfer 50uL of bacteria suspension into each well of 96-well black clear bottom plate. Add 50uL of Luciferase reagent and take the luminescence readings immediately at 135 gains.

**Outer cytoplasmic membrane depolarization**

The outer cytoplasmic membrane depolarization activity of polymer was determined using the membrane potential-sensitive fluorescent dye 1-N-Phenylnaphthylamine (NPN). *E.coli* K12 and *P. aeruginosa* O1 bacteria were harvested at mid-log phase and washed three times with HEPES buffer (5 mM HEPES, pH 7.4). The bacteria were resuspended to an O.D 600 of 0.2 in HEPES buffer. Subsequently the bacterial suspensions were diluted to $10^6$ CFU/mL by HEPES buffer and incubated with NPN (20 nM). Fluorescence was recorded for subtraction with Perkin Elmer LS-55 luminescence spectrometer (excitation $\lambda = 350$ nm, emission $\lambda = 420$ nm, high stirring speed), then polymers were added at a concentration of 100 μg/mL, and the fluorescence was recorded. Polymyxin B with same concentration as polymer (100 μg/mL) is used as positive control.

**Stimulated emission depletion microscopy (STED)**

To prepare samples for super resolution STED microscopy, bacteria from logarithmic phase cultures were pelleted by centrifugation at 3,000 X *g* for 10 min, suspended in culture media at a concentration of $10^8$ CFU $mL^{-1}$ and incubated for 1 h in darkness with the rhodamine-labeled copolymer (CSM5-K5). Membrane stain FM1-43FX (5 μg/mL; Life Technologies) was added to the samples for 5 min, as suggested by the manufacturer, before washing the bacteria three times with PBS and resuspending in a fixative solution of 2% paraformaldehyde in PBS [pH 7.0]. Bacteria were fixed for 2 h at room temperature, washed three times in PBS and applied to a sterile glass bottom collagen coated dish (MatTek Corporation). STED super resolution microscopy was performed on a Leica TCSM SP8 STED-3X (Leica Microsystems, Wetzlar, Germany) at SingHealth Advanced Bioimaging Core. Further image processing required deconvolution, which was done using Huygens Professional software (Scientific Volume Imaging, Hilversum, Netherlands). ImageJ was utilized for further image processing.

**Cryo-Electron Microscopy**

To prepare samples for super resolution Cryo-Electron microscopy, bacteria from logarithmic phase cultures were pelleted by centrifugation at 3,000 X *g* for 10 min, washed by PBS for 3 times and diluted to concentration of $10^8$ CFU $mL^{-1}$. The bacteria were then incubated with polymer at concentration of specific concentrations of polymer (times of MIC value) in PBS at 37˚C for 3 hours.

A 4 μL prepared bacteria culture was applied on a Quatafoil 2/2 grids and plunged frozen into liquid ethane at liquid nitrogen temperature using a Vitrobot Mark IV (FEI Company, USA/Netherland). The grids were imaged at liquid nitrogen temperature with a nominal magnification of 18000X on a 300 kV Titan Krios transmission electron microscope (FEI Company, USA/Netherland), equipped with a Falcon II electron detector (FEI Company, USA/Netherland). The pixel size of final image is 4.6 angstrom.

**Anti-microbial activity assay**

**Microbial Strains, culture medium and inoculums preparation:** The test microorganism strains selected to evaluate the antibacterial activity of cationic polymers were both Gram-negative and Gram-positive species which obtained from ATCC. Gram-negative species which involved in this study were *Escherichia coli* (ATCC 8739), *Pseudomonas aeruginosa* (PA01), *Pseudomonas aeruginosa* (ATCC 27853), and Gram-positive species were *Staphylococcus aureus* (ATCC 29213), *MRSA* (ATCC BAA 40) and *Enterococuss faecalis* (ATCC 29212). The mid log phase (4hr) microbial cell suspension was mixed to homogeneity and the optical density (OD) was measured to give a final density of $10^5$ CFU/ml in the test plate and these were confirmed by viable counts (Colony Forming Units, CFU/ml).

**Determination of Minimum Inhibitory Concentration (MIC):** The MICs values of the cationic polymers against the test microorganism were determined by broth microdilution method using 96-well microtiter plates as recommended by (CLSI, 2011) with slight modification. The MHB broth was placed into 96-well plate and the stock solutions were serially diluted and the bacterial cultures were added sequentially into the each well. The final concentrations of the polymers into the test plate were ranging from 512 ug/ml to 1 ug/ml and the

microplate were aerobically incubated at 37 °C for 24 hr. The well with inoculums and without test polymers serves as controls. The bacterial growth was examined by measuring the optical density at a wavelength of 600nm (TECAN, infinite F200) as well as visual examination of turbidity. This MIC values are defining as the lowest concentration that showed no growth or non-turbid and which kills the bacterial growth by more than 90%. The entire test was carried out in triplicate.

**Cytotoxicity assay**

**a) Mammalian Cell Biocompatibility test via MTT cell proliferation assay;** The mammalian cell biocompatibility test was done according to the published protocol using 3T3 cells. In a 96-well plate, 3T3 cells were co-cultured for 24 h at 37 ºC with polymer (100 µg/mL and 200 µg/mL) at initial cell density of $1\times10^5$ cells per well. At the end of the incubation period the culture medium was removed, each well was washed with PBS followed by addition of MTT solution, and the plate was incubated for 4 h at 37 ºC. The MTT medium was then removed, 100 µL of DMSO was added to each well, the plate was shaken at 100 rpm for 15 mins and the absorbance at 570 nm was measured with plated reader (BIO-RAD Benchmark Plus, US).

**b) Hemolytic activity test;** Fresh human blood was collected from a healthy donor (age 23, Male). 1 mL blood was mixed with 9 mL Tris buffer (10 mM Tris, 150 mM NaCl, pH 7.2) and centrifuged at 1000 rpm for 5 min. The red blood cell (RBC) pellet was collected and subsequently washed with Tris buffer three times and diluted to a final concentration of 5% v/v. 50 µL of antimicrobial solution at different concentrations mixed with 50 µL red blood cell stock were added to a 96-well microplate and incubated for 1 hr or 8hr at 37 ℃ with 150 rpm shaking. The microplate was centrifuged at 1,000 rpm for 10 min. 80 mL aliquots of the supernatant were then transferred to a new 96-well microplate and diluted with another 80 mL of Tris buffer. Hemolytic activity was determined by absorbance measured at 540 nm with a 96-well plate spectrophotometer (Benchmark Plus, BIO-RAD). Triton X-100 (0.1% in Tris buffer) which is able to lyse RBCSM completely

was used as positive control, while Tris buffer was used as negative control. The hemolysis percentage (H) was calculated from the following equation:

$$hemolysis\% = \frac{[(O_p - O_b)]}{[(O_t - O_b)]} \times 100\%$$

where $O_p$ is the absorbance for the antimicrobial agent, $O_b$ is the absorbance for the negative control (Tris buffer), and $O_t$ is the absorbance for the positive control of Triton X-100.

**b) *In vitro* cytokine release assay**

The *in vitro* cytokine release studies were carried out with acute monocytic leukemia cells THP-1 (ATCC TIB-202). Cell culture media used were RPMI-1640 with 10% fetal bovine serum (FBS) and 0.05 mM 2-mercaptoethanol. THP-1 cells were cultured in 96-well plates with cell density of $1 \times 10^4$ cells in each well, and addition of 100 ng/mL 12-O-tetradecanoylphorbol-13-acetate (TPA) and incubated in a $CO_2$ incubator at 37 °C for 24 h for differentiation into macrophages and cell attachment. The cells were then washed with phosphate buffered saline (PBS) once and the different samples were added into each well and further incubated for 24 h. LPS at 100ng/mL is used as positive control to trigger the expression of cytokines. After incubation, the culture media from each well were retrieved and centrifuged to remove floating cells and debris and aliquots of 100 µL were used for the cytokines (IL-6, IL-8 and TNF-α) release assay tested by Eve technologies, Canada.

**Animal Test**:

**Murine excisional wound model**

Bacterial cultures of *S. aureus* BAA40 were prepared and used to infect 8-week-old female BALB/c mice (InVivos Pte Ltd.). Wound were prepared as previously described[67] with minor modifications. Mice were anesthetized by inhalation of 3% isoflurane followed by wound preparation. Mice were shaved, skin sterilized

by 70% ethanol swabbing, and an excisional wound punctured with a single 6 mm diameter biopsy through the skin. 2.5 µL of bacterial cultures ($1\times10^3$CFU/wound) were administered to the wound site, and then 2.5 µL of treatment solutions were applied after 4 hours of wound infection. The wound site was sealed using Tegaderm TM dressing (3M, St Paul Minnesota, USA). Mice euthanization at indicated time points (24hrs) was achieved by $CO_2$ asphyxiation followed by cervical dislocation. Wound sites were excised and the bacteria present in the wound were determined by homogenization and colony forming unity plating of serially diluted samples to selective media. Statistical significance was determined by the Mann-Whitney test with Dunn's post-test for multiple comparisons using Prism (GraphPad) software. Recovered titres of zero were set to the limit of detection for statistical analysis and graphical representation. All studies and protocols were approved by the Nanyang Technological University Institutional Care and Use Committee (NTU IACUC).

**Fluorescence-activated cell sorting (FACS)**: Single cell suspensions from wound samples were obtained using MACSM Dissociator (Miltenyi Biotec). The digested tissue solution was gently filtered through a 40 µm nylon filter cup by gravity. The single cell suspension was pelleted. The cell pellet was resuspended, transferred to a 1.5 mL microfuge tube and blocked in 1 mL of 3% BSA (in PBS) on ice for 30 minutes. Cells were then probed with the fluorescence-labelled antibodies against CD11b and Ly6G (Miltenyi Biotec) in the dark for 30 minutes on ice, followed by washing using PBS buffer. The washed pellet was then re-suspended in 300 µL of PBS for flow cytometry using Accuri C6 flow cytometer (BD Biosciences). Data was analyzed using Flowjo software version 7.6.5.

**Computational Simulation**

**a) Well-tempered meta-dynamics simulation[68] of chitosan-*graft*-oligolysine**: Well-tempered meta-dynamics simulation of two chains of CSM5-K5 copolymer was performed in NPT ensemble to investigate the self-assembly mechanism. Deacetylation degree of chitosan in experiment is 80%; thus the simulation

model of CSM5-K5 contains one chitosan chain with the length of 5-sugar-unit, and four oligolysine chains, whose length is 1, 2, 1, and 1 respectively and are grafted on the amino groups of the sugar units. Protonation degree of lysine was set as 100% so altogether there are 9 positive charges in each molecule. We finished 400 ns meta-dynamics simulation with the help of PLUMED 2.1.3[69]. The system temperature was maintained at 300 K by V-rescale temperature coupling method and pressure maintained at 1 bar by Parrinello-Rahman pressure coupling method. Force field parameters Glycam_06j[70] and AMBER99SB[71] were employed to characterize the chitosan and polylysine parts, respectively. Distance and angle between two molecules were defined as two collective variables (CV) for the free energy calculation. Gaussian height was set to 2 kJ/mol and Gaussian widths for distance and angle were set to 0.1 nm and 0.05 rad respectively. Gaussian potential was deposited every 500 calculation steps (1 ps). A constrained potential was added on distance CV to limit the size of CV space and enhance the simulation efficiency. Bias factor used in the simulation was 8 (More parameters could be found in Supporting Information).

**b) Interaction between polycations and membrane:** Two kinds of membrane were constructed in our simulation. Mammalian cell membrane was mimicked by zwitterionic POPC. Each leaflet of the mammalian cell membrane was composed of 81 POPC molecules. Bacterial inner membrane was modelled by a mixture of zwitterionic POPC and negatively charged POPG with a ratio of 4:1. Each leaflet of the bacterial inner membrane was composed of 65 POPC and 16 POPG molecules. The membrane models were built by a web server MemBuilder II and parameterized with a Slipid/AMBER force field published by Jambeck and Lyubertsev [72-73].

Six different systems were simulated for 200 ns: a) pure mammalian membrane (MM); b) mammalian membrane and two aggregated CSM5-K5 molecules (MM-dimer); c) pure bacterial inner membrane (IM); d) bacterial inner membrane and two aggregated CSM5-K5 molecules (IM-dimer); e) bacterial inner membrane and two separated CSM5-K5 molecules (IM-2mon); f) bacterial membrane and two polylysine (PK) chains with nine residues each (IM-2PK). These simulations were also performed in NPT ensemble at 300 K and 1

bar and a Nose-Hoover temperature coupling method and a semi-isotropic Parrinello-Rahman pressure d coupling method were exerted. In systems b, d, e, and f, all membrane models were equilibrated for 200 ns before they were simulated with polycations and all polycations were placed above center of mass of membrane with a distance of 5 nm.

**Supporting Information**: Supplementary synthesis scheme, equations, NMR spectra, summary of biological activity for all the synthesized polymers as well as published antimicrobial peptides, GPC and MALDI-TOF spectra, calculations based on light scattering and pH-potentiometric titration, energy profile of Isothermal Titration Calorimetry and Computational Simulation procedures. This material is available free of charge via the internet at http://pubs.acs.org/.

## Notes

The authors declare no competing financial interests.

## ORCID

Feiqing Ding: 0000-0002-0211-7101

Scott A. Rice: 0000-0002-9486-2343

Hongwei Duan: 0000-0003-2841-3344

Xue-Wei Liu: 0000-0002-8327-6664

Kam (Michael) Chiu Tam: 0000-0002-7603-5635

Kevin Pethe: 0000-0003-0916-8873

Mary B Chan-Park: 0000-0003-3761-7517

## Acknowledgement

We thank the funding support from a Singapore Ministry of Education Academic Research Fund Tier 3 (MOE2013-T3-1-002) and a Singapore Ministry of Health Industry Alignment Fund (NMRC/MOHIAFCAT2/0 03/2014). Zheng Hou and Yang Liu acknowledge the support of Nanyang Technological University through PhD Research Scholarships. We acknowledge the assistance of Alex Li and Sheethal Reghu in the animal study and MIC testing.

## References

(1) Hughes, D.; Andersson, D. Evolutionary Consequences of Drug Resistance: Shared Principles Across Diverse Targets and Organisms. *Nature Reviews Genetics* **2015,** *16*, 459-471.

(2) Dever, L.; Dermody, T. Mechanisms of Bacterial Resistance to Antibiotics. *Archives of Internal Medicine* **1991,** *151* (5), 886-895.

(3) Kim, B. Antimicrobial Peptides: Pore Formers or Metabolic Inhibitors in Bacteria? *Nature Reviews Microbiology* **2005,** *3* (3), 238-250.

(4) Afacan, N.; Yeung, A.; Pena, O.; Hancock, R. Therapeutic Potential of Host Defense Peptides in Antibiotic-resistant Infections. *Current Pharmaceutical Design* **2012,** *18*, 807-819.

(5) Fox, J. Antimicrobial Peptides Stage a Comeback: Better Understanding of the Mechanisms of Action, Modification and Synthesis of Antimicrobial Peptides is Reigniting Commercial Development. *Nature Biotechnology* **2013,** *31* (12), 379-382.

(6) He, Y.; Lazaridis, T. Activity Determinants of Helical Antimicrobial Peptides: A Large-Scale Computational Study. *PLOS one* **2013,** *8* (6), 66440.

(7) Epand, R.; Walker, C.; Epand, R.; Nathan, M. Molecular Mechanisms of Membrane Targeting Antibiotics. *Biochim. Biophys. Acta-Biomembr.* **2016,** *1858* (5), 980-987, DOI: 10.1016/j.bbamem.2015.10.018.

(8) Epand, R.; Epand, R. Bacterial Membrane Lipids in the Action of Antimicrobial Agents. *J. Pept. Sci.* **2011,** *17* (5), 298-305, DOI: 10.1002/psc.1319.

(9) Sahariah, P.; Gaware, V.; Lieder, R.; Jónsdóttir, S.; Hjalmarsdottir, M.; Sigurjonsson, O.; Másson, M. The Effect of Substituent, Degree of Acetylation and Positioning of the Cationic Charge on the Antibacterial Activity of Quaternary Chitosan Derivatives. *Mar. Drugs* **2014,** *12* (8), 4635-4658, DOI: 10.3390/md12084635.

(10) Li, P.; Poon, Y.-F.; Li, W.; Zhu, H.-Y.; Yeap, S.-H.; Cao, Y.; Qi, X.; Zhou, C.; Lamrani, M.; Beuerman, R.; Kang, E.-T.; Mu, Y.; Li, C.-M.; Chang, M.; Su, S.; Chan-Park, M. B. A Polycationic Antimicrobial and Biocompatible Hydrogel with Microbe Membrane Suctioning Ability. *Nature Material* **2011,** *10* (2), 149-56, DOI: 10.1038/nmat2915.

(11) Sajomsang, W.; Tantayanon, S.; Tangpasuthadol, V.; Daly, W. Quaternization of N-aryl Chitosan Derivatives: Synthesis, Characterization, and Antibacterial Activity. *Carbohydrate Research* **2009,** *344*, 2502–2511.

(12) Vinová, J.; Vavíková, E. Chitosan Derivatives with Antimicrobial, Antitumour and Antioxidant Activities-a Review. *Current Pharmaceutical Design* **2011,** *17*, 3596-3607.

(13) Guo, A.; Wang, F.; Lin, W.; Xu, X.; Tang, T.; Shen, Y.; Guo, S. Evaluation of Antibacterial Activity of N-phosphonium Chitosan as a Novel Polymeric Antibacterial Agent. *Int. J. Biol. Macromol.* **2014,** *67*, 163-171, DOI: 10.1016/j.ijbiomac.2014.03.024.

(14) Dragostin, O.; Samal, S.; Dashc, M.; Lupascu, F.; Pânzariu, A.; Tuchilus, C.; Ghetu, N.; Danciu, M.; Dubruel, P.; Pieptu, D.; Vasile, C.; Tatia, R.; Profire, L. New Antimicrobial Chitosan Derivatives For Wound Dressing Applications. *Carbohydr. Polym.* **2016,** *141*, 28-40, DOI: 10.1016/j.carbpol.2015.12.078.

(15) Sahariah, P.; Sørensen, K. K.; Hjalmarsdottir, M.; Sigurjonsson, O.; Jensen, K.; Masson, M.; Thygesen, M. Antimicrobial Peptide Shows Enhanced Activity and Reduced Toxicity upon Grafting to Chitosan Polymers. *Chemistry Communications* **2015**.

(16) Su, Y.; Tian, L.; Yu, M.; Gao, Q.; Wang, D.; Xi, Y.; Yang, P.; Lei, **B.**; Ma, P.; Li, P. Cationic Peptidopolysaccharides Synthesized by 'Click' Chemistry with Enhanced Broad-spectrum Antimicrobial Activities. *Polymer Chemistry* **2017,** *8* (25), 3788-3800.
(17) Li, P.; Zhou, C.; Rayatpisheh, S.; Ye, K.; Poon, Y.-F.; Hammond, P.; Duan, H.; Chan-Park, M. B. Cationic Peptidopolysaccharides Show Excellent Broad-Spectrum Antimicrobial Activities and High Selectivity. *Adv Mater* **2012,** *24* (30), 4130-4137, DOI: 10.1002/adma.201104186.
(18) Liu, L.; Xu, K.; Wang, H.; Tan, J.; Fan, W.; Venkatraman, S.; Li, L.; Yang, Y.-Y. Self-assembled Cationic Peptide Nanoparticles as an Efficient Antimicrobial Agent. *Nature Nanotechnology* **2009,** *4*, 457-463.
(19) Andreu, D.; Rivas, L. Animal Antimicrobial Peptides: An Overview. *Biopolymers* **1998,** *47*, 415-433.
(20) Hancock, R.; Sahl, H.-G. Antimicrobial and Host-defense Peptides as New Anti-infective Therapeutic Strategies. *Nature Biotechnology* **2006,** *24*, 1551-1557.
(21) Schneider, T.; Gries, K.; Josten, M.; Wiedemann, I.; Pelzer, S.; Labischinski, H.; Sahl, H. The Lipopeptide Antibiotic Friulimicin B Inhibits Cell Wall Biosynthesis through Complex Formation with Bactoprenol Phosphate. *Antimicrobial agents and chemotherapy* **2009,** *53* (4), 1610-1618.
(22) Makovitzki, A.; Avrahami, D.; Shai, Y. Ultrashort Antibacterial and Antifungal Lipopeptides. *Proceedings of the National Academy of Sciences of the United States of America* **2006,** *103* (43), 15997-6002, DOI: 10.1073/pnas.0606129103.
(23) Franca, E.; Lins, R.; Freitas, L.; Straatsma, T., P;. Characterization of Chitin and Chitosan Molecular Structure in Aqueous Solution. *Journal of chemical theory and computation* **2008,** *4* (12).
(24) Beyth, N.; Houri-Haddad, Y.; Domb, A.; Khan, W.; Hazan, R. Alternative Antimicrobial Approach: Nano-Antimicrobial Materials. *Evidence - Based Complementary and Alternative Medicine* **2015,** *2015*.
(25) Sader, H.; Fedler, K.; Rennie, R.; Stevens, S.; Jones, R. Omiganan Pentahydrochloride (MBI 226), a Topical 12-Amino-Acid Cationic Peptide: Spectrum of Antimicrobial Activity and Measurements of Bactericidal Activity. *Antimicrobial agents and chemotherapy* **2004,** *48* (8), 3112–3118.
(26) Gottler, L.; Ramamoorthy, A. Structure, Membrane Orientation, Mechanism, and Function of Pexiganan-A Highly Potent Antimicrobial Peptide Designed from Magainin. *Biochimica et Biophysica Acta* **2009,** *1788* (8), 1680-1686.
(27) Mygind, P. H.; Fischer, R. L.; Schnorr, K. M.; Hansen, M. T.; Sönksen, C. P.; Ludvigsen, S.; Raventós, D.; Buskov, S.; Christensen, B.; De Maria, L.; Taboureau, O.; Yaver, D.; Elvig-Jørgensen, S. G.; Sørensen, M. V.; Christensen, B. E.; Kjærulff, S.; Frimodt-Moller, N.; Lehrer, R. I.; Zasloff, M.; Kristensen, H.-H. Plectasin is a Peptide Antibiotic with Therapeutic Potential from a Saprophytic Fungus. *Nature* **2005,** *437* (7061), 975-980, DOI: 10.1038/nature04051.
(28) Liyanage, S.; Gardner, P.; Ribeiro, J.; Cristante, E.; Sampson, R.; Luhmann, U.; Ali, R.; Bainbridge, J. Flow Cytometric Analysis of Inflammatory and Resident Myeloid Populations in Mouse Oular Inflammatory Models. *Methods in eye research* **2016,** *151*, 160-170.
(29) Jun, J.-I.; Kim, K.-H.; Lau, L. The Matricellular Protein CCN1 Mediates Neutrophil Efferocytosis in Cutaneous Wound Healing. *Nature Communication* **2015,** *6*.
(30) Won, H.-S.; Kang, S.-J.; Choi, W.-S.; Lee, B.-J. Activity Optimization of an Undecapeptide Analogue Derived from a Frog-Skin Antimicrobial Peptide. *Molecules and Cells* **2011,** *31*, 49-54.
(31) Radzishevsky, I.; Rotem, S.; Bourdetsky, D.; Navon-Venezia, S.; Carmeli, Y.; Mor, A. Improved Antimicrobial Peptides Based on Acyl-lysine Oligomers. *Nature Biotechnology* **2007,** *25* (6), 657-659.
(32) Duque, G.; Descoteaux, A. Macrophage cytokines: involvement in immunity and infectious diseases. *Frontiers in immunology* **2014,** *5*, 1-12.
(33) Cao, A. Light Scattering. Recent Applications. *Analytical Letters* **2003,** *36* (15), 3185-3225.
(34) Baysal, B.; Karadag, C. Quasielastic Light Scattering Studies of Polypeptides: Evidence for Chain Extension in Solution. *Turkish Journal of Chemistry* **2013,** *37* (4), 480-491.
(35) Skorik, Y.; Petrova, V.; Okatova, O.; Strelina, I.; Gasilova, E. Characterization of Clusters and Unimers in Associating Solutions of Chitosan by Dynamic and Static Light Scattering. *Macromolecular Chemistry and Physics* **2016,** *217* (14), 1636-1644
(36) Lal, M.; Lillford, P.; Naik, V.; Prakash, V. Supramolecular and Colloidal Structures in Biomaterials and Biosubstrates. **2000**.
(37) Greenfield, N. Analysis of The Kinetics of Folding of Proteins and Peptides Using Circular Dichroism. *Nature Protocols* **2007,** *1* (6), 2891-2899.

(38) Liu, X.; Dan, W.; Ju, H.; Dan, N.; Gong, J. Preparation and Evaluation of a Novel pADM-derived Micro- and Nano-electrospun Collagen Membrane. *RSC Advances* **2015,** *5* (64), 52079-52087
(39) Borkovec, M.; Koper, G. Proton Binding Characteristics of Branched Polyelectrolytes. *Macromolecules* **1997,** *30* (7), 2151.
(40) Farris, S.; Mora, L.; Capretti, G.; Piergiovanni, L. Charge Density Quantification of Polyelectrolyte Polysaccharides by Conductometric Titration: An Analytical Chemistry Experiment. *Journal of Chemical Education* **2012,** *89* (1), 121-124
(41) Wu, C.; Hao, J.; Deng, X.; Liu, Y. Random Branched Poly(hydroxyetheramine): a Novel Polycation with Proton Sponge Effect and High Density of Discrete Charge. *Polymer Bulletin* **2008,** *60*, 635–645.
(42) Akinc, A.; Thomas, M.; Klibanov, A., M.; Langer, R., ;. Exploring Polyethylenimine-Mediated DNA Transfection and the Proton Sponge Hypothesis. *The Journal of gene medicine* **2005,** *7*, 657-663.
(43) Hovakeemian, S.; Liu, R.; Gellman, S.; Heerklotz, H. Correlating Antimicrobial Activity and Model Membrane Leakage Induced by Nylon-3 Polymers and Detergents. *Soft Matter* **2015,** *11*, 6840.
(44) Tian, J.; Sethi, A.; Swanson, B.; Goldstein, B.; Gnanakaran, S. Taste of Sugar at the Membrane: Thermodynamics and Kinetics of the Interaction of a Disaccharide with Lipid Bilayers. *Biophysical Journal* **2013,** *104*, 622-632.
(45) Bronowska, A. Thermodynamics of Ligand-Protein Interactions: Implications for Molecular Design. **2011**, 1-41.
(46) Richter, G. W.; Kress, Y. Electron Microscopy of a Strain of Bordetella Bronchiseptica. *Journal of Bacteriology* **1967,** *94* (4), 1216.
(47) Matias, V.; Beveridge, T. Native Cell Wall Organization Shown by Cryo-Electron Microscopy Confirms the Existence of a Periplasmic Space in Staphylococcus aureus. *Journal of bacteriology* **2006,** *188* (3), 1011-1021.
(48) Zuber, B.; Haenni, M.; Ribeiro, T.; Minnig, K.; Lopes, F.; Moreillon, P.; Dubochet, J. Granular Layer in the Periplasmic Space of Gram-Positive Bacteria and Fine Structures of Enterococcus gallinarum and Streptococcus gordonii Septa Revealed by Cryo-Electron Microscopy of Vitreous Sections. *Journal of Bacteriology* **2006,** *188* (18), 6652–6660.
(49) Wang, A.; Lupoli, T.; Sumida, Y.; Tsukamoto, H.; Wu, Y.; Rebets, Y.; Kahne, D.; Walker, S. Primer Preactivation of Peptidoglycan Polymerases. *Journal of the American Chemical Society* **2011,** *133* (22), 8528-8530
(50) Egan, A.; Biboy, J.; Veer, I.; Breukink, E.; Vollmer, W. Activities and Regulation of Peptidoglycan Synthases. *Philosophical Transactions of Royal Society Biological sciences* **2015,** *370* (1679), 20150031
(51) Misra, G.; Rojas, E.; Gopinathan, A.; Huang, K. Mechanical Consequences of Cell-Wall Turnover in the Elongation of a Gram-Positive Bacterium. *Biophysical Journal* **2013,** *104*, 2342-2352.
(52) Elhenawy, W.; Davis, R., M.; Fero, J.; Salama, N.; Felman, M.; Ruiz, N. The O-Antigen Flippase Wzk Can Substitute for MurJ in Peptidoglycan Synthesis in Helicobacter pylori and Escherichia coli. *PLOS one* **2016,** *11* (8), 1-16.
(53) Müllera, A.; Wenzel, M.; Strahl, H.; Grein, F.; Saaki, T.; Kohl, B.; Siersm, T.; Bandow, J.; Sahl, H.-G.; Schneider, T.; Hamoen, L. Daptomycin Inhibits Cell Envelope Synthesis by Interfering with Fluid Membrane Microdomains. *Proceedings of the National Academy of Sciences of the United States of America* **2016**.
(54) Epand, R.; Epand, R. Domains in Bacterial Membranes and The Action of Antimicrobial Agents. *Molecular BioSystems* **2009,** *5* (6), 580-7, DOI: 10.1039/b900278m.
(55) Epand, R.; Epand, R. Lipid Domains in Bacterial Membranes and the Action of Antimicrobial Agents. *Biochimica et Biophysica Acta* **2009,** *1788* (1), 289-94, DOI: 10.1016/j.bbamem.2008.08.023.
(56) Hyyrylainen, H.-L.; Vitikainen, M.; Thwaite, J.; Wu, H.; Sarvas, M.; Harwood, C.; Kontinen, V.; Stephenson, K. D-Alanine Substitution of Teichoic Acids as a Modulator of Protein Folding and Stability at the Cytoplasmic Membrane/Cell Wall Interface of Bacillus subtilis. *Journal of Biological Chemistry* **2000,** *275* (35), 26696–26703.
(57) Jorgenson, M.; Young, K. Interrupting Biosynthesis of O-Antigen or the Lipopolysaccharide Core Produces Morphological Defects in Escherichia coli by Sequestering Undecaprenyl Phosphate. *Journal of Bacteriology* **2016,** *198* (22), 3070-3079
(58) Jintapattanakit, A.; Mao, S.; Kissel, T.; Junyaprasert, V. B. Physicochemical properties and biocompatibility of N-trimethyl chitosan: Effect of quaternization and dimethylation. *European Journal of Pharmaceutics and Biopharmaceutics* **2008,** *70*, 563-571.
(59) Zhong, Z.; Li, P.; Xing, R.; Liu, S. Antimicrobial activity of hydroxylbenzenesulfonailides derivatives of chitosan, chitosan sulfates and carboxymethyl chitosan. *Int. J. Biol. Macromol.* **2009,** *45*, 163–168.
(60) Zhong, Z.; Xing, R.; Liu, S.; Wang, L.; Cai, S.; Li, P. Synthesis of acyl thiourea derivatives of chitosan and their antimicrobial activities in vitro. *Carbohydrate Research* **2008,** *343*, 566–570.

(61) Sajomsang, W.; Tantayanon, S.; Tangpasuthadol, V.; Daly, W. H. Quaternization of N-aryl chitosan derivatives: synthesis, characterization, and antibacterial activity. *Carbohydrate Research* **2009,** *344*, 2502–2511.
(62) Sajomsang, W.; Tantayanon, S.; Tangpasuthadol, V.; Daly, W. H. Synthesis of Methylated Chitosan Containing Aromatic Moieties: Chemoselectivity and Effect on Molecular Weight. *Carbohydr. Polym.* **2008,** *72*, 740–750.
(63) Yu, H.; Chen, X.; Lu, T.; Sun, J.; Tian, H.; Hu, J.; Wang, Y.; Zhang, P.; Xiabin;, J. Poly(L-lysine)-Graft-Chitosan Copolymers: Synthesis, Characterization, and Gene Transfection Effect. *Biomacromolecules* **2007,** *8*, 1425-1435.
(64) Poché, D.; Moore, M.; Bowles, J. An Unconventional Method for Purifying the N-carboxyanhydride Derivatives of γ-alkyl-L-glutamates. *Synthetic Communications* **1999,** *29* (5), 843-854.
(65) Schillen, K.; Wyn;, B.; Johnsen, R. Micellar Sphere-to-Rod Transition in an Aqueous Triblock Copolymer System. A Dynamic Light Scattering Study of Translational and Rotational Diffusion. *Macromolecules* **1994,** *27* (17), 4825-4832
(66) Wang, C.; Tam, K. C.; Jenkins, R. D.; Bassett, D. R. Potentiometric Titration and Dynamic Light Scattering of Hydrophobically Modified Alkali Soluble Emulsion (HASE) Polymer Solutions. *Physical Chemistry Chemical Physics* **2000,** *2* (9), 1967-1972
(67) Keogh, D.; Tay, W.-H.; Ho, Y.-Y.; Dale, J.; Chen, S.; Umashankar, S.; Williams, R.; Chen, S.; Dunny, G.; Kline, K. Enterococcal Metabolite Cues Facilitate Interspecies Niche Modulation and Polymicrobial Infection. *Cell host and microbe* **2016,** *20* (4), 493-503
(68) Barducci, A.; Bussi, G.; Parrinello, M. Well-Tempered Metadynamics: a Smoothly Converging and Tunable Free-Energy Method. *Phys. Rev. Lett.* **2008,** *100*, 020603.
(69) Bonomia, M.; Branduardi, D.; Bussi, G.; Camilloni, C.; Provasi, D.; Raiteri, P.; Donadio, D.; Marinelli, F.; Pietrucci, F.; Broglia, R. A.; Parrinel, M. PLUMED: A Protable Plugin for Free-Energy Calculations with Molecular Dynamics. *Comp. Phys. Comm.* **2009,** *180*, 1961-1972.
(70) Kirschner, K.; Yongye, A.; Tschampel, S.; González-Outeiriño, J.; Daniels, C.; Foley, L.; Woods, R. GLYCAM06: A Generalizable Biomolecular Force Field, Carbohydrates. *Journal of Computational Chemistry* **2008,** *29*, 622.
(71) Hornak, V.; Abel, R.; Okur, A.; Strockbine, B.; Roitberg, A.; Simmerling, C. Comparison of Multiple Amber Force Fields and Development of Improved Protein Backbone Parameters. *Proteins : Structure, Function, and Bioinformatics* **2006,** *65* (3), 712-725
(72) Jämbeck, J. P. M.; Lyubartsev, A. Derivation and Systematic Vaidation of a Refined All-atom Force Field for Phosphatidylcholine Lipids. *Journal of Physical Chemistry B* **2012,** *116*, 3164-3179.
(73) Jämbeck, J. P. M.; Lyubartsev, A. An Extension and Further Validation of an All-Atomistic Force Field for Biological Membranes. *Journal of Chemical Theory and Computation* **2012,** *8*, 2938-2948.

**Table 1** Molecular weight and Light scattering study of CSM5-K5, and K100

| Polymer | $M_n$[†] | $M_w$[†] | $R_h$ for individual polymer (nm) | Polymer aggregates (DI water, pH=7) | | |
|---|---|---|---|---|---|---|
| | | | | $R_g$ (nm) | $R_h$ (nm) | Aggregation number |
| CSM5-K5 | 3648Da | 4084Da | 7.75 | 42.7±3.4 | 36.5±3.5 | 110[$] |
| K100 | 10947Da | 12522Da | 9.25 | No aggregation | | |

[†]Using GPC

[$]Based on $M_n$ from GPC

**Table 2** MIC (in μg/mL) of CSM5-K5 (and K100) against Gram-positive and Gram-negative bacteria

| | **CSM5-K5** | **K100** |
|---|---|---|
| **Gram-positive Strains** | | |
| *S. aureus* 29213 | 32 | 128 |
| *S. aureus* BAA-40 (MRSA) | 16 | |
| *S. aureus* USA-300 (ORSA) | 16 | |
| *S. aureus* MRSA-1 | 32 | |
| *S. aureus* MRSA-2 | 32 | |
| *S. aureus* MRSA-3 | 16 | |
| *S. aureus* MRSA-4 | 32 | |
| *S. aureus* MRSA-5 | 32 | |
| *S. aureus* MRSA-6 | 32 | |
| *S. aureus* MRSA-7 | 32 | |
| *Bacillus subtilis* | 8 | |
| *Enterococcus faecium* 19434 | 128 | |
| *Enterococcus faecalis* OG1RF | 256 | |
| *Enterococcus faecalis* V583 | 128 | |
| **Gram-negative strains** | | |
| *E. coli* K12 | 32 | 256 |
| *E. coli* W3110 | 32 | |
| *E. coli* UTI89 | 64 | |
| *E. coli* EC958 | 64 | |
| *E. coli* PTR3 | 64 | |
| *E. coli* 8739 | 16 | |
| *E. coli* 25922 | 64 | |
| *P. aeruginosa* PAO1 | 64 | 512 |
| *P. aeurginosa* PAD1 | 64 | |
| *P. aeruginosa* PAD25 | 64 | |
| *P. aeruginosa* PAW238 | 64 | |
| *P. aeruginosa* PAES | 128 | |
| *P. aeruginosa* PAER | 128 | |
| *Salmonella enterica subsp. enterica* 13076 | 64 | |
| *Vibrio parahaemolyticus* 17802 | 64 | |

**Table 3 Summary of thermodynamic parameters of CSM5-K5 with various liposomes as determined by isothermal titration calorimetry (ITC)**

| Components | ΔG(kcal/mol) | ΔH(kcal/mol) | -TΔS (kcal/mol) | ΔS(kcal/K·mol) | $K_A(M^{-1})$ | *Binding Site, n |
|---|---|---|---|---|---|---|
| **OM interaction** | | | | | | |
| a. POPC:LPS(*E. coli*) (4:1) | -6.21 | -0.21 | -6.00 | -0.0194 | 23753 | 0.392 |
| b. POPC:LPS(*P. aeruginosa*) (4:1) | -5.20 | -1.10 | -4.10 | -0.0132 | 4608 | 0.296 |
| **IM interaction** | | | | | | |
| c. POPC:POPG (4:1) | -5.86 | -8.96 | +3.10 | 0.01 | 13333 | 0.173 |

*Binding Site, n is determined based on no. of moles of CSM5-K5 polymer binding with no. of moles of liposome.

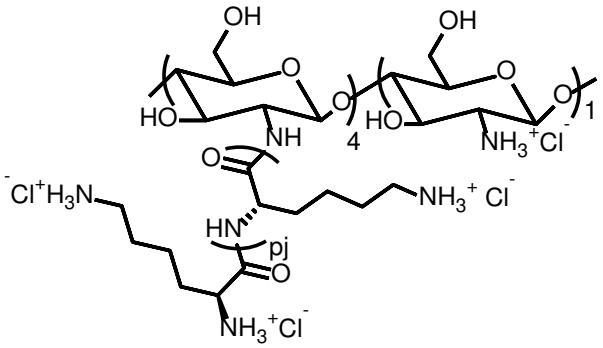


**Scheme 1** Schematic of CSM5-K5 ($\sum_{j=1}^{4} p_j \approx 5$)

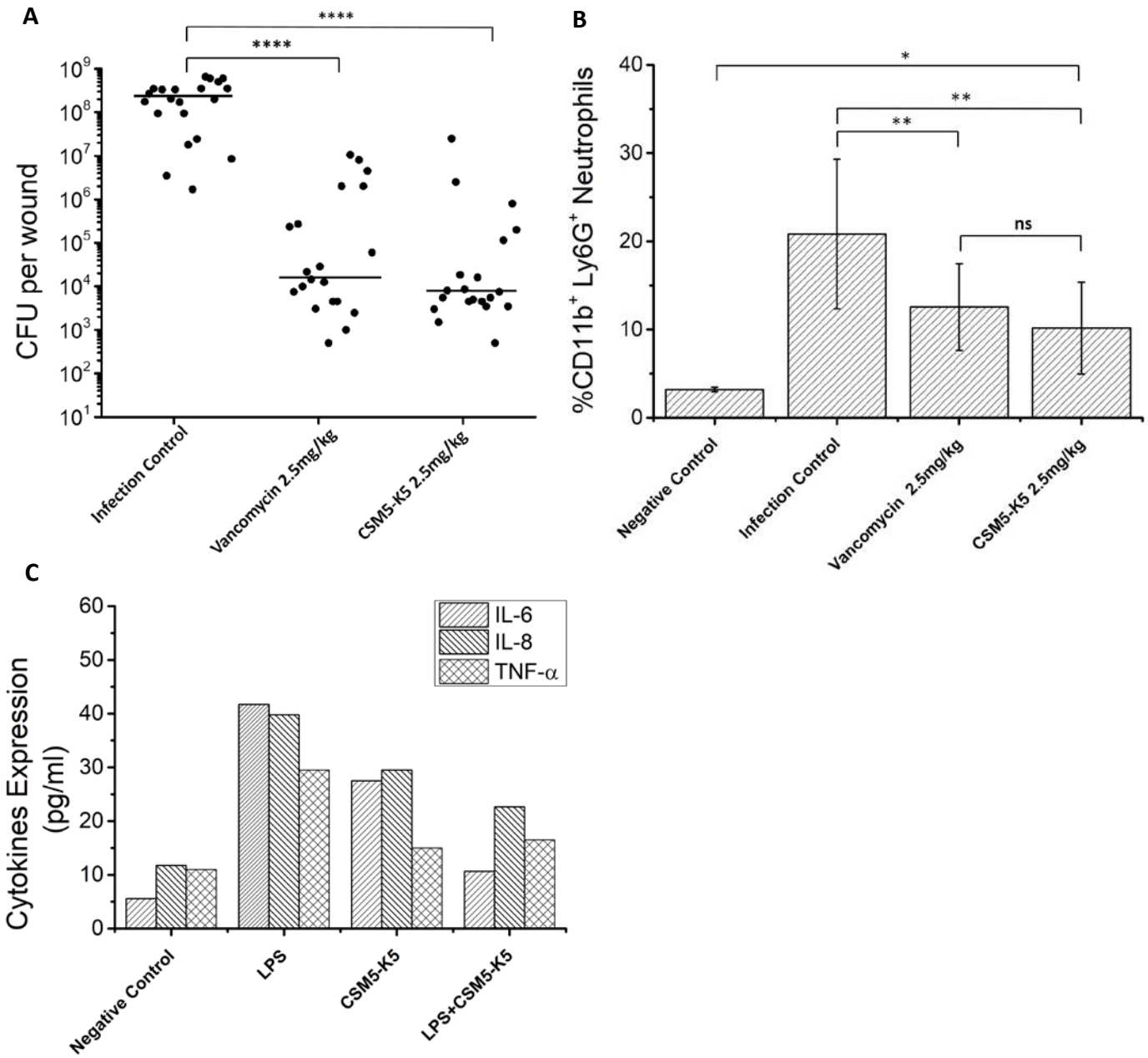


**Figure 1 (A)** *In vivo* test of antibacterial activity of CSM5-K5 in a murine excisional wound model. Bacteria (MRSA BAA-40) concentration (CFU per wound) of control mice was compared with treated mice (the median is presented by the horizontal line for each group). The values were obtained from 3 experimental replicates with **** P≤0.0001, Mann-Whitney test compared to infection control (with bacteria and no treatment). **(B)** The FACS analysis of *in vivo* immune cell neutrophils characterized by positive expression of both CD11b and Ly6G antibody. The values were obtained based on experimental replicates, with **p≤0.01 Mann-Whitney test compared to infection control (CSM5-K5 treated group) and *p<0.1 Mann-Whitney test compared to negative control (negative control is wound without bacteria and without any treatment). **(C)** *In vitro* cytokines secretion from macrophages by LPS, CSM5-K5 nanoparticle and their combination; negative control is macrophage cells without addition of LPS or CSM5-K5.

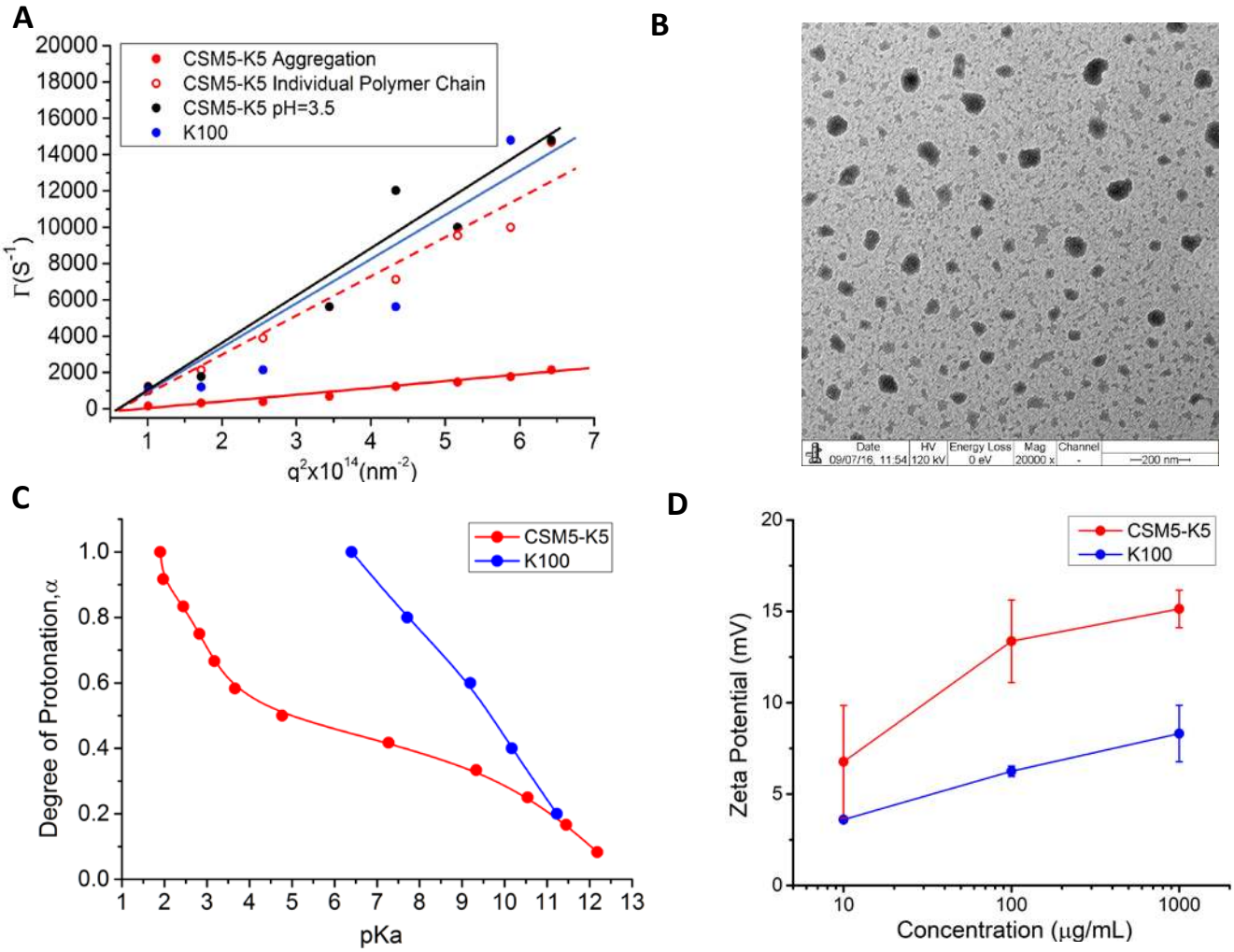


**Figure 2**. Solution properties of CSM5-K5 compared with K100: **(A)** Dynamic light scattering (DLS) data: decay rate (Γ) versus wave vector ($q^2$) for CSM5-K5 suspension at pH=7 (red), CSM5-K5 suspension at acidic pH (pH=3.5) (black) and K100 (blue). The decay rate (Γ) variations with wave vectors ($q^2$) were evaluated using the relaxation function measured at specific angles (Figure S5); the relaxation function is the inverse Laplace Transformation of the autocorrelation function of intensity versus time. **(B)** TEM image of CSM5-K5 at pH=7. **(C)** Degree of protonation (α) of CSM5-K5 and K100 change versus pKa. **(D)** Zeta-potential of CSM5-K5 and K100 measured at different concentrations at physiological pH (PBS, pH=7.4).

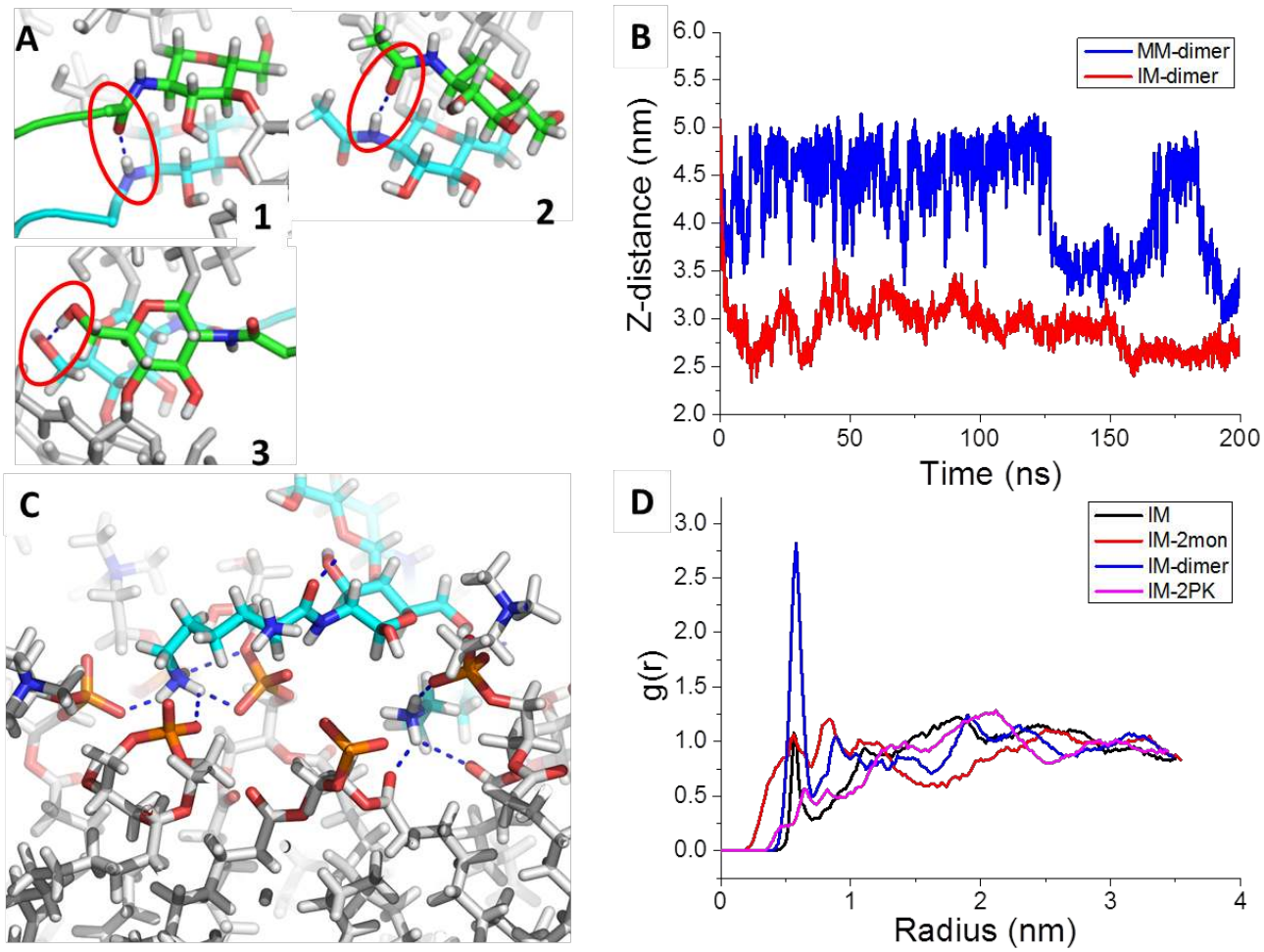


**Figure 3 (A)** H-bonds between the chitosan chains that maintain the dimerization of two copolymer can be divided into two categories: the –NHC(=O)•••–NHC(=O) H-bonds and the –OH•••–OH H-bonds. The former are defined as H-bonds between the two 2-position amide groups which are directly attached to chitosan backbone of CSM5-K5 (A1 and A2); and the latter are defined as the H-bonds between hydroxyl groups of chitosan (A3). **(B)** IM-dimer system has a relatively lower Z-distance between center of mass (COM) of CSM5-K5 dimer and membrane than versus the MM-dimer system indicating a stronger binding of dimer with bacterial inner membrane than with mammalian cell membrane. **(C)** A snapshot of IM-dimer system showed oligolysine of CSM5-K5 were mainly H-bonded with phosphate groups ($PO_4^-$) of lipids, but some could reach deeper to H-bonded with carbonyl groups of lipids. **(D)**POPG clustering effect within bacterial model membrane (POPC: POPG = 4:1) was shown by the lateral radial distribution function (RDF) of POPG with respect to itself in membrane systems with or without presence of polycations. Polycations showed different capability of gathering negatively charged POPG. CSM5-K5 dimer was the most effective for POPG domain formation over three kinds of polycations. Nitrogen, oxygen, and hydrogen atoms are colored as blue, red, and white respectively, carbon atoms are colored as green and cyan (A) or cyan and gray (C) to differentiate different molecules.

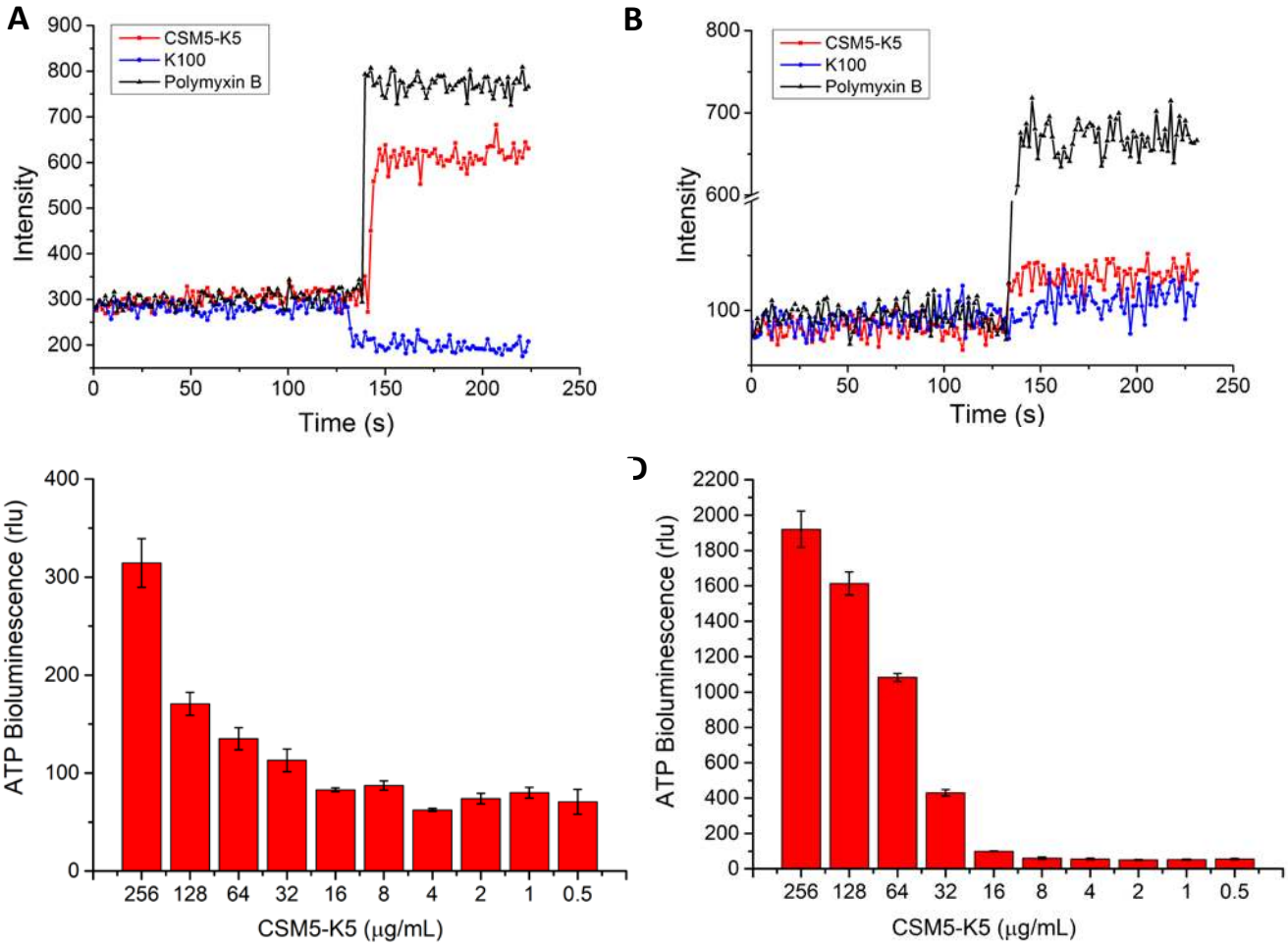


**Figure 4** NPN dye leakage assay of **(A)** *E. coli* K12, and **(B)** *P. aeruginosa* PA01 Polymyxin B was used as control with same concentration as polymer (100 μg/mL); ATPase assay of **(C)** *E. coli* K12, and **(D)** MRSA BAA-40.

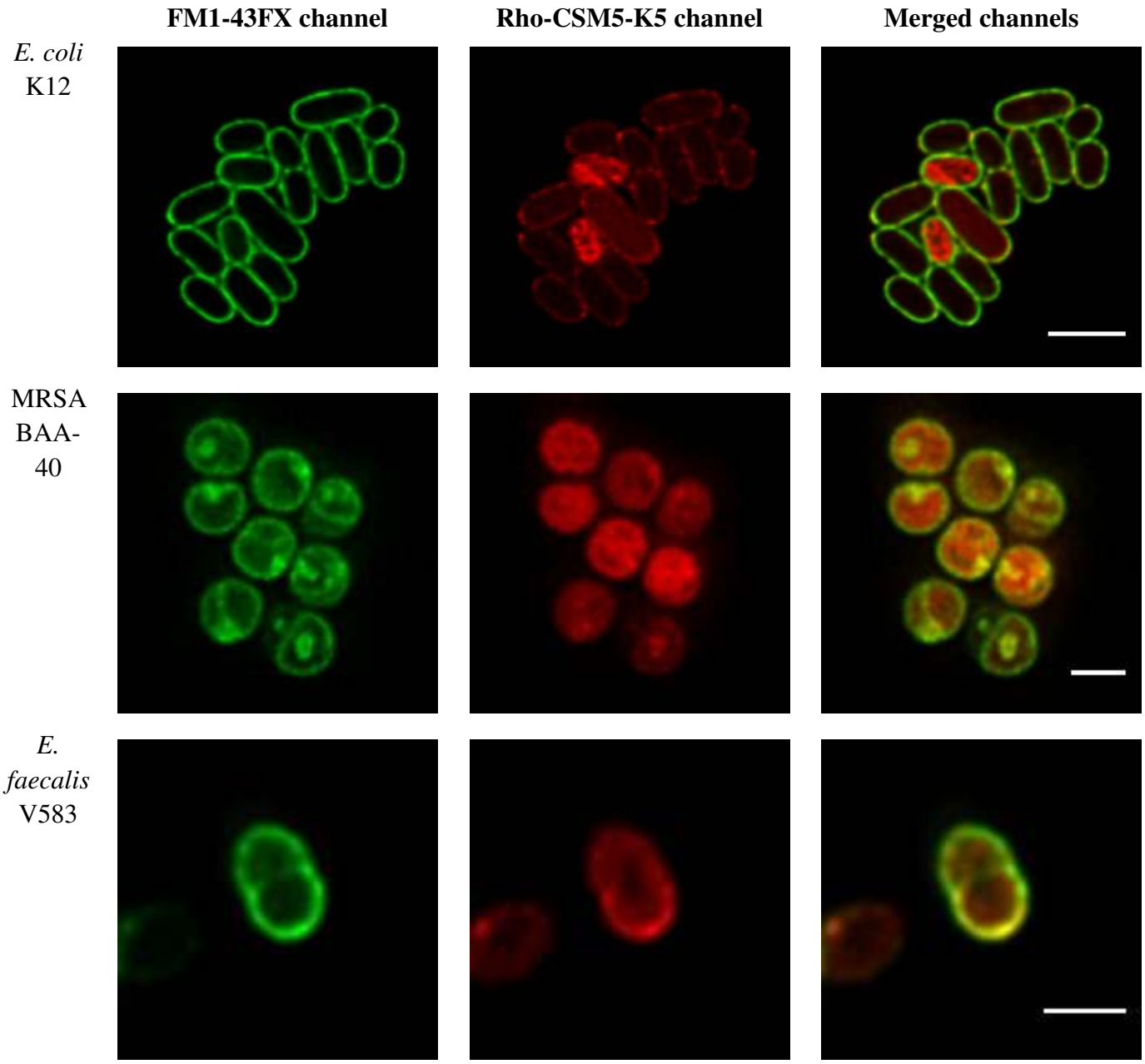


**Figure 5** Fluorescence microscopy images of *E. coli* K12, MRSA BAA-40 and *E. faecalis* V583 incubated with Rho-CSM5-K5 (first column is the FM1-43FX membrane dye; second column is CSM5-K5 conjugated with Rhodamine dye; third column is the merging of both channels). *E. coli* K12 scale bar = 2 µm. MRSA BAA-40 and *E. faecalis* V583 scale bars = 1 µm.

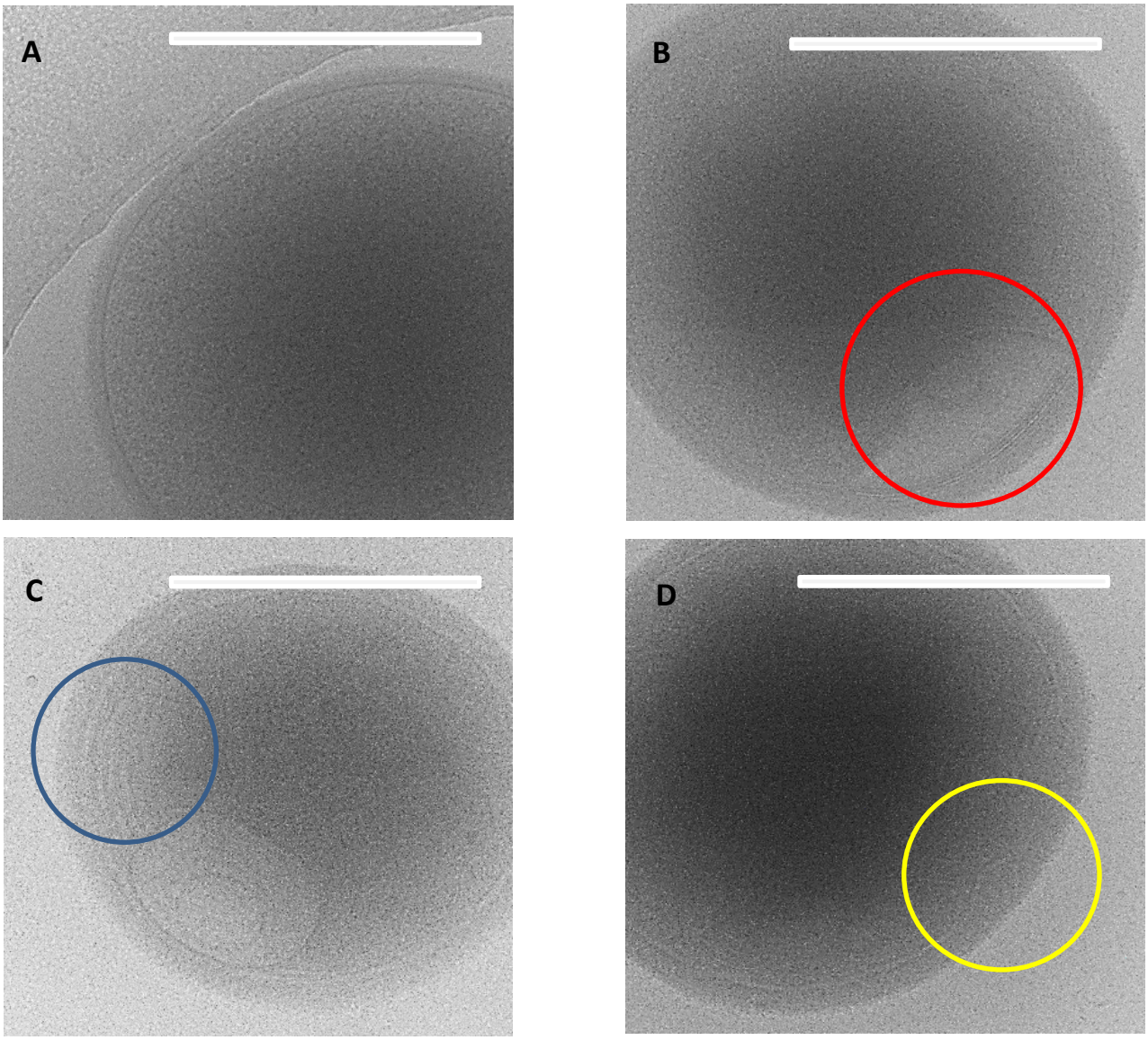


**Figure 6** Cryo-TEM images of MRSA treated with CSM5-K5 at 8×MIC. **(A)** MRSA Control without treatment by CSM5-K5; **(B)** Circle shows separation of Cell membrane from cell wall after treatment of CSM5-K5; **(C)** Circle shows shrinking of cell membrane after treatment of CSM5-K5; **(D)** Circle shows irregular cell wall after treatment of CSM5-K5; Magnification is same in all the sub-figures; Scale bar=500nm.

**Table of Content**

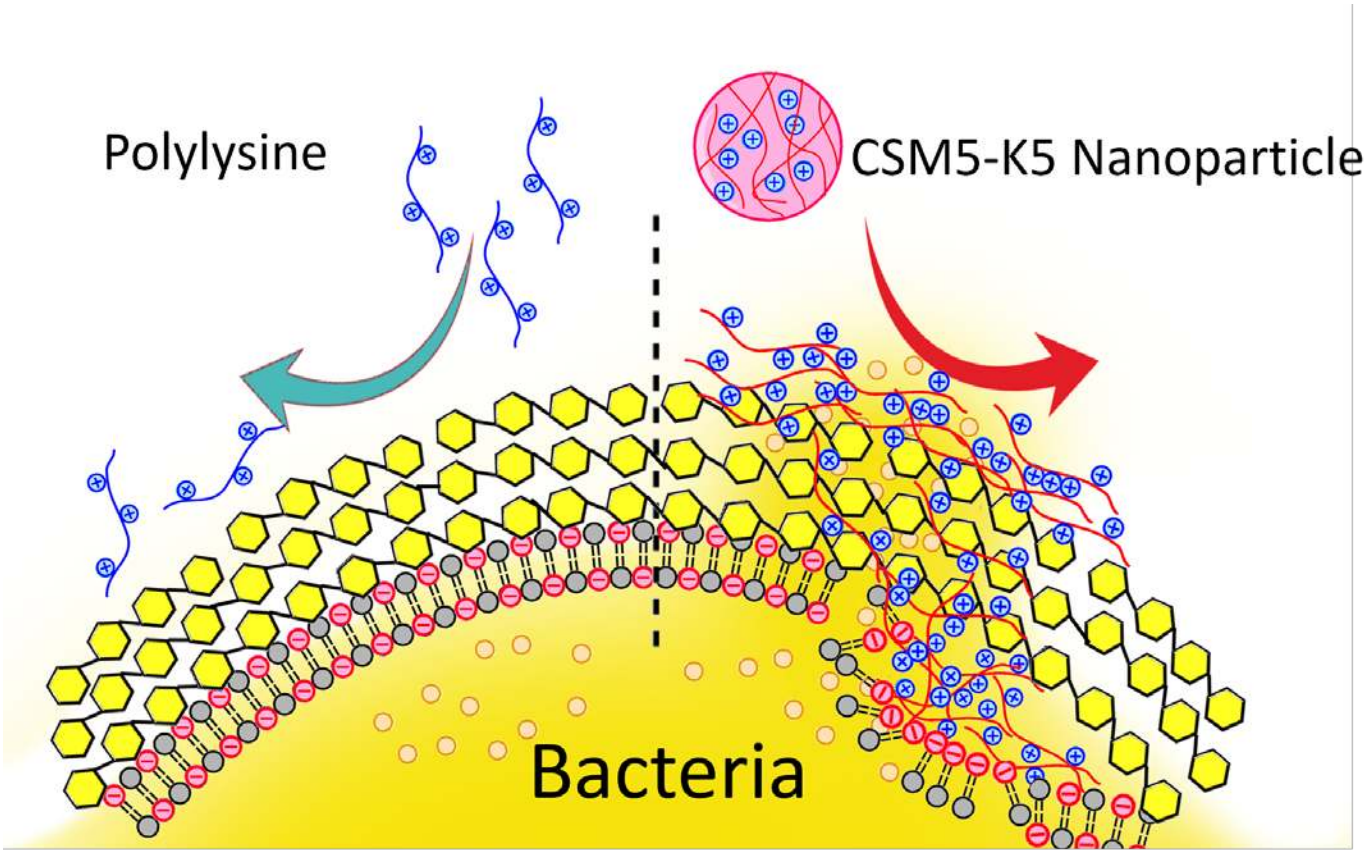

# Supporting Information

## Nanoparticles of Short Cationic Peptidopolysaccharide Self-Assembled by Hydrogen Bonding with Antibacterial Effect against Multi-Drug Resistant Bacteria

*Zheng Hou[†1,2], Yogesh Vikhe Shankar[†1,2], Yang Liu[†3], Feiqing Ding[1,2], Jothy Lachumy Subramanion[1,2], Vikashini Ravikumar[5], Rubí Zamudio-Vázquez[1,2], Damien Keogh[1,2], Huiwen Lim[8], Moon Yue Feng Tay[1,9], Surajit Bhattacharjya[3], Scott A. Rice[3,5], Jian Shi[6], Hongwei Duan[1,2], Xue-Wei Liu[2,4], Yuguang Mu[3], Nguan Soon Tan[3,8], Kam (Michael) Chiu Tam[7], Kevin Pethe[8], Mary B. Chan-Park*[1,2,3]*

[1]School of Chemical and Biomedical Engineering, Nanyang Technological University (NTU), 62 Nanyang Drive, Singapore 637459

[2]Centre for Antimicrobial Bioengineering, NTU, 62 Nanyang Drive, Singapore 637459

[3]School of Biological Sciences, NTU, 60 Nanyang Drive, Singapore 637551

[4]Division of Chemistry and Biological Chemistry, NTU, 50 Nanyang Ave, 639798

[5]Singapore Center for Environmental and Life Sciences (SCELSE), 60 Nanyang Drive, Singapore 637551

[6]NUS Centre for Bioimaging Sciences, National University of Singapore, 14 Science Drive 4 Singapore 117557

[7]Department of Chemical Engineering, Waterloo Institute for Nanotechnology, University of Waterloo, Canada, 200 University Ave. W. Waterloo, ON. N2L 3G1

[8]Lee Kong Chian School of Medicine, NTU, 11 Mandalay Road. Singapore 308232

[9]Nanyang Technological University Food Technology Centre (NAFTEC), NTU, 62 Nanyang

Drive, Singapore 637459

† These authors contribute equally.

*mbechan@ntu.edu.sg

# List of Tables

# Table of Contents

**Table S1** Antimicrobial activity, mammalian cell biocompatibility and hemolysis of Chitosan-*graft*-oligolysine and comparison with polylysine and some published antimicrobial peptides

| Entry | | MIC[a] (μg/mL ) | | | | [b] %Cell Viability Test with 100 μg/mL of compound | Hemolytic Activity (HC10, RBC) (μg/mL) | [c]Selectivity based on HC10 |
|---|---|---|---|---|---|---|---|---|
| | | Gram-negative | | Gram-positive | | | | |
| | | *E. coli* K12 | *P. aeruginosa* PAO1 | *S. aureus* 29213 | MRSA BAA-40 | | | |
| **1(a)** | **[d]CSM-K5** | **16** | **64-128** | **32** | **32** | **83.34** | **>5000** | **>312.5** |
| 2(a) | K10 | >512 | >512 | >512 | >512 | 96.26 | >5000 | |
| 2(b) | K20 | >512 | >512 | >512 | >512 | 97.4 | >5000 | - |
| 2(c) | K40 | 512 | 512 | >512 | >512 | 86.7 | >5000 | |
| 2(d) | K100 | 256 | >512 | 128 | 128 | 82.12 | >5000 | |
| 3(a) | Magainin-2 | 64 | 512 | 512 | 512 | 98.22 | >500 | >7.8125 |
| 3(b) | LL-37 | 512 | 64 | 512 | 512 | 75.8 | - | - |
| 3(c) | Melittin | 32 | 64 | 8 | 8 | 2.16 | 16 | 0.5 |
| 3(d) | polymyxin B | 2 | 1 | 32 | 64 | 99.64 | >2500 | >1250 |
| 4(a) | Rho-CSM5-K5 | 32 | 128 | 32 | 32 | | | |

[a] The strains used in this study were: *E. coli* (K12), *P. aeruginosa* (PA01), *S. aureus* (ATCC 29213), *E. faecalis* (ATCC 8739), methicillin-resistant *S. aureus* (MRSA, BAA-40), as well as oxacillin resistant *S. aureus* (ORSA, USA-300). The MIC value may vary for different strains of the same bacterial species. [b] Cell Viability is tested against 3T3 cells at 100000 cells per well. [c]Selectivity is HC10/MIC of *E coli* K12. [d]More strains: *E. coli* (ATCC 8730, K12, W3110, UTI89, EC958, and PTR3), *P. aeruginosa* (PA01, and D25), S. *aureus* (ATCC 29213), *E. faecalis* (OG1RF, and V583), methicillin-resistant *S. aureus* (MRSA, BAA-40), as well as oxacillin resistant *S. aureus* (ORSA, USA-300) were tested against CSM5-K5 and summarized in Table 2.

**Table S2** Dynamic Light scattering of CSM5-K5 nanoparticle in various fluids

| Concentration (µg/mL) | Hydrodynamic Radius ($R_h$) in nm | | | |
|---|---|---|---|---|
| | DI water (pH=7) | PBS buffer (pH=7.4) | Urea (8M) | Acidic condition (pH=3.5) |
| 1000 | 36.5±3.5 | 48.7±5.5 | 122±3 | 6.5±0.4 |
| 100 | 34.8±2.6 | 30.4±2.4 | 6.4±0.8 | 5.1±0.4 |
| 10 | 6.1±0.5 | 8.1±0.7 | 6.1±0.9 | 3.5±0.7 |

**Table S3** Calculated results of moles of amine per unit weight (moles/g) of polymer

| | HCl used for amine neutralization (mM) | Moles of amine/g |
|---|---|---|
| K100 | 0.34 | 0.047 |
| CSM-K5 | 0.91 | 0.121 |

**Table S4** Hydrodynamic radii ($R_h$, nm) of different liposomes and liposome mixture with different polymer, in nm determined by Dynamic Light Scattering (DLS)

| | **POPC: LPS** | **POPC: POPG** | **POPC** |
|---|---|---|---|
| Control[a] | 75.0 | 60.1 | 70.0 |
| CSM5-K5 | 682.0 | 81.4 | 70.6 |
| Chitosan 3kDa | 75.9 | 70.0 | 64.5 |
| K100 | 69.2 | 66.2 | 68.0 |

[a]Control is Liposome with no test agent

**Table S5** Total number of water molecules that penetrated the membrane hydrophobic area in different time interval was counted for different systems.

| | **IM** | **IM-2mon** | **IM-dimer** | **IM-2PK** |
|---|---|---|---|---|
| Time interval 1 | 21 | 20 | 26 | 23 |
| Time interval 2 | 9 | 15 | 35 | 15 |
| Time interval 3 | 26 | 31 | 30 | 24 |

Average ± s.d: 19±7, 22±7, 30±4, and 21±4 water molecules captured in 20 ns for system IM, IM-2mon, IM-dimer, IM-2PK respectively.

To compare the membrane defects generated in different systems, the total number of water molecules that penetrated the hydrophobic area of membrane was averaged over the last three time intervals of each simulation, 20 ns each (Table S5). Averages of 19±7, 22±7, 30±4, and 21±4 water molecules were captured for IM, IM-2mon, IM-dimer, IM-2PK respectively, suggesting that the copolymer increased the permeability of the bacterial membrane, and the dimer was more effective than two monomers. No statistically significant permeability change was caused by linear polylysine, consistent with the experimental findings about K100, and indicating the importance of the chitosan backbone and shorter lysine chains for increasing the charge concentration.

**Table S6** Summary of reported MIC and cytotoxicity and mechanism of promising AMPs

| Antimicrobial peptide | MIC (μg/mL) | | | **Hemolysis/Cytotoxicity** |
|---|---|---|---|---|
| | *E. coli* | *P. aeruginosa* | *S. aureus* | |
| omiganan[1] | 32 | 64-256 | 32 | 100μg/mL (HC10)[2] |
| pexiganan[3] | 16 | 16 | 64 | 40μg/mL (HC10)[4] |
| plectasin[5] | - | - | 32 | >512μg/mL (HC10)[6] |

**Table S7** Summary of reported MIC and cytotoxicity of chitosan derivatives

| Chitosan derivatives | MIC (μg/mL) | | | Hemolytic activity/Cytotoxicity |
|---|---|---|---|---|
| | *E. coli* | *P. aeruginosa* | *S. aureus* | |
| CS[$]-sulfate[7] | 31.25 | 31.25 | 62.49 | |
| CS-Trimethyl ammonium[8] | 16-64 | - | 8-64 | 10~1000μg/mL ($IC_{50}$) |
| CS-N-pyridinium/ aryltrimethylammonium[9] | 64 | - | 32 | - |
| CS-thiourea[10] | 15.62 | 62.49 | 62.46 | - |
| CS-PHGH[‡11] | 15.6 | - | - | - |

[$]CS=chitosan

[‡]PHGH= polyhexamethylene guanidine hydrochloride

# Synthesis Schemes

## Synthesis of CSM5-K5

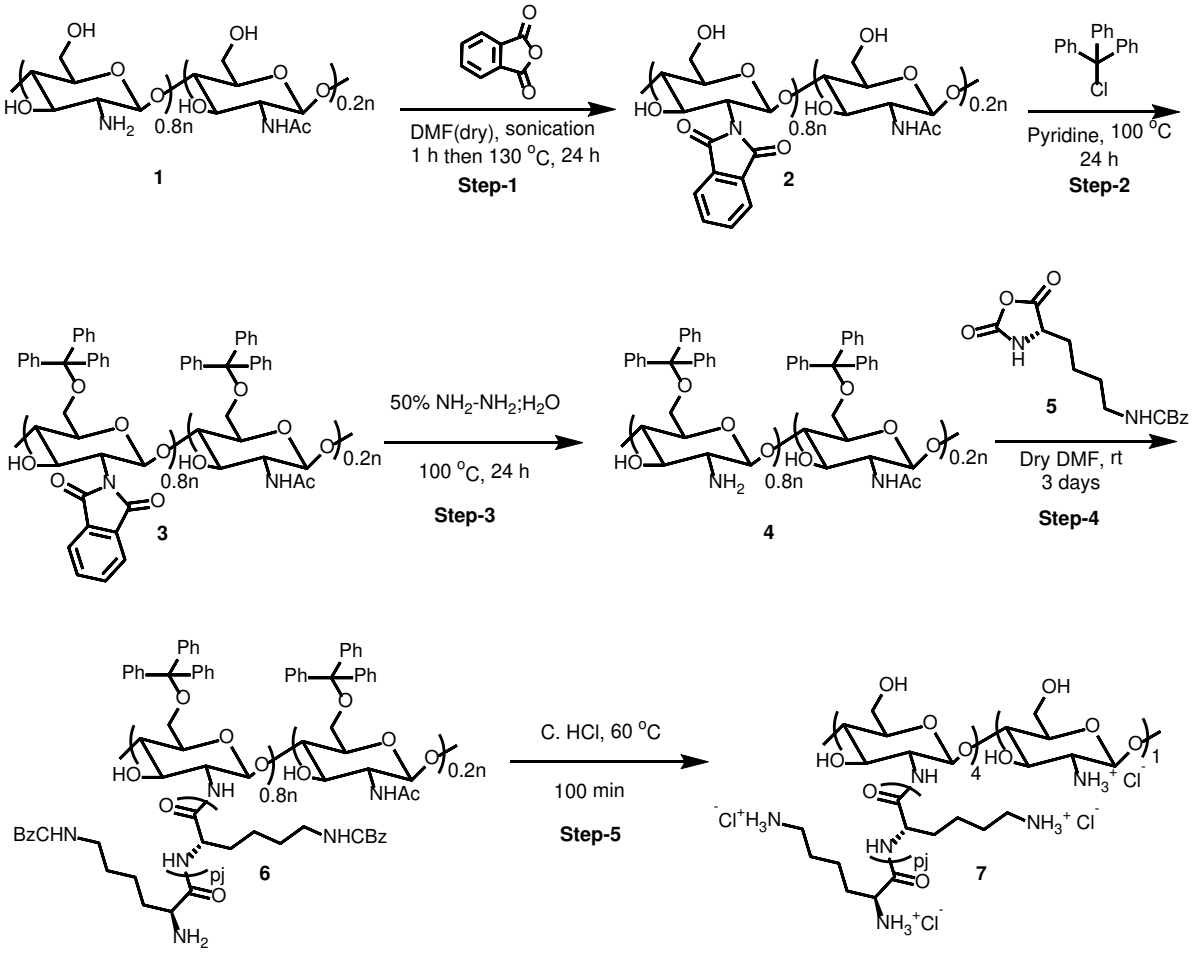


Figure S1A Synthesis scheme for CSM-K5 copolymer (CBz is Benzyl carbamates protection group for side chain amine of lysine)

**Protocol:**

CSM5-K5 (Scheme 1) was synthesized via NCA polymerization initiating from protected chitosan followed by acidic hydrolysis (Figure S1A). GPC of protected CS-Kn(CBz) shows that the "grafting from" the protected CS backbone was mostly successful with only a single major peak attributed to the protected CS-Kn(CBz) (Figure S3A). The major peak attributed to the protected CS-Kn(CBz) moved to the left indicating increased molecular weight and successful grafting from NCA polymerization, which requires very pure NCA monomer. The left minor peak at around 10 mins is due to the secondary structure formed as the polylysine chain length increased above 10 repeated units[12]. The right minor peak at around 13.9 min is due to unreacted chitosan. It

appears that not all the chitosan macroinitiator can initiate the NCA ring-opening polymerization, possibly because of the aggregation of chitosan macroinitiator in DMF, as shown by dynamic light scattering study of DMF solution of chitosan. The aggregation of the CS macroinitiator will lead to shielding of some of the amine groups.

Different reaction times and temperature conditions were evaluated for deprotection of trityl and CBz groups. The reaction time 100 min was found best to obtain >98% deprotection and molecular weight range from 3,500-4,000 Da by water phase GPC (**Figure S3B**). After deprotection the chitosan macroinitiator peak also disappeared in GPC spectrum. This can be attributed to the drastic cleavage of chitosan backbone during HCl deprotection process. The unreacted chitosan backbone is hydrolyzed to lower molecular weight N-glucosamine oligomers, and removed during dialysis. Further, after deprotection, there are no high molecular weight peaks found in water phase GPC (**Figure S3B**), as all the polylysine chains are in random coil.

The removal of trityl and CBz groups was verified by absence of chemical shift δH in the range from 7.0 to 7.5, which corresponds to the benzyl rings in both trityl and CBz groups. The crude product 7 was adjusted to pH=7 with NaOH solution (1M) and dialyzed with cellulose membrane (spectrum chemicals M.W. 1000 Da.) against DI water. After 5 days of dialysis, the residue was lyophilized to give off-white solid.

## Synthesis of Linear Polylysine

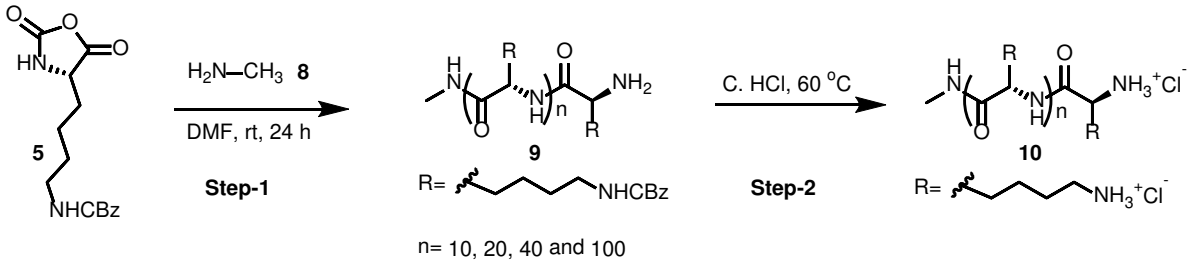


**Figure S1B** Synthesis of different linear L-polylysines**.**

**Protocol:**

The series of L-polylysine (K10, 20, 30, 40 and 100) (**10**) were synthesized from the compound **5**. The Methyl amine **8** was used as initiator for polymerization of NCA monomer **5** to produce compound **9** with good yield. The salt of compound **10** was obtained from **9** by using concentrated HCl deprotection.

## Synthesis of dye-attached CSM5-K5

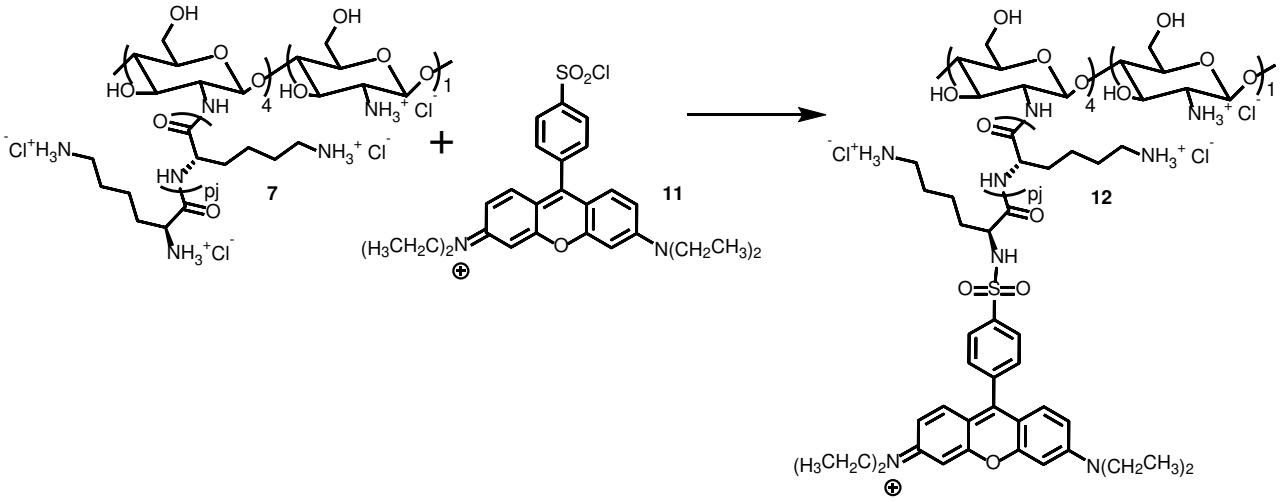


**Figure S1C** Synthesis of Lisamine Rhodamine B dye attached CSM5-K5

# NMR Characterization of Intermediates

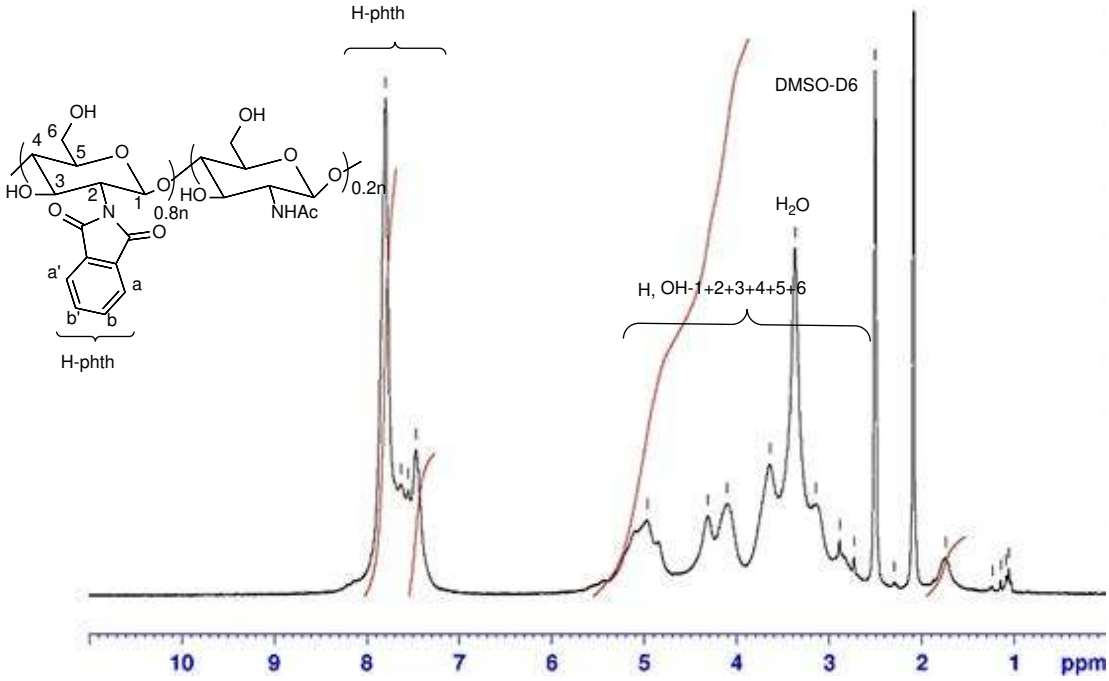


**Scheme S1** Synthesis of N-Phthaloyl Chitosan (compound **2**)

$$\text{Phthaloylation percentage} = \frac{(intergation\ \ from\ \ 7.5\ \ to\ \ 8)/4}{(intergration\ \ from\ \ 4\ \ to\ \ 5.5)/4} \times 100$$

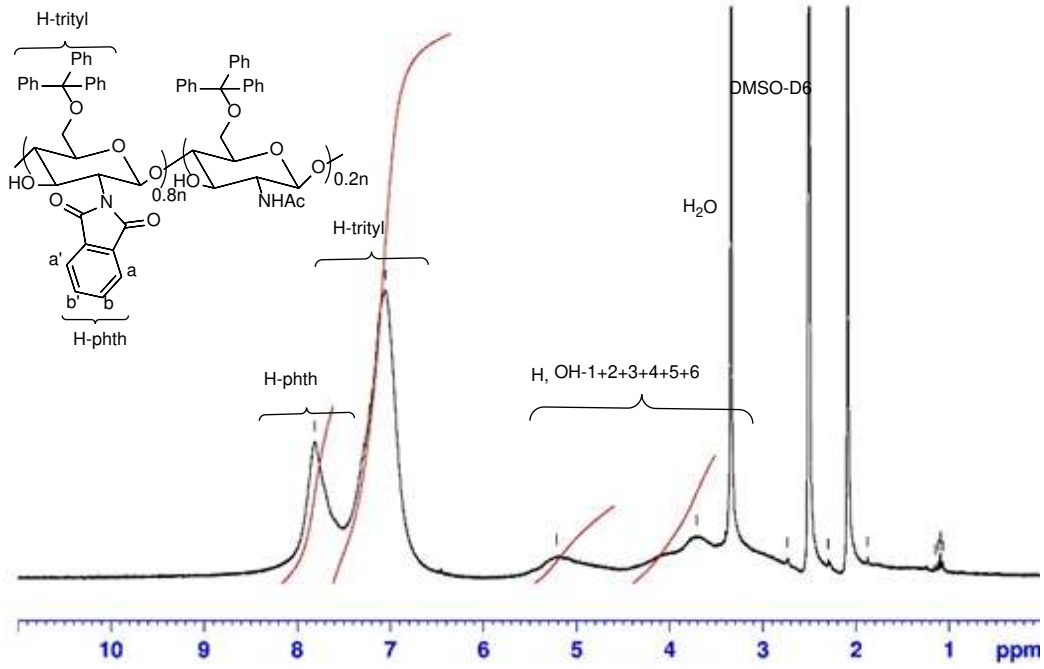


**Scheme S2** Synthesis of N-Phthaloyl-*6*-O-triphenylmethyl chitosan (compound **3**)

$$\text{Trityl Percentage} = \frac{(integration\ \ from\ \ 6.5\ \ to\ \ 7.5)/15}{(integration\ \ from\ \ 3.5\ \ to\ \ 5.5)/5} \times 100\%$$

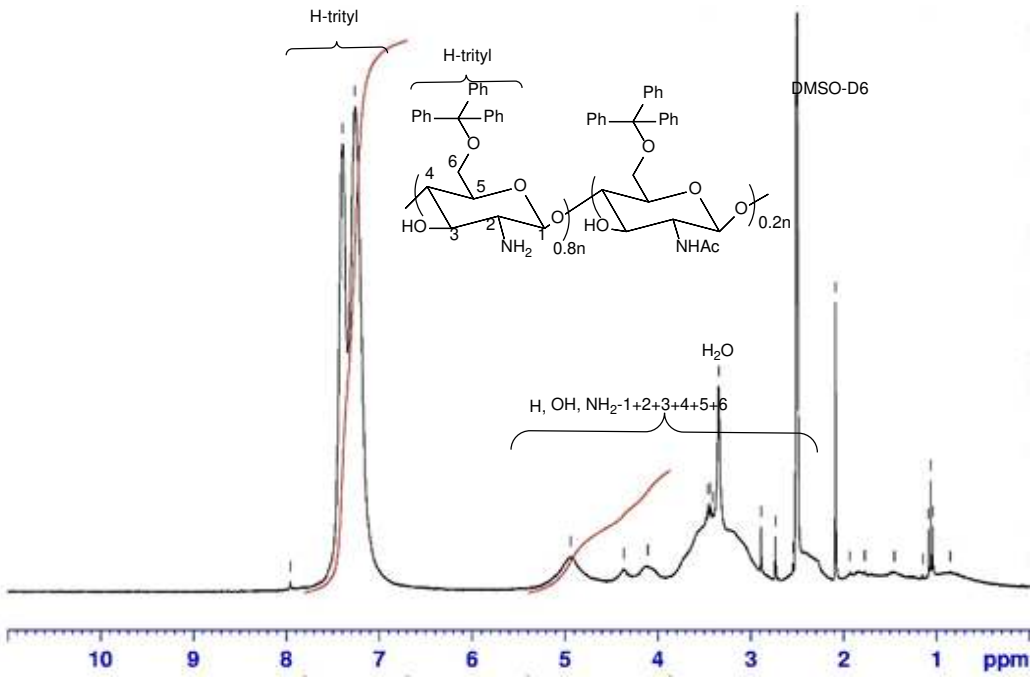


**Scheme S3** Synthesis of *6*-O-triphenylmethyl chitosan (compound **4**):

$$\text{Trityl Percentage} = \frac{(integration\ from\ 7\ to\ 8)/15}{(integration\ from\ 4\ to\ 5)/3} \times 100\%$$

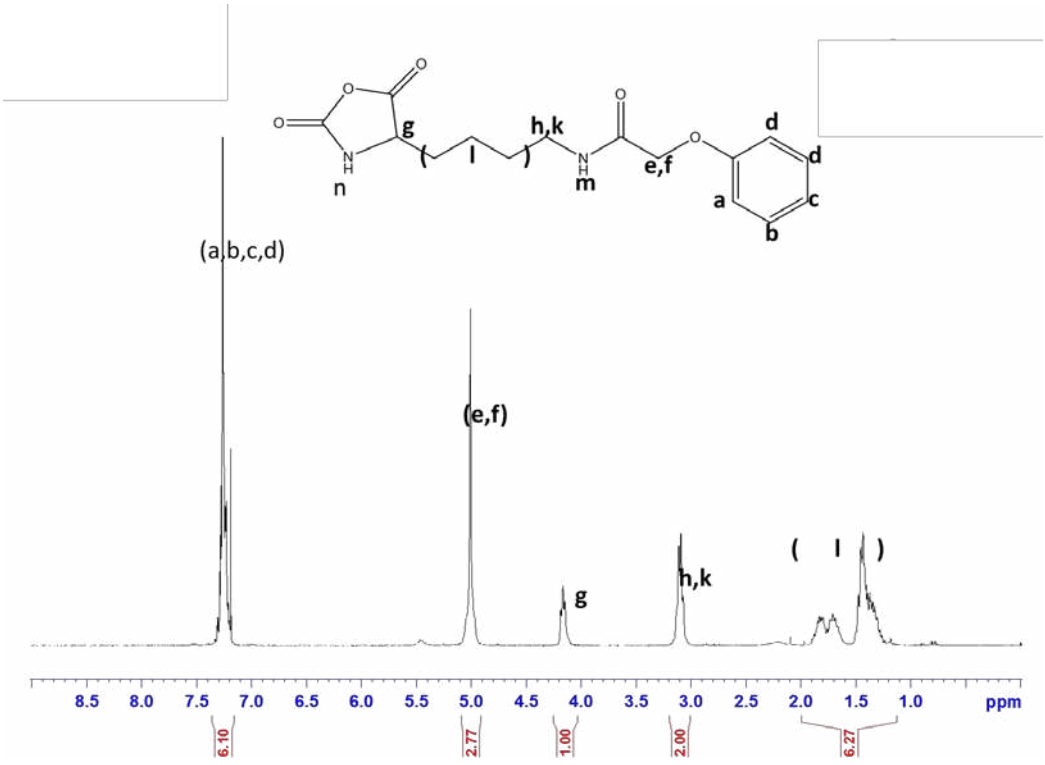


**Scheme S4** Synthesis Lysine NCA monomers (compound **5**)

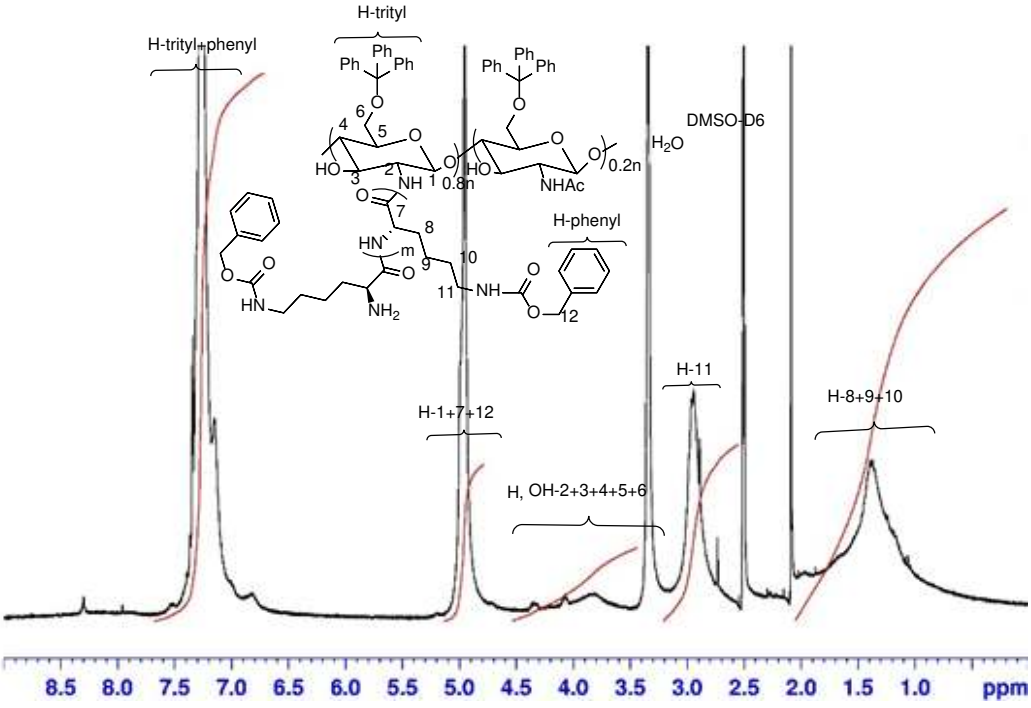


**Scheme S5** Synthesis of Protected CSM5-K5 copolymers (compound **6**);

$$\text{N of protected polymer} = \frac{(integration\ at\ 5)/3}{(integration\ from\ 3.5\ to\ 5.5)/5}$$

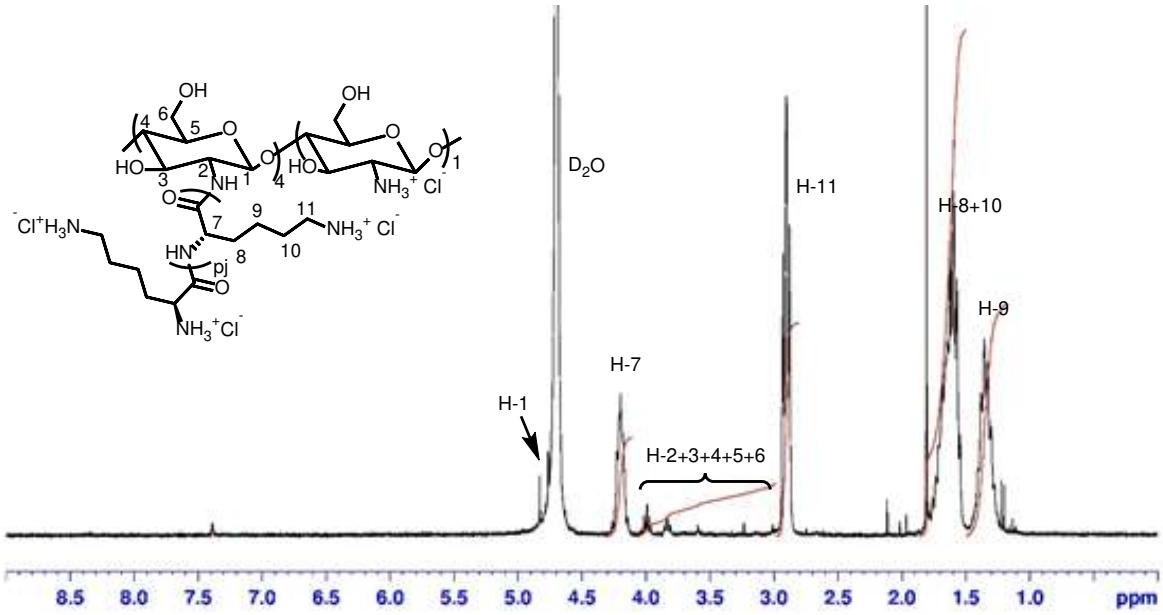


**Scheme S6** Deprotected CSM5-K5

$$\text{polysine chain length per glucosamine units} = \frac{(integration\ form\ 4.1\ to\ 4.3)}{(integration\ from\ 3\ to\ 4)/6}$$

$$Degree\ of\ Deprotection = \frac{(integration\ from\ 7.3\ to\ 7.4)/5}{(intergation\ from\ 4.1\ to\ 4.3)} \times 100\%$$

# Summary of molecular weight characterization

## a) Maldi-Tof Spectrum of CSM5-Kn

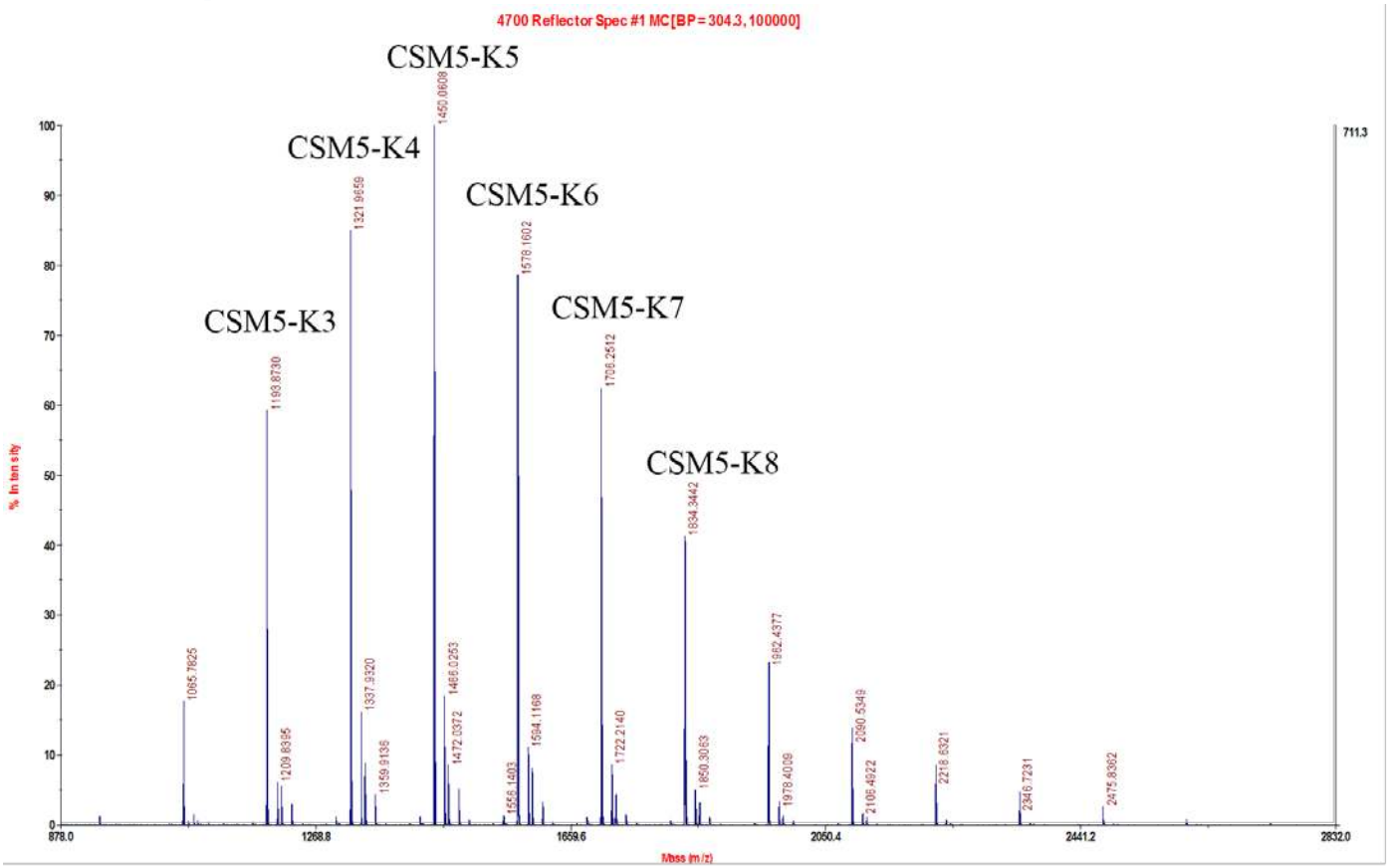


**Figure S2** Maldi-Tof Spectrum of CSM5-K5 (Molecular weight: CSM5-K3=1194Da, CSM5-K4=1322Da, CSM5-K5=1450Da, CSM5-K6=1578Da, CSM5-K7=1706, CSM5-K8=1834Da)

## b) GPC characterization

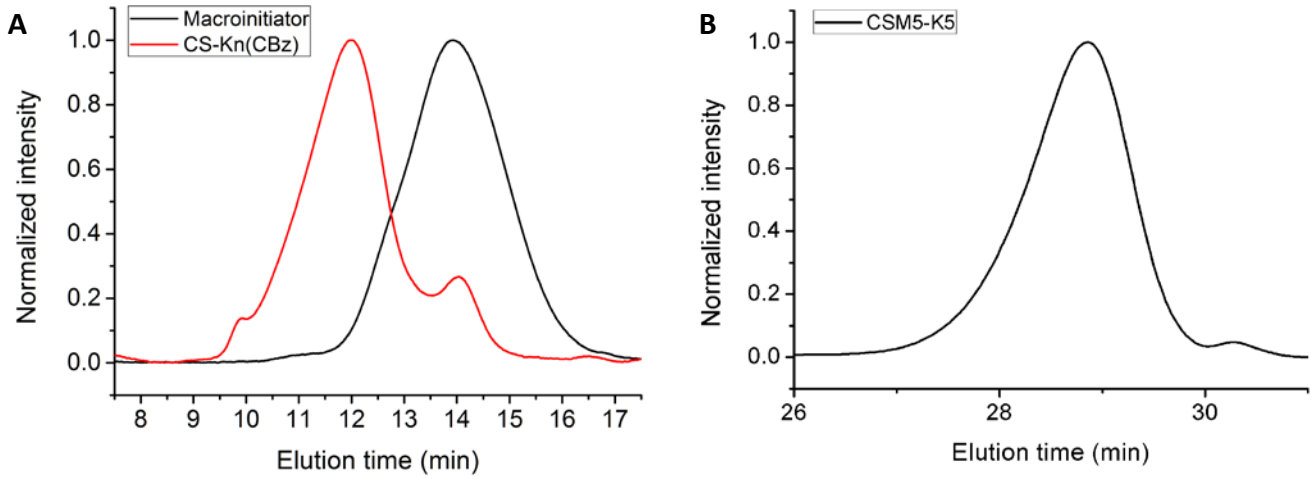


**Figure S3** (A) Summary of DMF phase GPC spectra for protected chitosan-*graft*-oligolysine (CS-Kn(CBz)) compared with macroinitiator. (B) water phase GPC spectra for deprotected chitosan-*graft*-oligolysine (CSM5-K5) via HCl deprotection method

# Light Scattering Study

## Calculation of Radius of Gyration ($R_g$)[13]

The Radius of Gyration of nanoparticles can be obtained by static light scattering interpreted by Zimm plot at specific concentration:

The basic static light scattering principle equation is Rayleigh-Debye-Zimm Formulism:

$$\frac{Kc}{R_\theta} = (\frac{1}{M_W} + 2A_2c)\frac{1}{P_\theta}$$

where $M_w$ is the aggregated molecular weight of nanoparticle; c is the concentration of solution.

The constant K is calculated from:

$$K = \frac{2\pi^2}{\lambda_o^4 N_A}(n_0\frac{dn}{dc})^2$$

where $\lambda_0$ is laser wavelength; $N_A$ is Avogadro's Number; $n_0$ is refractive index number of solvent; and $\frac{dn}{dc}$ is the differential refractive index number of solvent increment.

The $P_\theta$ is calculated from:

$$P_\theta = 1 + \frac{16\pi^2 {n_0}^2 R_g^2}{3\lambda_0^2} sin^2(\frac{\theta}{2})$$

where $R_g$ is Radius of Gyration, and θ is the angle of measurement.

The $R_\theta$ can be calculated based on average light scattering intensity of solution over time:

$$R_\theta = \frac{I_A n_0^2}{I_T n_T^2} R_T$$

where $I_A$ is the average intensity of solution over time, $I_T$ is the intensity of standard (Toluene); $n_T$ is refractive index of standard (Toluene); and $R_T$ is Rayleigh ratio of standard (Toluene).

The Rayleigh-Debye-Zimm Formulism can be further simplified into:

$$\frac{Kc}{\Delta R_{(\theta,c)}} = \frac{1}{M_W}\left(1 + \frac{R_g^2}{3}q^2\right) + 2A_2c$$

where $A_2$ is the second coefficient, and ΔR(θ,c) is measured on specific angle of measurement (θ) and concentration of solution (c); and wave factor q2 is calculated as:

$$q = \frac{4\pi n_0}{\lambda}\sin(\frac{\theta}{2})$$

The Radius of gyration ($R_g$) at specific concentration can be then calculated out by plotting of measured $I_A^{-1}$ against wave factors $q^2$ at different angles,

$$\frac{Kc}{I_A} = \frac{R_T n_0^2 R_g^2}{3 I_T n_T^2 M_W} q^2 + (\frac{R_T n_0^2}{M_W I_T n_T^2} + \frac{2R_T n_0^2 A_2 c}{I_T n_T^2})$$

## Zimm plot and aggregation number:

The Zimm plot also utilizes the equation:

$$\frac{Kc}{\Delta R_{(\theta,c)}} = \frac{1}{M_W}\left(1 + \frac{R_g^2}{3}q^2\right) + 2A_2c$$

With different concentration of solution measured at different angles (Figures S4), the extrapolated Y-intercept

at (θ,c)=(0,0) is the aggregated molecular weight.

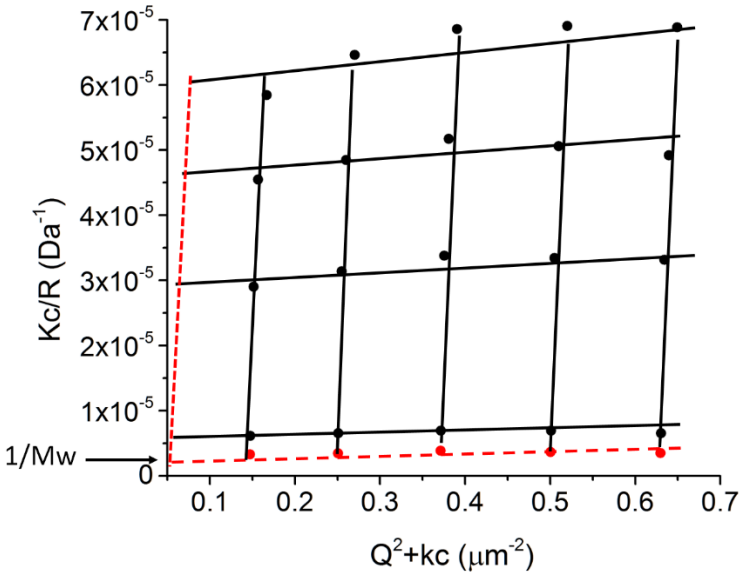


**Figure S4:** Zimm plot of CSM5-K5, the average molecular weight of CSM5-K5 nanoparticle is:

$$Mw = \frac{1}{0.248 \times 10^5} = 403325Da$$

Therefore, the average aggregation number of CSM5-K5 nanoparticle is:

$$N = \frac{Molecular\ \ weight\ \ of\ \ CSM5-K5\ \ nanoparticle}{Molecular\ \ weight\ \ of\ \ CSM5-K5} = \frac{403325Da}{3648Da} = 110$$

The molecular weight of CSM5-K5 is based on GPC study.

## Determination of ($R_h$) Hydrodynamic Radius using Correlation functions measured by dynamic light scattering:

The intensity autocorrelation functions of light scattered by the copolymer were measured at angles: 45, 60, 75, 90, 105,120, 135 and 150.

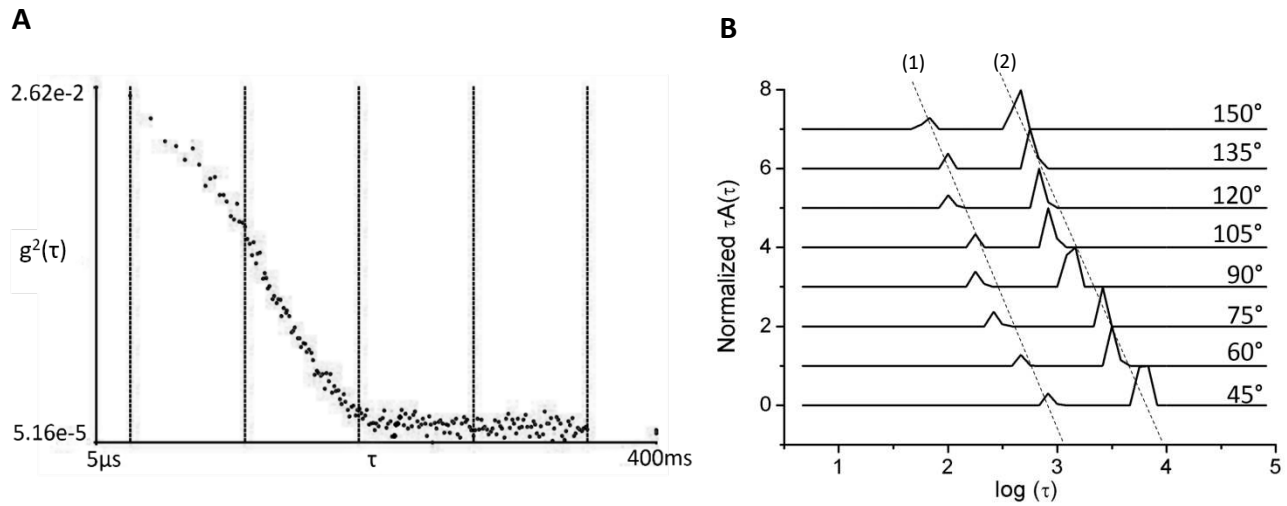


**Figure S5** The mathematical analysis of dynamic light scattering followed method presented by Schillen *et al*[14]: (A) Autocorrelation function of scattered light ($g^2(\tau)$ vs $\tau$) measured at 90 degrees. The g2(τ) is the intensity measured at τ, τ is time in logarithmic scale; (B) Normalized relaxation time distribution function τA(τ) $vs.\log(\tau)$ at different angles (θ) (45, 60, 75, 90, 105,120, 135 and 150)

The autocorrelation functions (Figure S4A) were processed using GENDIST package. The autocorrelation function was firstly processed by Regularized Inverse Laplace Transformation (RILT), to obtain relaxation time distribution functions (τA(τ) $vs.\log(\tau)$) at different angles (Figure S4B).[14]

The hydrodynamic radius ($R_h$) is calculated based on Stokes-Einstein Equation:

$$R_h = \frac{k_B T}{6\pi\eta D_T}$$

where $k_B$ is the Boltzmann constant, $\eta$ is the viscosity of the polymer solution and T is absolute temperature in Kelvin (K).

To obtain the diffusion coefficient ($D_T$) of the polymer suspension, the wave vector q at different angles (θ) are firstly calculated via:

$$q = \frac{4\pi n_0}{\lambda}\sin(\frac{\theta}{2})$$

where $n_0$ is the refractive index of copolymer solution, and $\lambda$ is incident wavelength, 637 nm.

Then, the decay rates (Γ) at different angles are obtained from relaxation time distribution function, with respect of $\tau$:

$$\Gamma = 1/\tau$$

The decay rates (Γ) at different angles are then plotted against square of wave vector ($q^2$) as a straight line passing origin point (0,0). The diffusion coefficient ($D_T$) is the gradient of the of decay rate Γ variation with $q^2$:

$$D_T = \frac{\Delta\Gamma}{\Delta q^2}$$

Finally, the hydrodynamic radius $R_H$ was calculated using this diffusion coefficient in the Stokes-Einstein Equation, giving:

$$R_h = \frac{k_B T}{6\pi\eta D_T}$$

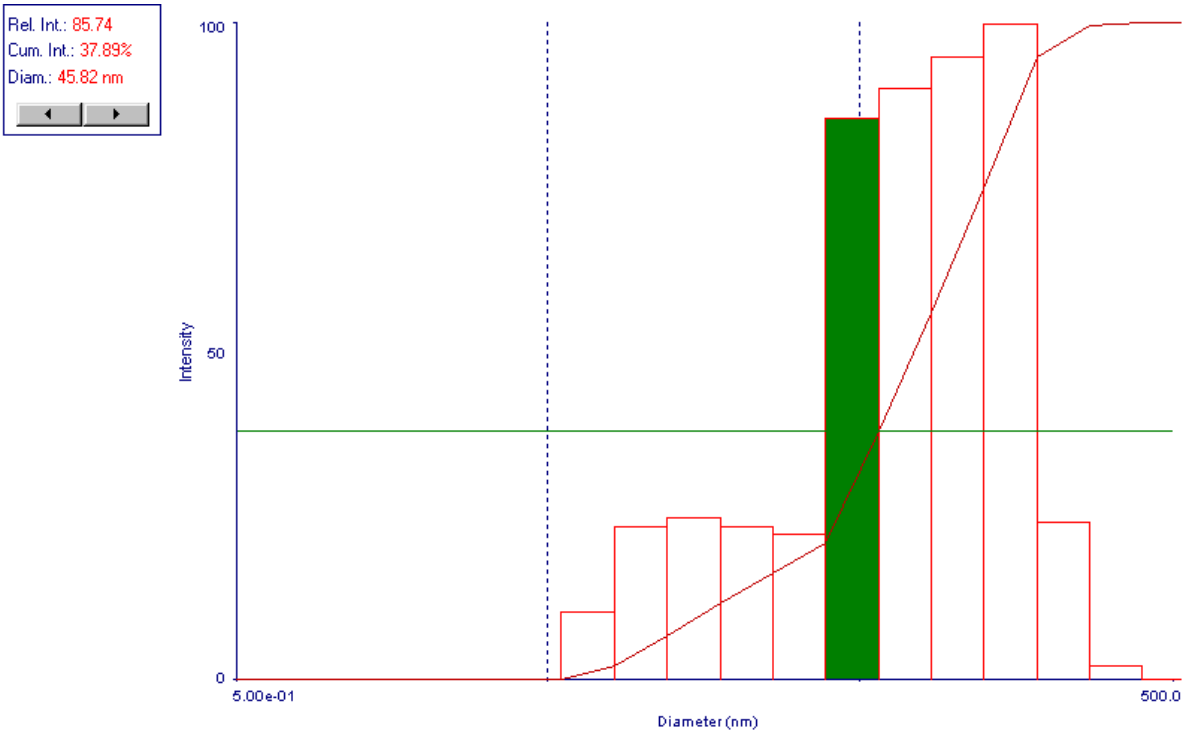


**Figure S6** Distribution of hydrodynamic radii for CSM5-K5 measured by dynamic light scattering at 90 Degree. Orange bins: size frequency histogram normalized to 100 at peak. Red line: cumulative size. Green Bar: tracking of intensity at different diameter in curse modal.

## Correlation of Rg/Rh to the morphology of a nanoparticle

The structure information can be understood by studying the shape factor, which is calculated via Rg/Rh[13]:

| Rg/Rh | Structure |
|---|---|
| < 0.6 | Core-shell |
| ~ 0.774 | Hard Sphere |
| ~ 1 | Vesicle |
| ~ 1.5 | Gaussian Chain |
| >2 | Long Rod |

# Circular Dichroism

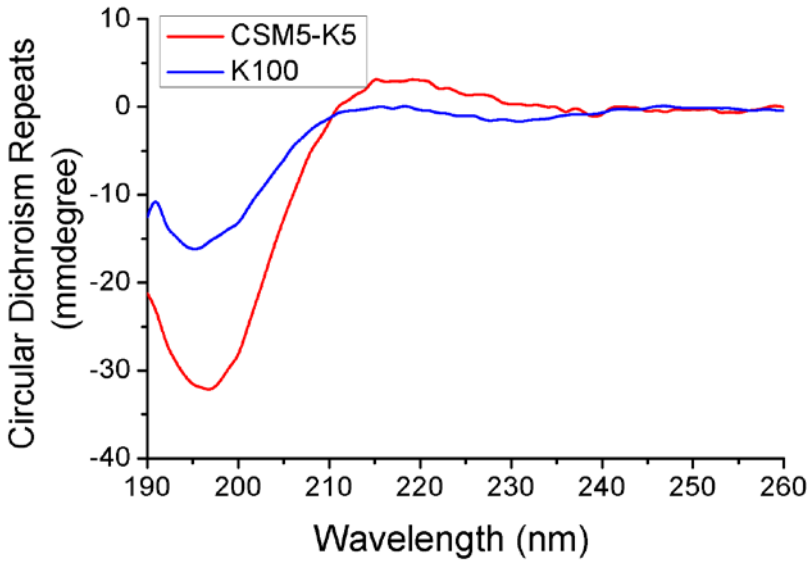


**Figure S7** Far-UV Circular Dichroism spectra of chitosan-*graft*-oligolysine (CSM5-5) and homo-polylysine K100 in DI water, 298.13K.

The CSM5-K5 and K100 show similar negative bands at 195 nm, indicating that the polylysine chains are in the random coil conformation, suggesting a lack of intramolecular hydrogen bonds between the amine groups of lysine repeat units due to protonation

# Computational simulation of chitosan-*graft*-oligolysine (CSM5-K5) Aggregation behavior

**a) General MD simulation parameters**

All MD simulations were performed with GROMACS package, version 4.6.3[15]. A leap-frog algorithm was used to integrate Newton's equation of motion, and the time step was set to 2 fs along with the application of LINCS algorithm[16], by which all the covalent bonds between hydrogen atoms and heavy atoms were constrained. Simulation systems were solvated in TIP3P water model[17]. Sodium and chlorine ions, characterized by Joung *et al.*[18], were used as the counter ions and added to reach a concentration of 0.17 M

physiological salt solution. A cutoff of 1.2 nm was used for both van der Waals interaction calculation and short-range electrostatic interaction calculation, and correspondingly Particle mesh Ewald (PME)[19] method was employed to deal with the long-range electrostatic interaction. All the visualization work was done by PyMol, version 1.5.0.3.

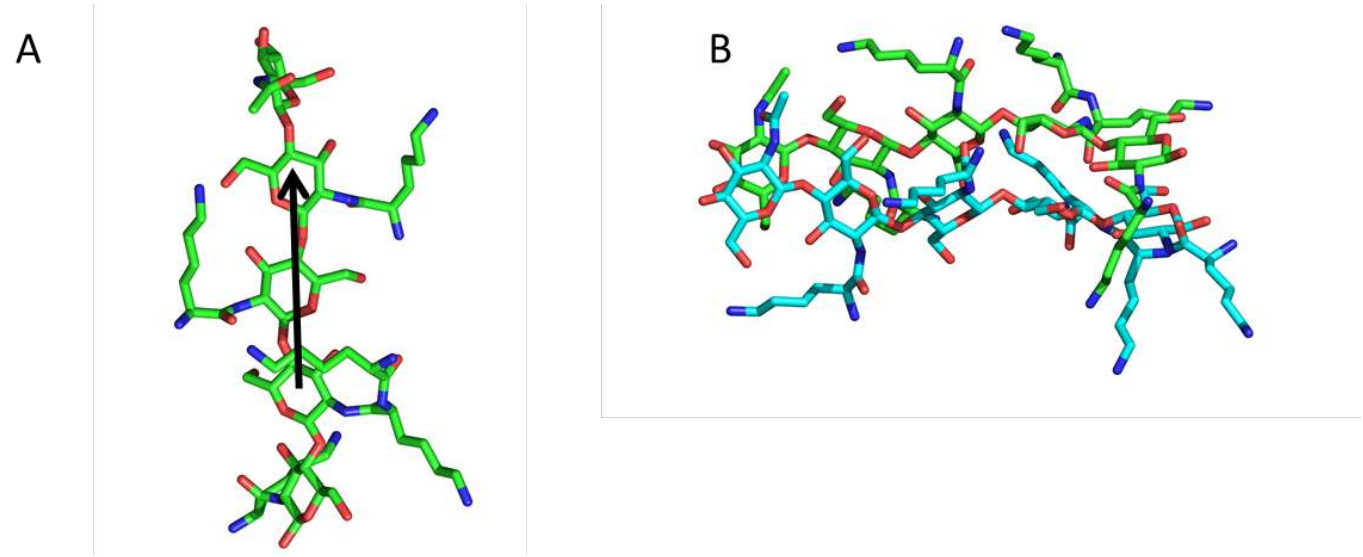


**Figure S8A** Molecular structure of CSM5-K5 (A) one CSM5-K5 is composed of one chitosan chain with 5 sugar repeat units and 4 oligolysine side chains (length 1, 2, 1, and 1 respectively), which are grafted onto the amino group of sugar units. (B) Two CSM5-K5 exist in an aggregated state in solution. This self-assembly happens with a configuration of two parallel chitosan chains, which is favorable for the chitosan-chitosan H-bonds formation. Nitrogen and oxygen atoms are colored as blue and red respectively, carbon atoms are colored as green and cyan to differentiate different molecules.

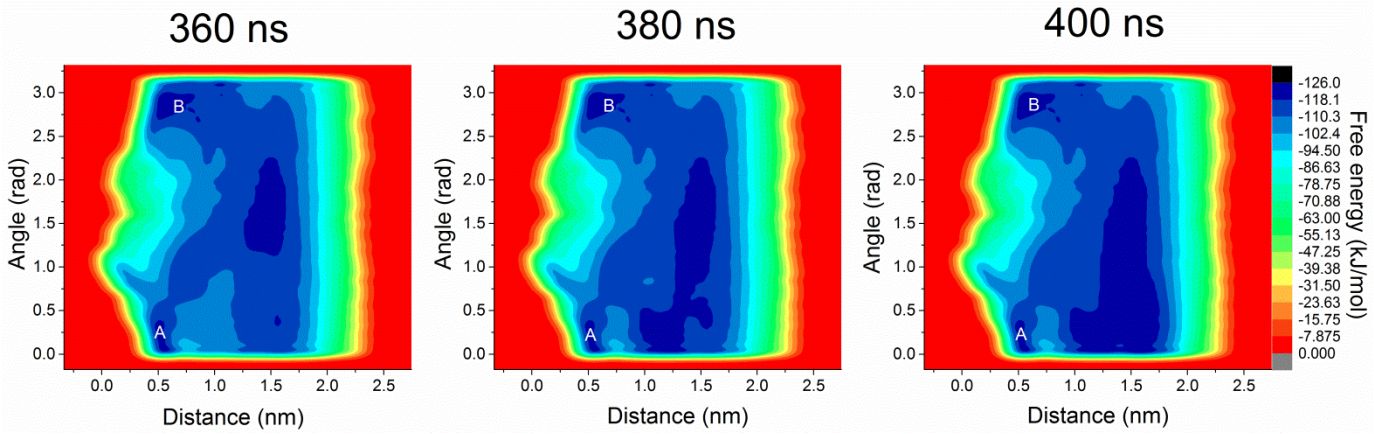


**Figure S8B** Free energy surfaces (FES) of CSM5-K5's dimerization. A well-tempered meta-dynamics simulation was performed using the distance and angle as collective variables (CVs). Distance is defined as center of mass distance between the chitosan chains of two CSM5-K5 molecules, and angle is the included angle between two vectors, each of which points from the 2nd sugar residue to the 4th sugar residue, as the black arrow shown in Figure S8A. FES was similar at different simulation time, especially in the area with small distance value, indicating the convergence of the simulation Two local minima, labelled as A and B, were found in the FES, and both of them appeared in the area with small chitosan-chitosan distance and small

or large chitosan-chitosan angle.

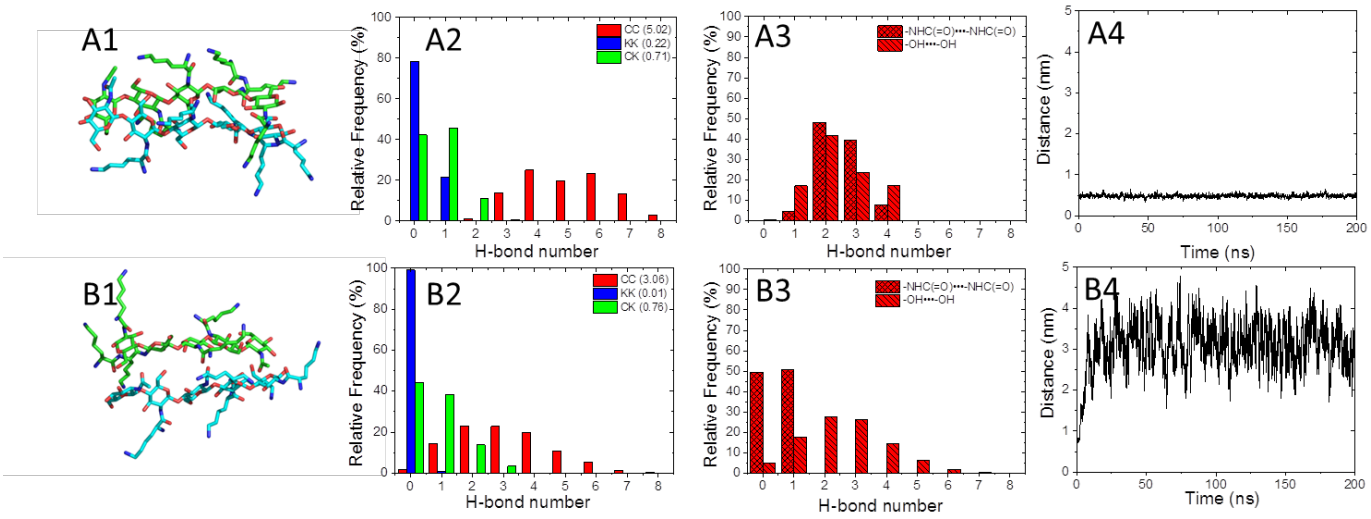


**Figure S8C** H-bonds and stability of structures in minimum A and B. Representative dimer conformations of minimum A (A1) and minimum B (B1) were obtained by clustering structures in each minimum based on RMSD with respect to the two chitosan chains with a cutoff of 0.1 nm using gromos method[20]. A2 and B2 presented frequency distributions of H-bonds, distinguishing chitosan (C) and polylysine (K), between the 2 molecules of configurations within each minimum. H-bonds between chitosan and chitosan, chitosan and polylysine, polylysine and polylysine were denoted as CC, CK, KK respectively. Also shown in A2 and B2 was the average number of H-bonds (inside the parenthesis). CC H-bond played a critical role in aggregation of CSM5-K5. CC H-bonds could be divided into two categories: the –NHC(=O)•••-NHC(=O) H-bonds and –OH•••-OH H-bonds, and their frequency distribution were shown in A3 and B3. Minimum A has more NHC(=O)•••-NHC(=O) H-bonds than minimum B. Started from the representative structures, 200 ns simulation was performed for each FES minimum. COM distance between two CSM5-K5 (A4 and B4) showed that minimum A was more stable than minimum B. indicating that more –NHC(=O)•••–NHC(=O) H-bonds promoted a more stable dimer conformation.

# pH potentiometric titration of chitosan-*graft*-oligolysine and linear polylysines

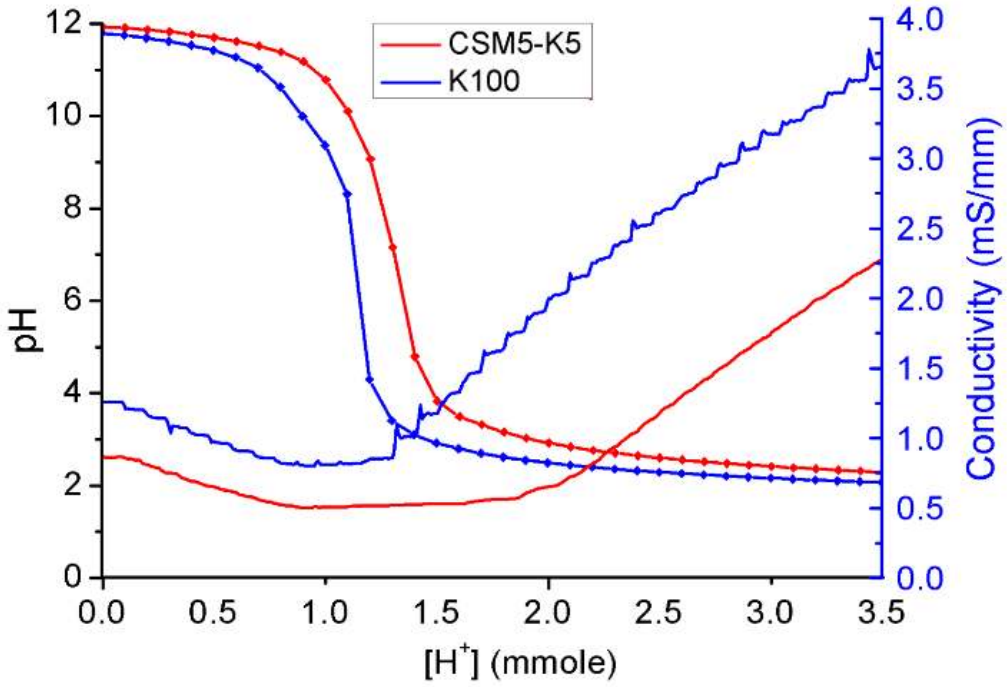


**Figure S9A** pH potentiometric titration curves for (A) Chitosan-*graft*-oligolysine (CSM5-K5) and (B) Linear polylysine (K100)

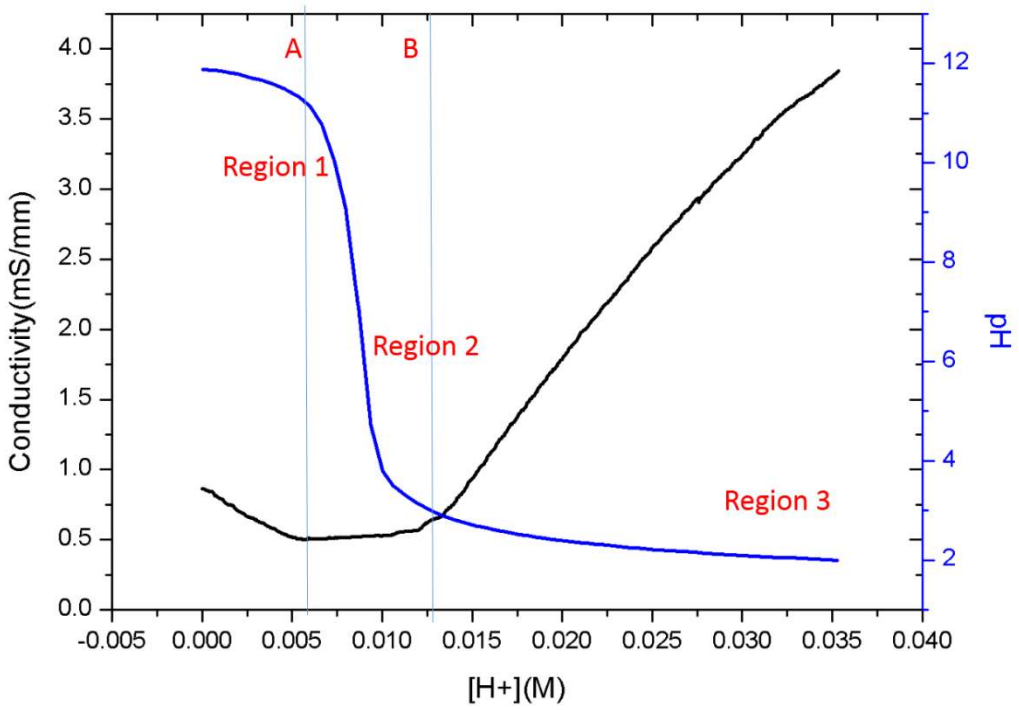


**Figure S9B** Illustration of pH titration calculation

pH-potentiometric titrations of CSM5-K5 (Figure S9B) show the protonation process as pH is tuned from 12 to 2. As pH is reduced from 11.5 to 3.0 (Region 2) the conductivity of the solution increases slowly as the

amine groups are protonated. As pH is reduced further to values below 3.0 (Region 3), the conductivity increases more rapidly, suggesting that the amine groups are fully protonated by pH about 3.0

The acidic dissociation constant (pKa) of the polymer corresponding to protonation curve (Figure 3C) is obtained from the pH-potentiometric titration curve. Taking Figure S9B as an example, the protonation process of amine groups (Region 2) on polymer is detected by conductivity curve between point (A) and (B), with point (A) as 0% protonation (α=0), and point (B) as 100% protonation (α=1). The acidic dissociation constant (pKa) value is calculated based on the pH value corresponding to each degree of protonation in Region 2 via the Henderson-Hasselbalch Equation:

$$pK_a = pH + \log\left(\frac{1-\alpha}{\alpha}\right)$$

pKa is not defined for the limits α = 0 and 1, corresponding to the pH values of ~11.5 and ~3.0. For intermediate values of pH, α is interpolated between these two limits and pKa at the corresponding pH computed from the above relation.

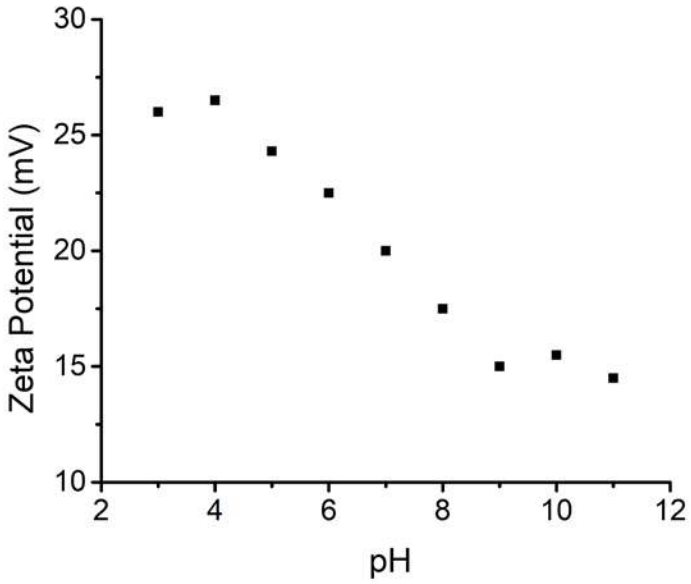


**Figure S9C** Zeta-potential of CSM5-K5 nanoparticle measured from pH=3 to pH=11 in water

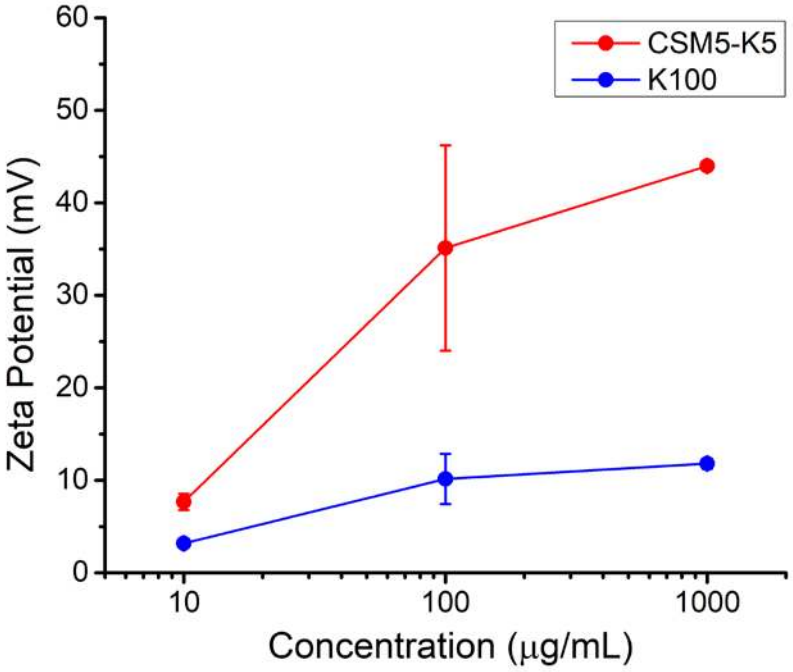


**Figure S9D** Zeta-potential of CSM5-K5 and K100 measured at different concentration in DI water.

# Isothermal Titration Calorimetry Studies

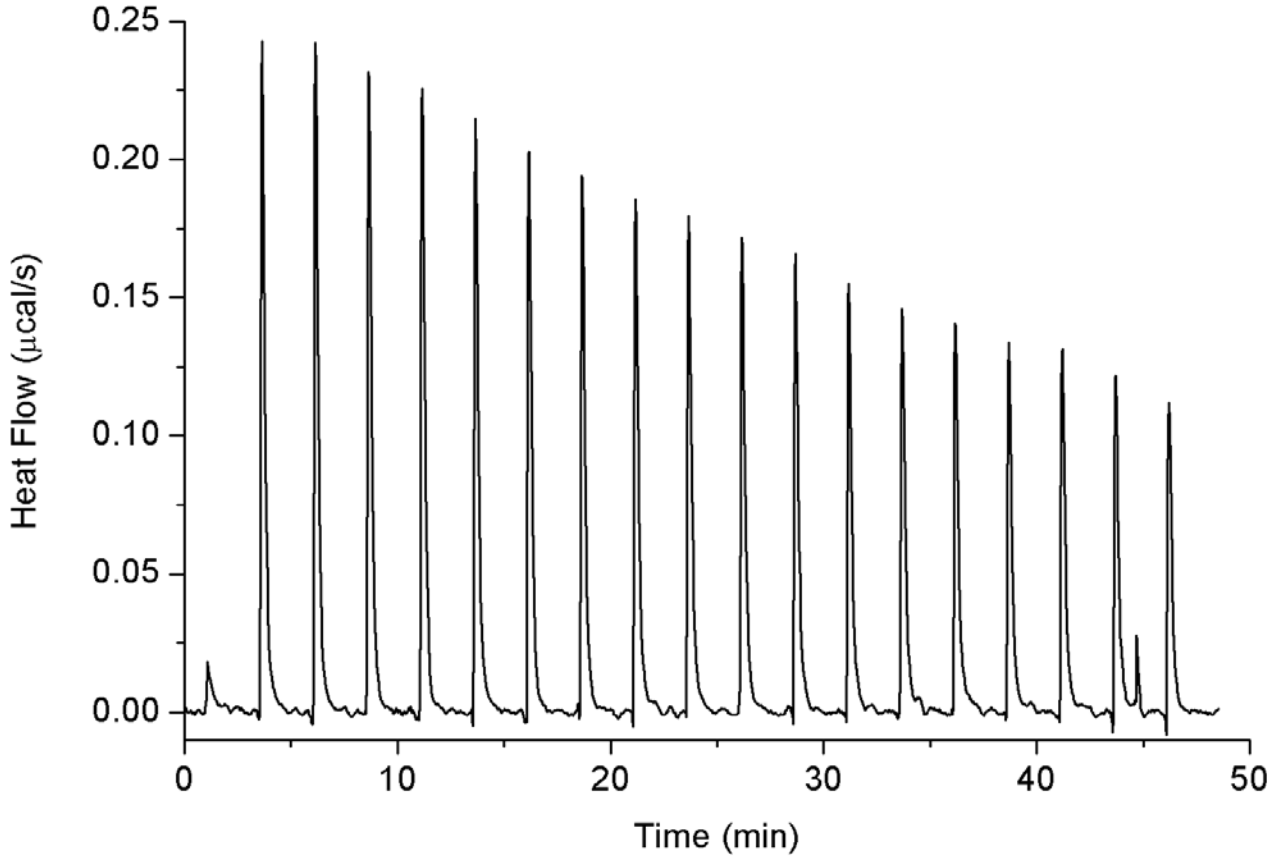


**Figure S10A** Isothermal Titration Calorimetry Spectrum of CSM5-K5 with pure MES buffer (pH=6.5)
For CSM5-K5 titrated with pure MES buffer (pH=6.5), trace amount of enthalpy heat is released at first, followed by greater increase in entropy, suggesting the dilution effect of concentrated CSM5-K5 solution.

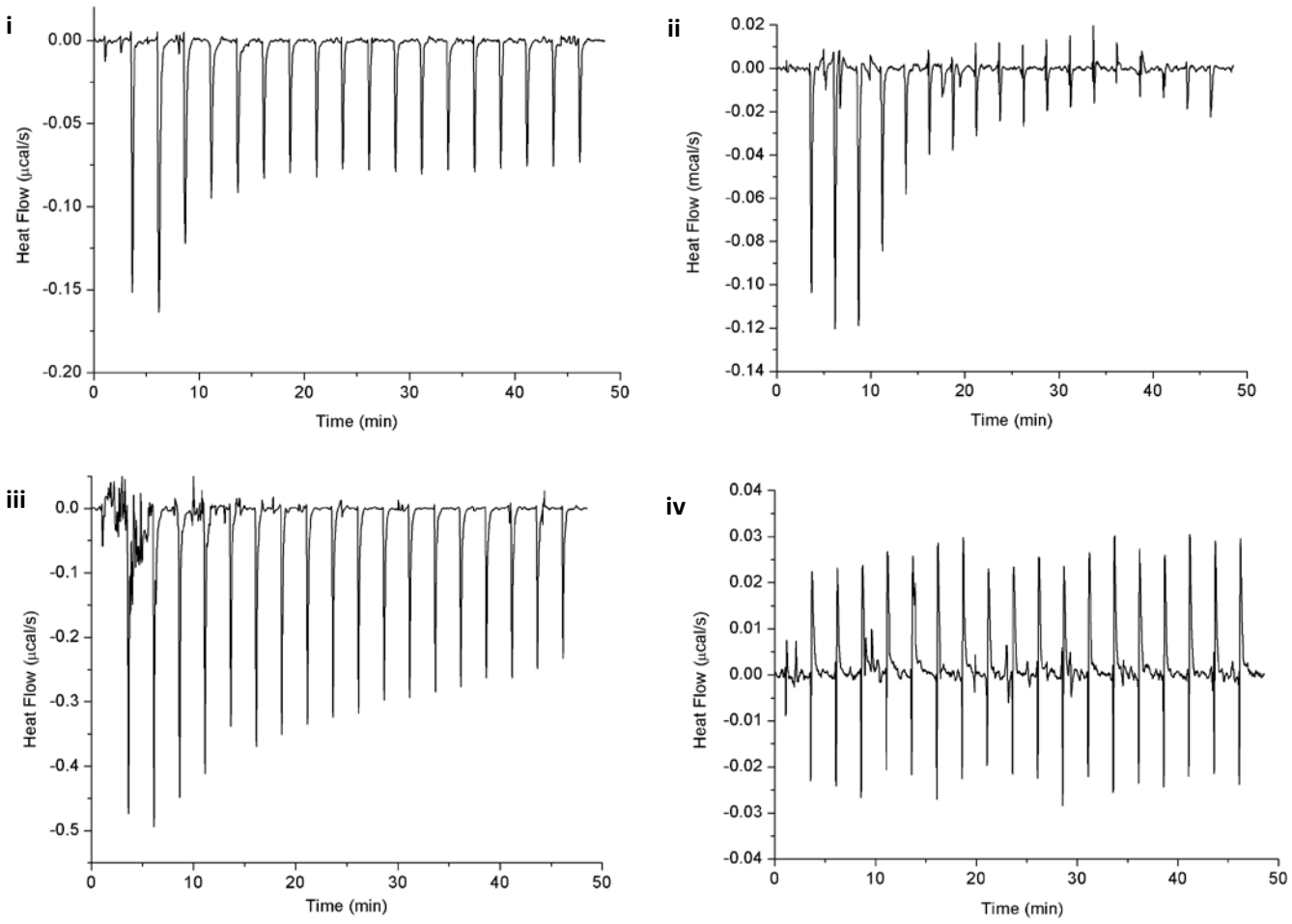


**Figure S10B** Summary of heat flow (µcal/s) change with time determined by isothermal titration calorimetry study of CSM5-K5 interaction with **(i)** POPC: LPS liposome with LPS from *E. coli*; **(ii)** POPC: LPS liposome with LPS from *P. aeruginosa* PA01; **(iii)** POPC: POPG liposome; **(iv)** Purely POPC liposome

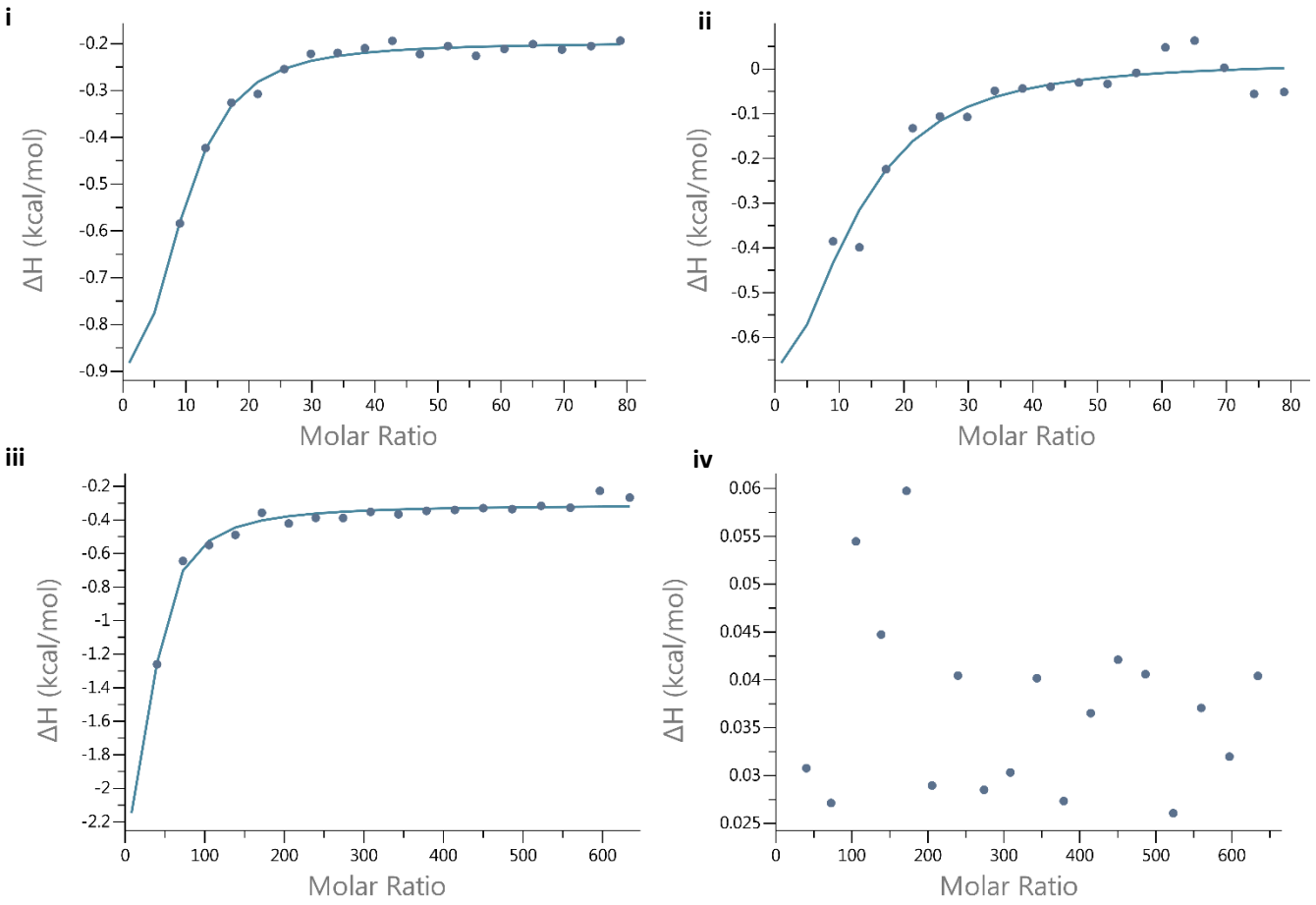


**Figure S10C** Summary of enthalpy profile (kcal/mol) change with mole ratio of polymer added into liposomes determined by isothermal titration calorimetry study of CSM5-K5 interaction with (i) POPC: LPS liposome with LPS from *E coli*; (ii) POPC: LPS liposome with LPS from *P.aeruginosa* PAO1; (iii) POPC: POPG liposome; (iv) Pure POPC liposome.

# Dynamic Light Scattering Study of liposome interaction with polymers

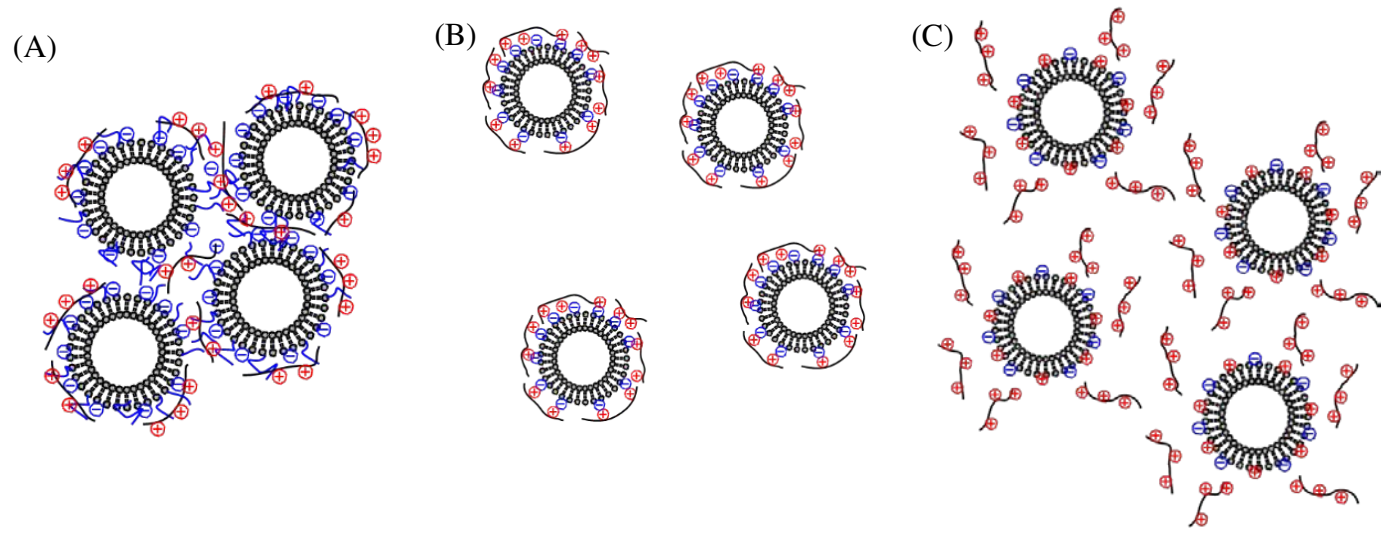


**Figure S11** Illustration of cationic copolymer binding on model liposomes: (A) the polymer has very strong interaction with POPC:LPS liposomes and mediates aggregation, (B) the polymer can bind with POPC:POPG liposomes, (C) the polymer has no interaction with Pure POPC liposomes).

We applied dynamic light scattering (DLS) to study the interaction of CSM5-K5 with different model liposomes. Pristine chitosan (3kDa molecular weight) and linear K100 salt were used as comparisons (Table S5). Pristine chitosan 3kDa and linear polylysine individually did not cause any change in hydrodynamic radius, indicating negligible interaction. However, CSM5-K5 copolymers show strong binding interaction with POPC:LPS liposome model: the hydrodynamic radii of POPC:LPS liposome incubated with the CSM5-K5 series increase dramatically from around 75 nm to 682 nm, suggesting aggregation of liposomes mediated by the copolymer (Figure S11A). This result is consistent with the ITC finding that the binding of LPS with CSM5-K5 is thermodynamically favorable. CSM5-K5 also shows some interaction with POPC:POPG liposome, as the size slightly increases. The polymers might be adsorbed on the surface of the liposomes (Figure S11B). For the pure POPC model, which represents mammalian cells, the interaction with CSM5-K5 copolymer is not significant as the size of liposome shows almost no changes from DLS (Figure S11C). These

DLS results suggest CSM5-K5 preferentially interacts with bacterial membrane.

# Computational Simulation of chitosan-*graft*-oligolysine Interaction with membrane

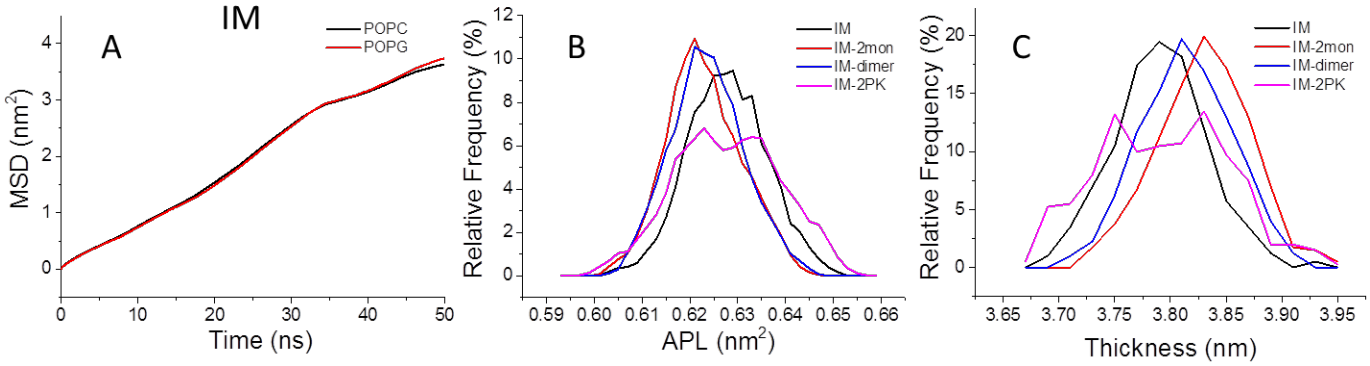


**Figure S12A** Lateral mean square displacements (MSD) of POPC and POPG in IM system is shown in (A). Based on the least squares fitting to Einstein relation $MSD = 4Dt + c$, where D is the diffusion coefficient and c is a constant, diffusion coefficients for POPC and POPG were 2.19 ± 0.25 (1e-7 cm$^2$/s) and 2.23 ± 0.08 (1e-7 cm$^2$/s) respectively. The high diffusion constant indicated that our membrane was in a fluid phase. Area per lipid (APL) in IM-2mon and IM-dimer systems showed a slight decrease as compared to APL in IM system (B), and correspondingly, a slight increase of thickness for membranes in IM-2mon and IM-dimer systems was observed (C). Distance of phosphorus atoms in different membrane leaflet were used to calculate membrane thickness.

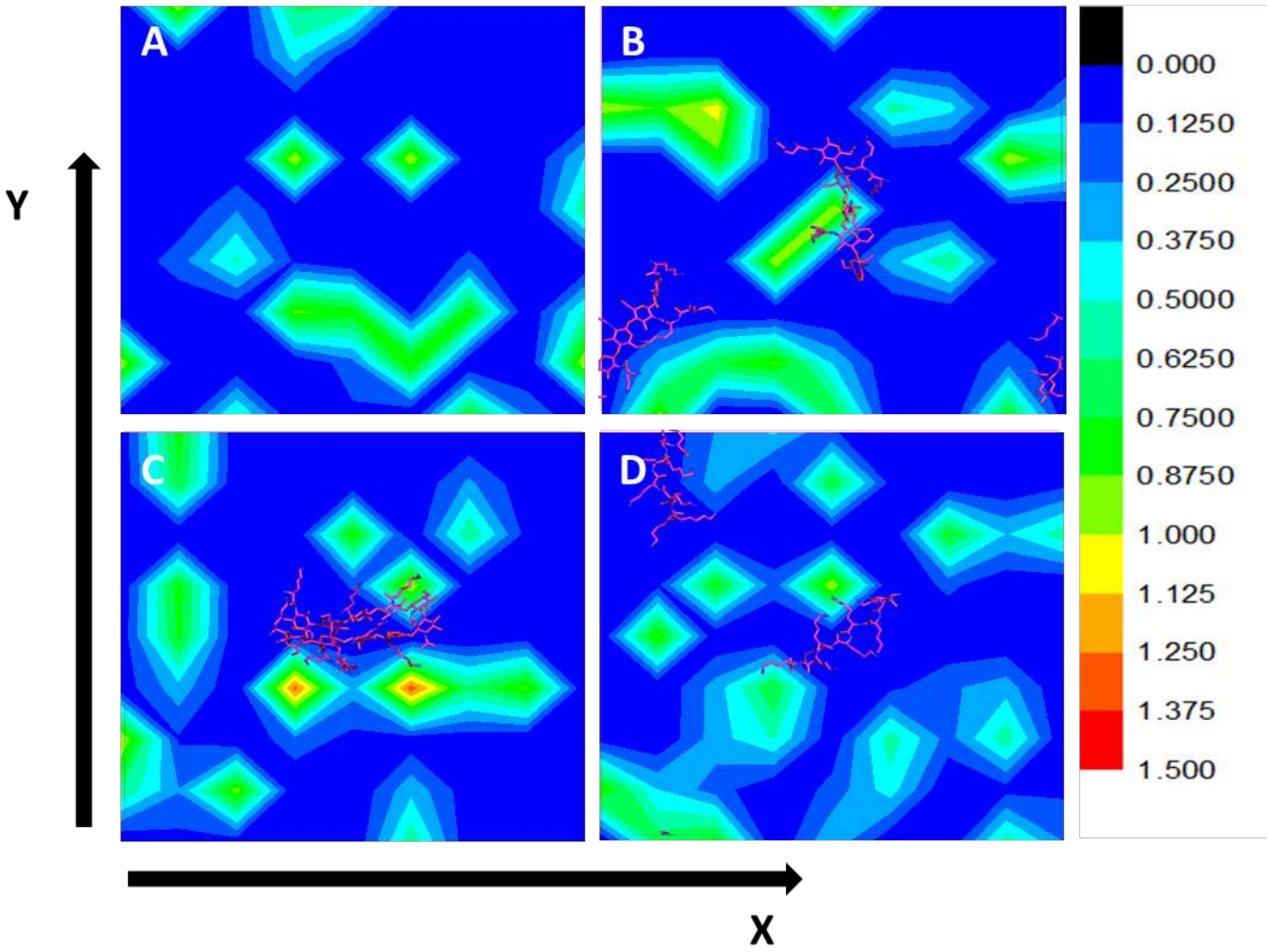


**Figure S12B**. Accumulation of POPG in system IM (A), IM-2mon (B), IM-dimer (C) and IM-2PK (D). 100 frames in the last 1 ns simulation were picked out to compute the average number of lipid molecules as a function of X,Y coordinates. Each window is a top view of simulation box and has a size of approximately 7.1nm * 7.1nm. The positions of the polycations are labeled with red lines. One molecule in (B) is divided at the simulation boundary due to the periodic boundary conditions (PBC). POPG in IM-dimer system was more concentrated than others.

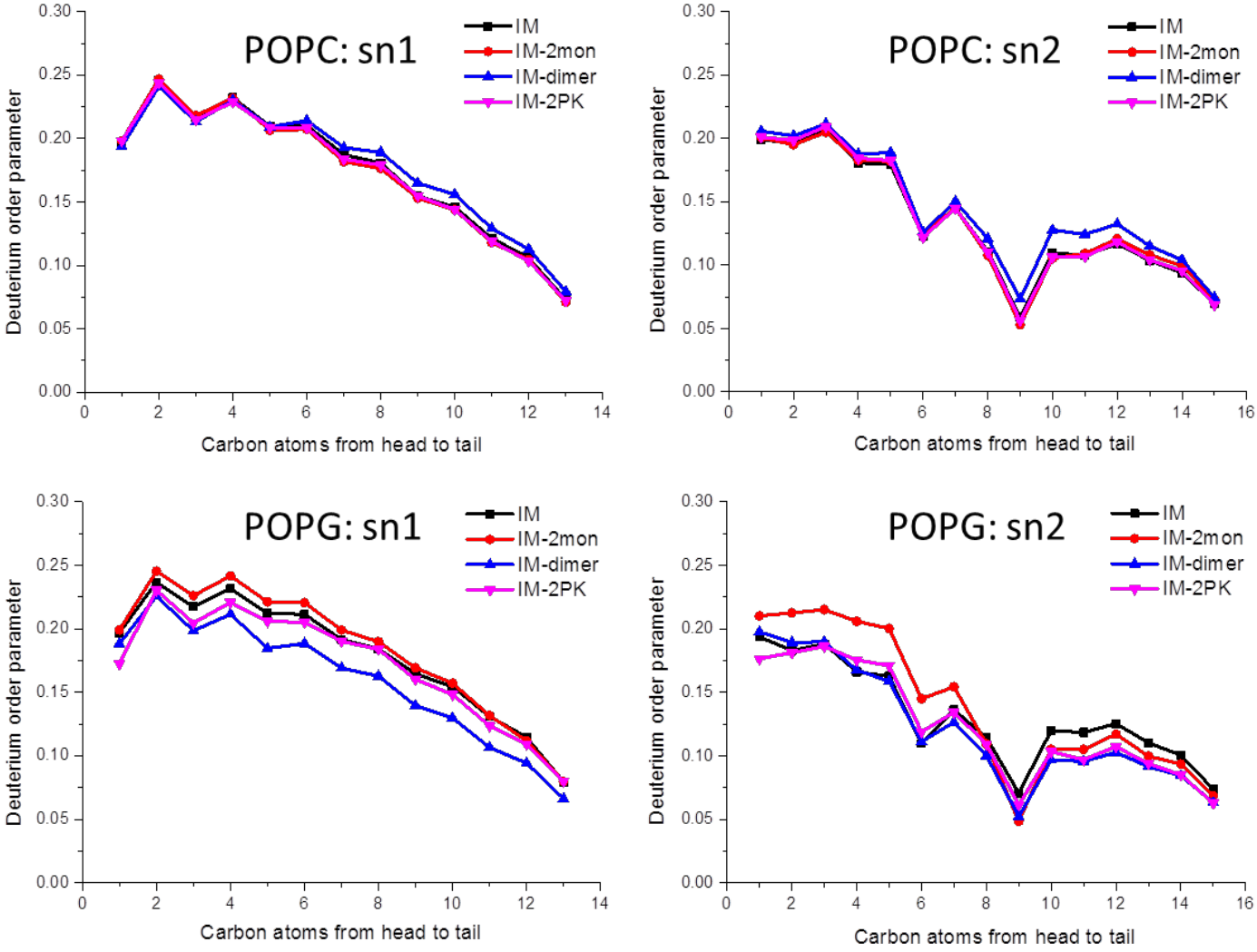


**Figure S12C** Deuterium order parameters for two acyl chains of POPC and POPG in different systems. Parameters were calculated based on $S_{cd}(z) = \frac{3}{2}\langle cos^2\theta(z)\rangle - \frac{1}{2}$ , where θ(z) is the angle between the normal to the bilayer and the C-C vector located at z. CSM5-K5 were more effective to POPG than to POPC, but the effect was limited based on our simulation.

# Cryo-TEM images of MRSA BAA-40 treated with CSM5-K5

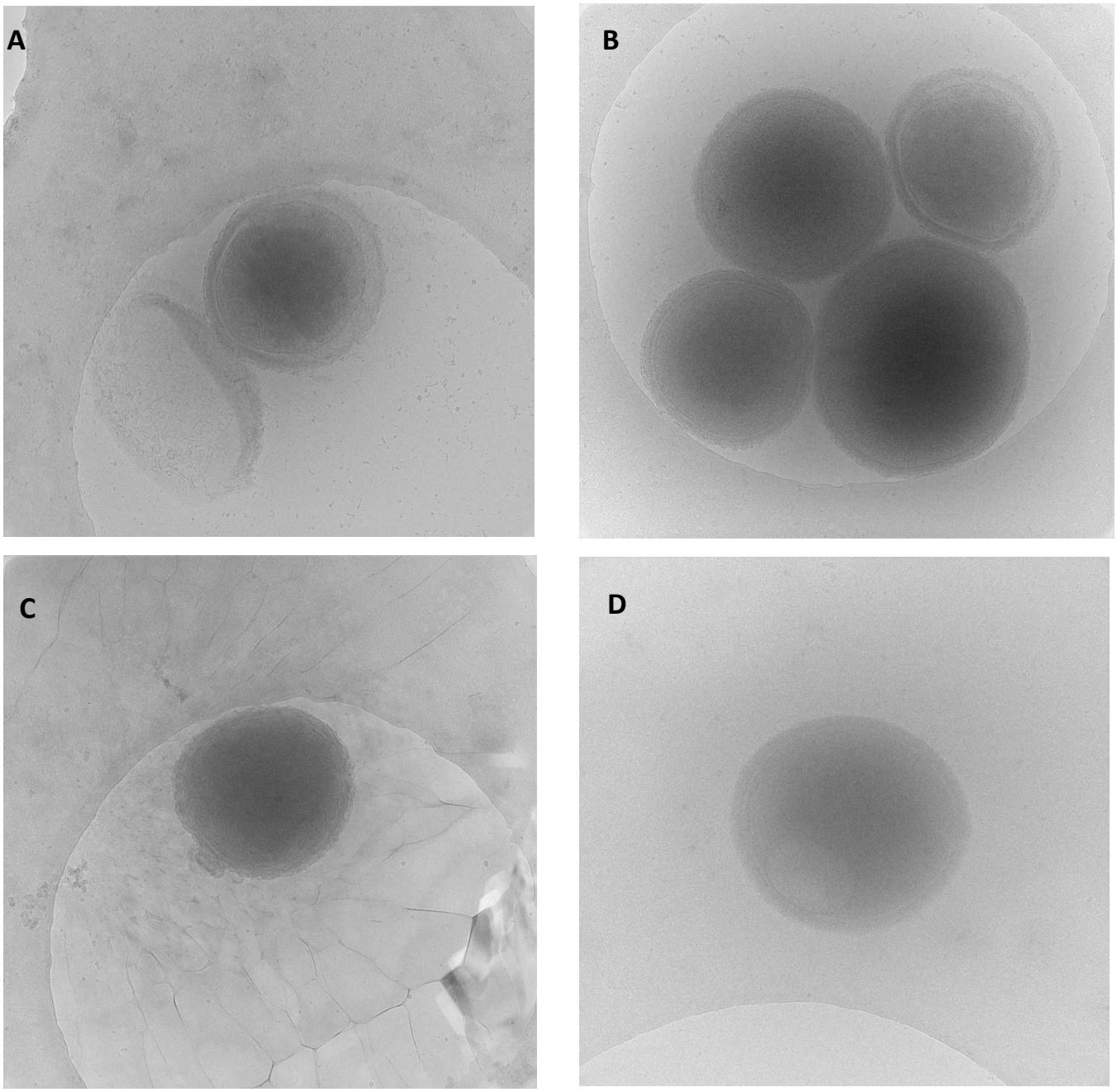


**Figure S13** Cryo-TEM images of MRSA BAA-40 treated with (A)1×MIC, (B)2×MIC, (C)4×MIC and (D)8×MIC concentration of CSM5-K5

## References

(1) Sader, H.; Fedler, K.; Rennie, R.; Stevens, S.; Jones, R. Omiganan Pentahydrochloride (MBI 226), a Topical 12-Amino-Acid Cationic Peptide: Spectrum of Antimicrobial Activity and Measurements of Bactericidal Activity. *Antimicrobial agents and chemotherapy* **2004,** *48* (8), 3112–3118.

(2) Won, H.-S.; Kang, S.-J.; Choi, W.-S.; Lee, B.-J. Activity Optimization of an Undecapeptide Analogue Derived from a Frog-Skin

Antimicrobial Peptide. *Molecules and Cells* **2011,** *31*, 49-54.
(3) Gottler, L., M.; Ramamoorthy, A. Structure, Membrane Orientation, Mechanism, and Function of Pexiganan — A Highly Potent Antimicrobial Peptide Designed from Magainin. *Biochimica et Biophysica Acta* **2009,** *1788* (8), 1680-1686.
(4) Radzishevsky, I.; Rotem, S.; Bourdetsky, D.; Navon-Venezia, S.; Carmeli, Y.; Mor, A. Improved Antimicrobial Peptides based on Acyl-lysine Oligomers. *Nature Biotechnology* **2007,** *25* (6), 657-659.
(5) Mygind, P. H.; Fischer, R. L.; Schnorr, K. M.; Hansen, M. T.; Sönksen, C. P.; Ludvigsen, S.; Raventós, D.; Buskov, S.; Christensen, B.; De Maria, L.; Taboureau, O.; Yaver, D.; Elvig-Jørgensen, S. G.; Sørensen, M. V.; Christensen, B. E.; Kjærulff, S.; Frimodt-Moller, N.; Lehrer, R. I.; Zasloff, M.; Kristensen, H.-H. Plectasin is a Peptide Antibiotic with Therapeutic Potential from a Saprophytic Fungus. *Nature* **2005,** *437* (13), 975-980.
(6) Cao, X.; Zhang, Y.; Mao, R.; Teng, D.; Wang, X.; Wang, J. Design and Recombination Expression of a Novel Plectasin-derived Peptide MP1106 and its Properties against Staphylococcus aureus. *Applied Microbiology and Biotechnology* **2015,** *99*, 2649–2662.
(7) Zhong, Z.; Li, P.; Xing, R.; Liu, S. Antimicrobial Activity of Hydroxylbenzenesulfonailides Derivatives of Chitosan, Chitosan Sulfates and Carboxymethyl Chitosan. *International Journal of Biological Macromolecules* **2009,** *45*, 163–168.
(8) Sajomsang, W.; Tantayanon, S.; Tangpasuthadol, V.; Daly, W. Quaternization of N-aryl chitosan derivatives: synthesis, characterization, and antibacterial activity. *Carbohydrate Research* **2009,** *344*, 2502–2511.
(9) Sajomsang, W.; Tantayanon, S.; Tangpasuthadol, V.; Daly, W. Synthesis of Methylated Chitosan Containing Aromatic Moieties: Chemoselectivity and Effect on Molecular Weight. *Carbohydrate Polymers* **2008,** *72*, 740–750.
(10) Zhong, Z.; Xing, R.; Liu, S.; Wang, L.; Cai, S.; Li, P. Synthesis of Acyl Thiourea Derivatives of Chitosan and their Antimicrobial Activities *in vitro*. *Carbohydrate Research* **2008,** *343*, 566–570.
(11) Sun, S.; An, Q.; Li, X.; Qian, L.; He, B.; Xiao, H. Synergistic effects of chitosan–guanidine complexes on enhancing antimicrobial activity and wet-strength of paper. *Bioresource Technology* **2010,** *101*, 5693–5700.
(12) Huesmann, D.; Birke, A.; Klinker, K.; Turk, S.; Rader, H.; Barz, M. Revisiting Secondary Structures in NCA Polymerization:Influences on the Analysis of Protected Polylysines. *Macromolecules* **2014,** *47* (3).
(13) Cao, A. Light Scattering. Recent Applications. *Analytical Letters* **2003,** *36* (15), 3185-3225.
(14) Schillen, K.; Brown, W.; Johnsen, R. Micellar Sphere-to-Rod Transition in an Aqueous Triblock Copolymer System. A Dynamic Light Scattering Study of Translational and Rotational Diffusion. *Macromolecules* **1994,** *27* (17), 4825-4832
(15) Berendsen, H. J. C.; Spoe, D., van der.; van Drunen, R. GROMACS: a Message Passing Parallel Molecular Dynamics Implementation. *Computer Physics Communications* **1995,** *95*, 43-56.
(16) Hess, B.; Bekker, H.; Berendsen, H.; Fraaije, J. LINCS: a Linear Constraint Solver for Molecular Simulations. *Journal of Computational Chemistry* **1997,** *18*, 1463-1472.
(17) Jorgensen, W.; Chandrasekhar, J.; Madura, J., D.; Impey, R., W.; Klein, M., L. Comparison of Simple Potential Functions for Simulating Liquid Water. *Journal of Chemical Physics* **1983,** *79* (2), 926, DOI: 10.1063/1.445869.
(18) Joung, I.-S.; Cheatham, T. Determination of Alkali and Halide Monovalent Ion Parameters for Use in Explicitly Solvated Biomolecular Simulations. *Journal of Physical Chemistry* **2008,** *112*, 9020-9041.
(19) Essmann, U.; Perera, L.; Berkowitz, M.; Darden, T.; Lee, H.; Pedersen, L., G;. A Smooth Particle Mesh Ewald Method. *Journal of Chemical Physics* **1995,** *103*, 8577-8593.
(20) Daura, X.; Gademann, K.; Jaun, B.; Seebach, D.; Gunsteren, W. F.; Mark, A. E. Peptide Folding: When Simulatioin Meets Experiment. *Angewandte Chemie International Edition.* **1999,** *38*, 236-240.